



**Cape Peninsula
University of Technology**

**THE DESIGN, NUMERICAL MODELLING AND DEVELOPMENT OF MEMS
FABRICATION PROCESS OF A MICROBOLOMETER FOR USE IN LONG WAVE
INFRARED DETECTION**

by

SENDA TUDIEJI PAUL

Thesis submitted in fulfilment of the requirements for the degree

Master of Technology: Mechanical Engineering

in the Faculty of Engineering

at the Cape Peninsula University of Technology

Supervisor: Prof Philander Oscar

Bellville Campus

Date of submission: April 2013

Acknowledgements

I acknowledge with sincere gratitude all the people who helped and supported me to complete this thesis.

Special thanks to my supervisor, Prof O. Philander, for his strong support, guidance, assistance and patience for the duration of this research and writing of this thesis.

I am indebted to the Cape Peninsula University of Technology Department of Mechanical Engineering and the postgraduate financial aid office of CPUT for providing me with bursary assistance.

Finally, to my family whose support and love helped me to focus and move forward with my research, I am deeply grateful.

Abstract

The Advanced Manufacturing Technology Strategy (AMTS), predecessor of the Technology Innovation Agency, was a national strategy focused principally on improving collaboration amongst industry, academia and science councils. The aerospace industries and training institutions in particular have been identified as key thrust areas for achieving economic development through the AMTS. Furthermore, the AMTS Aerospace Interest Group has been identified as one of the most important facets of Micro and Nano Manufacturing, Sensors and Electronics Flagship Program.

The manufacturing of Micro and Nano Electronics and sensors is essential for South Africa to sustain the technology capability development as seen in developed countries. For example, there is an urgent need to establish a Photo Lithography facility for South African industry and training Institutions.

The demand for the new generations of industrial, military, commercial, medical, automotive and aerospace products in South Africa in particular, and in the world in general, has fuelled research and development activities focused on advanced and smart materials. This situation has allowed for the emergence of a new generation of infrared sensors, the bolometer, based on an infrared thermal detection mechanism which is particularly suited to operate at ambient temperature, opening opportunities for achieving low cost infrared imaging systems for both military and commercial applications.

This work deals with different South African bolometer membranes of the second prototype in collaboration with the University of Pretoria and Denel Optronics. The bolometer is an infrared thermal sensor that measures thermal radiation by converting said radiation into a temperature change and subsequently measuring the induced change in electrical resistance. The term

infrared from Latin *Infra*, meaning *below*, is usually applied to wavelengths between 700nm and 1mm. It can be argued that the first occurrence of infrared sensing actually goes back several millennia, when men placed their hands over recently extinguished fire. However, until Herschel's experiment, this kind of infrared was between the sun and the earth.

Thermal imaging, which refers to the ability to measure the temperature of different points on a scene, requires either an array of infrared detectors operating in those wavelength ranges or a way to scan a scene using a single detector.

To realise this work, objectives have been assigned to different groups of the consortium represented by CPUT, UP and Denel. Analyses of thirteen bolometer membranes including metal bolometer (Titanium) and Vanadium oxide were assigned to CPUT, reason why this thesis focuses on the modelling, designing and testing of the bolometer membranes. Masks design of the second prototype bolometer test structures includes several thermally isolated bolometer devices. These devices have been modelled and analysed in order to study their electrical and thermal behaviour.

Table of Content

Acknowledgements.....	i
Abstract.....	ii
Table of Content.....	iv
List of Figures	vii
List of tables	ix
List of Abbreviations and Keywords	xi
List of Physical constants.....	xiv
List other variables	xv
Chapter One.....	1
1. Introduction.....	1
1.1 Background	5
1.2 Objectives	7
1.3 Methodology	8
1.4 Thesis outline	11
Chapter Two.....	12
2. Literature Review	12
2.1 Introduction.....	12
2.2 MEMS Technology	12
2.3 MEMS Applications and Markets	13
2.3.1 Automotive.....	15
2.3.2 Communication.....	15
2.3.3 Biotechnology	16
2.4 Advantages of MEMS	17
2.4.1 Advantage of MEMS manufacturing.....	17
2.4.2 Challenges facing MEMS.....	18
2.5 Brief theory of infrared radiation.....	19
2.5.1 Introduction.....	19

2.5.2 Theory of infrared (IR) absorption.....	20
2.5.4 Molecular vibrations	21
2.5.5 Vibrational coupling.....	22
2.5.6 Laws of radiation and definitions.....	22
2.5.7 Definitions	24
2.5.8 Spectral magnitudes	25
2.5.9 The emissivity	27
2.6 Un-cooled Infrared Imaging	29
2.7 Summary.....	29
Chapter Three.....	30
3. Principles and Fabrication of Uncooled Microbolometer Devices Analysed.....	30
3.1 Introduction.....	30
3.2 Ideal model of a microbolometer.....	31
3.2.1 Uncooled thermal detector structure	31
3.2.2 Microbolometer principles	32
3.2.3 Vanadium oxide and metal titanium bolometer analysed processing.....	33
3.3 Material selection.....	37
Gold's physical quantities and thermal properties.....	41
Gold's chemical qualities	42
3.4 Manufacturing process	44
3.4.1 CoventorWare.....	44
3.5 Fabrication process.....	45
3.5.1 Fabrication technologies	45
3.5.2 Bolometer process sequence for the prototype model.....	47
3.6 Summary.....	52
Chapter Four.....	53
4. Results and Discussions of Static Analysis.....	53
4.1 MEMS Processing and Virtual Fabrication	53
4.2 Numerical analyses	59
4.2.1 Thermal Loading for Static Analyses	60
4.2.2 Thermal Loading for Dynamic Analyses	60
4.3 Static Analyses and data treatment.....	61
4.4 Analysis approach	75
4.5 Static analysis at atmospheric pressure	82

4.6 Summary.....	85
Chapter Five.....	88
5. Results and Discussions of Dynamic Analyses.....	88
5.1 Thermal modelling.....	88
5.2 Determination of thermal properties.....	91
5.3 Summary.....	108
Chapter Six.....	109
6. Conclusion and Recommendations.....	109
6.1 Problems solved in the research.....	109
6.1.1 Solid model.....	110
6.1.2 Thermal conductance.....	110
6.1.3 Thermal time constant.....	111
6.2 Recommendations for future work.....	115
Bibliography.....	116
Appendix A.....	119
A. Using CoventorWare.....	119
Appendix B.....	127
B. MemMech Solver.....	127
Appendix C.....	129
C. Devices thermal conductance analysis.....	129

List of Figures

Figure 1-1: (a) Schematic drawing of monolithically integrated infrared bolometer focal plane array (FPA) and (b) placement of a focal plane array with an infrared lens system (Niklaus F, 2007, 2).....	9
Figure 1-2: Ideal bolometer schematic	9
Figure 2-1 MEMS Market trucker (Bouchaud J., 2011:4)	13
Figure 2-2: High value of MEMS devices (Bouchaud J., 2011:4).....	14
Figure 2-3: Top 20 MEMS suppliers' high value (Bouchaud J., 2011:4)	14
Figure 2-4: 2010 MEMS market (Bouchaud J., 2011:4)	16
Figure 2-5: Stretching vibrations (teaching.shu.ac.uk/hwb/chemistry/tutorials)	21
Figure 2-6: Bending vibrations (teaching.shu.ac.uk/hwb/chemistry/tutorials)	21
Figure 2-7: A schematic representation of electromagnetic radiation. The wavelength represented by λ (Pol, VDE, 2012, 1)	23
Figure 2-8: Graphical representation of radiance, irradiance and emittance (Cassanova J-L, 2007, 6).....	25
Figure 2-9: Wavelength and the λ_{max} displacement from the law of Wien (Cassanova J-L, 2007, 12).....	27
Figure 2-10: Emissivity of different materials (Cassanova J-L, 2007, 14).....	28
Figure 3-1: Schematic structure of thermal detector (Yon JJ)	32
Figure 3-2: Cross sectional view of a microbolometer	32
Figure 3-3: Metal bolometer solid model design built in Coventorware.....	33
Figure 3-4: Vanadium Oxide bolometer membrane solid model of the VOx bolometer prototype.....	34
Figure 4-1: Metal bolometer process editor	53
Figure 4-2: VOx bolometer process editor	53
Figure 4-3: Metal bolometer virtual fabrication used CoventorWare.....	54
Figure 4-4: VOX bolometer virtual fabrication as used in CoventorWare	55
Figure 4-5: Dimensioning of (a) MET and (b) VOX device	56
Figure 4-6: Metal bolometer masks layout.....	58
Figure 4-7: VOx bolometer masks layout.....	59
Figure 4-8: VOx bolometer heat flux variation at 300K	62
Figure 4-9: Titanium bolometer displacement at a heat flux of 10000 pW/ μm^2	63
Figure 4-10: Titanium bolometer at 1000 pW/ μm^2	63
Figure 4-11: Metal titanium thermomechanical layout.....	64
Figure 4-12: CoventorWare data collection of VOX2 at 300K	65
Figure 4-13: Displacement data collected of VOX2 at 300K.....	66
Figure 4-14: Thermal conductance equation of VOX2.....	68
Figure 4-15: Thermal conductance equation of MET2@300K.....	69

Figure 4-16: Titanium pixel bolometers' thermal conductance variations of three different metal titanium bolometer.....	72
Figure 4-17: Length and width of bolometer membrane variation.....	73
Figure 4-18: Vox devices thermal conductance	73
Figure 4-19: Length and width variation	74
Figure 4-20: Vox devices (set 3) Thermal conductance	74
Figure 4-21: Length and width variation	75
Figure 4-22: Titanium bolometer thermal deformations displacement	76
Figure 4-23: VOx bolometer thermal deformations displacement.....	77
Figure 4-24: VOX2 L vs W at ambient temperature of 300K.....	78
Figure 4-25: VOX3 L vs W at ambient temperature of 300K.....	78
Figure 4-26: MET2 L vs W at ambient temperature of 300K.....	79
Figure 4-27: VOX3 L vs W at ambient temperature of 263K.....	80
Figure 4-28: MET4 W vs L at ambient temperature of 298K.....	80
Figure 4-29: VOXA W vs L at ambient temperature of 273K.....	81
Figure 4-30: VOXB W vs L at ambient temperature of 278K.....	82
Figure 5-1: Applied heat on MET2 for 4 micron second	94
Figure 5-2: Heating vs Cooling curve of MET2 @ 4 μ s.....	94
Figure 5-3: Heating Curve for MET 2.....	94
Figure 5-4: Cooling Curve for MET2	95
Figure 5-5: Applied heat flux on MET3 @ 4 μ s.....	96
Figure 5-6: Heating and Cooling curve of MET3 over 3 μ s	96
Figure 5-7: Maximum temperature heating curve	97
Figure 5-8: Maximum temperature cooling curve.....	97
Figure 5-9: Heat load on VOX3 @ 35 μ s.....	98
Figure 5-10: Heating vs Cooling curves of VOX3	99
Figure 5-11: Heating curve of VOX3.....	99
Figure 5-12: Cooling curve of VOX3	100
Figure 5-13: Heating vs Cooling curves @ 35 μ s.....	101
Figure 5-14: Heating vs Cooling for VOXF @ 35 μ s.....	101
Figure 5-15: MET2 dynamic simulations data collected.....	102
Figure 5-16: Maximum temperature, Minimum temperature vs Time of VOX3.....	103
Figure 5-17: Elapsed time for MET2 dynamic simulations	103
Figure 5-18: Vox membrane pixel bolometer at peak temperature.....	104
Figure 5-19: window fit and plot applied to MET2	106
Figure 5-20: Determination of γ in Window Fit and Plot of VOXF	106
Figure 5-21: Output from Window Fit and Plot for MET3.....	107
Figure A-1: Gold properties in the MPD	120
Figure A-2: Titanium properties in the MPD.....	120
Figure A-3: VOx properties in the MPD	121
Figure A-4: Tetrahedrons mesher settings.....	124
Figure A-5: Titanium bolometer seen in the visualizer	126
Figure B-1: MemMech Settings and Results Flow.....	128

List of tables

Table 1-1 Bolometer masks (UP 2010)	10
Table 3-1: Metal (titanium) bolometer geometry dimensions	35
Table 3-2: Vanadium oxide (VOx) bolometer geometry dimensions.....	36
Table 3-3: VOx (second set) bolometer geometry dimensions.....	37
Table 4-1: Metal (titanium) bolometer geometry dimensions	56
Table 4-2: Vanadium oxide (VOx) bolometer geometry dimensions	56
Table 4-3: VOx (second set) bolometer geometry dimensions.....	57
Table 4-4: Mask definitions of bolometers analysed	58
Table 4-5 Data collection from CoventorWare	66
Table 4-6 Thermal conductance results of VOX2.....	67
Table 4-7: Thermal conductance results of MET2.....	68
Table 4-8: Thermal conductance results of MET3.....	69
Table 4-9: VOX4 thermal conductance results in vacuum.....	70
Table 4-10: VOXF thermal conductance results in vacuum	70
Table 4-11: thermal conductance of each device in W/K	71
Table 4-12 Bolometer devices' thermal conductance	71
Table 4-13 Calculated Thermal conductance at atmospheric conditions.....	85
Table 5-1 Thermal and physical parameters	91
Table 5-2 thermal parameters in vacuum.....	92
Table 5-3: Thermal parameters at atmospheric	92
Table 5-4: Bolometer pixel thermal responsivity in vacuum	93
Table 5-5: required time to reach the maximum temperature	107
Table 6-1: Bolometer properties for VOX2, 3, & 4	112
Table 6-2: Bolometer properties for MET2, 3 & 4	113
Table 6-3: Bolometer properties for VOXA, -B, -C, -E, -F, & -G	113
Table C-1: MET2 Thermal Conductance.....	129
Table C-2: MET3 Thermal Conductance.....	129
Table C-3: MET4 Thermal Conductance.....	130
Table C-4: VOX2 Thermal Conductance.....	130
Table C-5: VOX3 Thermal Conductance.....	131
Table C-6: VOX4 Thermal Conductance.....	131
Table C-7: VOXA Thermal Conductance	132
Table C-8: VOXB Thermal Conductance	132
Table C-9: VOXC Thermal Conductance	133

Table C-10: VOXD Thermal Conductance	133
Table C-11: VOXE Thermal Conductance	134
Table C-12: VOXF Thermal Conductance	134
Table C-13: VOXG Thermal Conductance.....	135

List of Abbreviations and Keywords

AMTS: Advanced Manufacturing Technology Strategy

MEMS: Micro Electro Mechanical Systems

AMAA: Advanced Microsystems for Automotive Applications

Bolometer: a bolometer is a device measuring the power of incident electromagnetic radiation via the heating of a material with a temperature-dependent electrical resistance.

CoventorWare: CoventorWare is an integrated suite of software tools for designing and simulating MicroElectroMechanical Systems (MEMS) and microfluidics devices. CoventorWare supports two distinct design flows, which may be used separately or in combination. The ARCHITECT module provides a unique system-level approach to MEMS design, whereas the DESIGNER and ANALYZER modules work together to provide a more conventional physical design flow. Both design flows require information about the fabrication process as a starting point, and this information is provided via a Process Editor and the Material Properties Database.

G: thermal conductance in Watt per Kelvin (W/K)

H: thermal time capacitance in Joules/Kelvin (J/K)

τ : time constant in seconds

IC: Integrated Circuit

CMOS: Complementary-Oxide-Semiconductor

BiCMoOS: Bipolar Complementary-Oxide-Semiconductor

UV: Ultraviolet

IR: Infrared Radiation

VOx: Vanadium Oxide

MET: Metal Bolometer membrane

TCR: Temperature Coefficient Resistance

FEA: Finite Element Analysis

UP: University of Pretoria

CPUT: Cape Peninsula University of Technology

pW : Pico Watt

BT: Brightness temperature

BB: Black Bodies

GB: Grey Bodies

A α -Si: Amorphous Silicon

VOx: Vanadium oxide

MET: Metal (Titanium) membrane bolometer devices

VOX: Vanadium oxide membrane bolometer devices

Sr: Steradian

List of Physical constants

Military VOX bolometer membrane time response: 15 ms

Commercial VOX bolometer membrane time response: 45 ms

Military Titanium bolometer membrane time response: 7 ms

Commercial Titanium bolometer membrane time response: 21 ms

Thermal static load variation interval: 500 to 10 000 pW/ μm^2

Zero absolute temperature: $-273\text{ }^\circ\text{C}$ or 0 K

Infrared electromagnetic spectrum ranges: 0.78 to 1000 μm

Near IR wavelength range: 0.78 to 2.5 μm

Near IR wave number range: 12800 to 4000 cm^{-1}

Middle IR wavelength range: 2.5 to 50 μm

Middle IR wave number range: 4000 to 200 cm^{-1}

Far IR wavelength range: 50 to 1000 μm

Far IR wave number range: 200 to 10 cm^{-1}

Useful IR wave number range: 4000 to 670 cm^{-1}

Velocity of propagation (in vacuum) of all radiation: 3×10^8 m/s

Speed of light: 299 792 458 m/s

Radiation of visible wavelength: 0.4 to 0.78 μm

Constant of Boltzmann: 5.67×10^{-8} $\text{Wm}^{-2}\text{K}^{-4}$

List other variables

Units

IR: Micro meter (μm)

$1 \mu\text{m} = 10^{-6} \text{ m}$

Power = Watts (W)

$1 \text{ W} = 1 \text{ J/s}$ (Joule per second)

Emittance: $\text{W/m}^2 \cdot \text{Sr}$

Irradiance: W/m^2

Thermal conductance: W/K (Watt per Kelvin)

Thermal Capacitance: J/K (Joule per Kelvin)

Responsivity: A/W or V/W

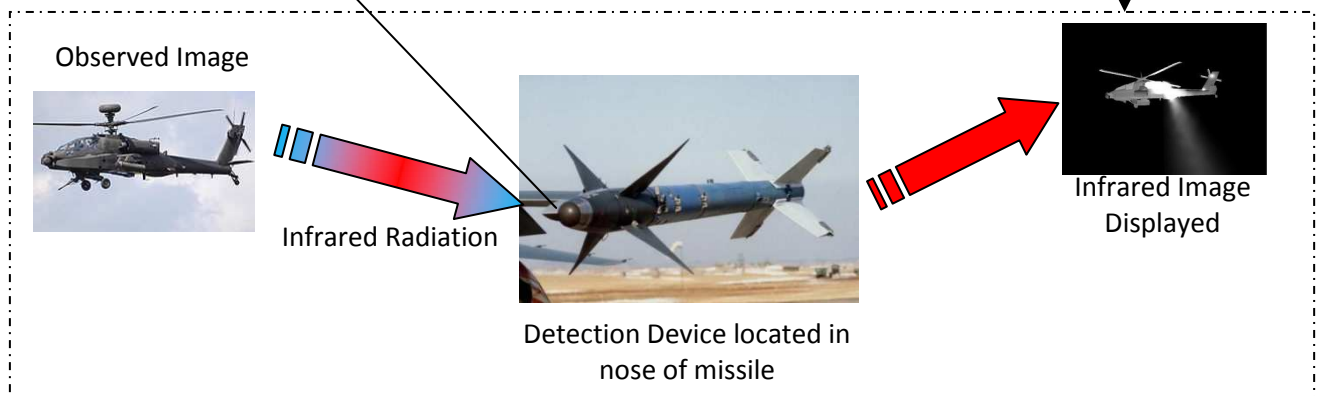
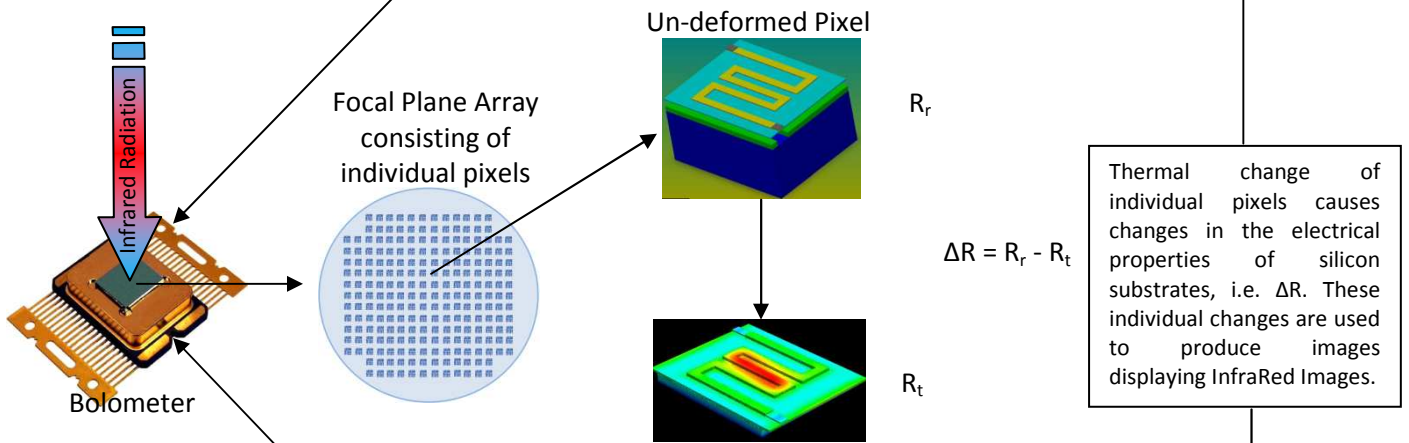
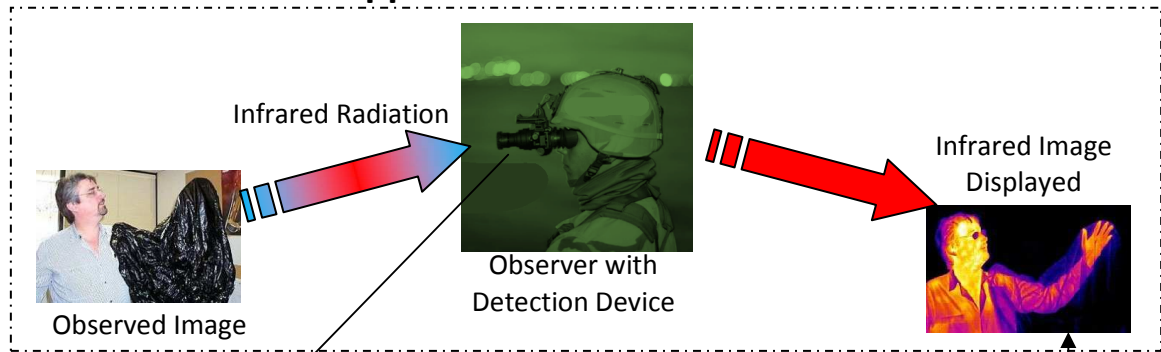
Chapter One

1. Introduction

The demand for the new generations of industrial, military, commercial, medical, automotive and aerospace products in South Africa in particular, and in the world in general, has fuelled research and development activities focused on advanced and smart materials. This situation has allowed for the emergence of a new generation of infrared sensors, the micro-electro-mechanical system (MEMS) silicon based uncooled bolometer, based on an infrared thermal detection mechanism which is particularly suited to operate at ambient temperature, opening opportunities for achieving low cost infrared imaging systems for both military and commercial applications.

BASIC OPERATION OF A SILICON MEMS BASED UNCOOLED BOLOMETER: Bolometers are typically located within detection devices such as Night Vision goggles and noses of heat seeking missiles for civilian and military application respectively. The bolometer consist of a silicon based focal plane array which acts as an infrared thermal imager that measures thermal radiation emits by animals, humans and a range of inanimate objects. Thermal detectors/pixels within the focal plane array deform due to resistance change caused by temperature change in the detector because of radiation fluxes and hence change the electrical properties of the bolometer's silicon structure. These changes in electrical properties, typically resistance, are then used to construct images digitally displayed of what the bolometer is observing.

Civilian Application for Infrared Detection



Defence Application for Infrared Detection

The sensitivity of bolometer devices depends on geometric and material properties and the combination of these and their specific effects on the device thermal properties such as Thermal Conductance (G), Thermal Capacitance (H) and Thermal Time Constant (τ), i.e. time taken by the device to absorb (heating) and dissipate (cooling) thermal radiation. The ultimate sensitivity of bolometer devices depend on small values for G , H and τ . Bolometer devices used for civilian applications typically have values for τ in the 7 - 15ms ranges while τ for military applications are less than 7 μ s as Helmut Budzier et. al. (Fast microbolometer-based infrared camera system).

The term *infrared* from Latin *Infra*, meaning *below*, is usually applied to wavelengths between 700nm and 1mm. It can be argued that the first occurrence of infrared sensing actually goes back several millennia, when men placed their hands over recently extinguished fire. However, until Herschel's experiment, this kind of infrared was between the sun and the earth.

There are many applications for thermal imaging, both civilian or military: night vision, fire fighting, surveillance, vehicles and personnel detection, driver vision enhancement, law enforcement, industrial process monitoring, public health (detecting industrials with fevers in airports), forecasting and medicine (blood control for example).

This thesis focuses on the Design, Solid Modelling, and Numerical Analyses of thirteen pixel membranes used in bolometer focal plane arrays. This study focussed on the effects of geometric and material parameters of both titanium and vanadium oxide bolometer pixels on sensitivity of the device. The mask design of the second prototype bolometer test structures, developed by our partners, i.e. DENEL Dynamics, University of Pretoria and Solid State Technologies, includes several thermally isolated bolometer devices. These devices were modelled and analysed in order to determine the effect of geometric and material parameters on electrical and thermal properties.

The research and development and research and technology of this AMTS funded project was the first of its kind in South Africa. The work presented in

this document, i.e. CPUT's component, is based on modelling and numerical analysis using the masks of South Africa's second prototype microbolometer focal plane array based on materials as stated above. All thirteen devices are thermally isolated, and their performances include different thermal parameters, however as uncooled thermal imaging devices, temperature is critical, and temperature change is measured by resistance change, as shown by Nicklaus et al. in 2007. This changing in resistance defines the sensitivity of the bolometer.

This thesis investigates the sensitivity of three sets of pixels with varying membrane areas and varying suspended leg lengths including three metal (Titanium) pixels, i.e. MET2, MET3 and MET4, three Vanadium oxide pixels, i.e. VOX2, VOX3 and VOX4, and seven Vanadium oxide pixels with variations in thermal properties; VOXA, VOXB, VOXC, VOXD, VOXE, VOXF and VOXG.

The literature review conducted in this study focussed on infrared technology, including uncooled infrared microbolometers, and their numerical analyses. It was found that the two most important properties influencing the device performance is its sensitivity and responsivity. In the first bolometer, invented by the American scientist Samuel P. Langley in 1880, a Wheatstone bridge was used along with galvanometer that produced a deflection proportional to the intensity of radiation for small deflections (deformation). A number of other resistive thin film bolometers have been proposed from 1947 to 1980. Publications of the late 80's indicated that uncooled infrared microbolometers and focal array technology was developed at Honeywell, and have become the dominating technology for the majority of commercial and military infrared imaging applications, as shown by F. Niklaus in 2008.

In the last few years thermal imaging has found its way into many more commercial applications. Most of these applications require a low cost product with an uncooled detector. Typically, these sensors detect the long wave infrared band, i.e. 7 – 14 μm . Microbolometer-based detectors are either made out of Vanadium Oxide (VOx) or Amorphous Silicon ($\alpha\text{-Si}$). A good microbolometer is the one with large temperature coefficient, low heat capacity and good thermal isolation. These parameters influence the change

in the electrical resistance of the device when subjected to incident infrared radiation.

Changes in scene temperature cause changes in the bolometer temperature, which in turn deforms bolometer membranes. These deformations in the bolometer bulk material, changes its electrical resistance and in turn is converted into electrical signals which is processed into an image. The combination of these parameters defines the sensitivity of the device. Military grade devices typically have higher responsivity over commercial devices, therefore they have better sensitivity. This however means higher capital injections are required to produce military grade devices and P. Capper et. al. (Kluwer Academic Publishers, 2001) showed that Vanadium oxide and Amorphous silicon when used in bolometers produce 15 ms - 45 ms, and 7 ms - 21 ms for commercial and military applications respectively.

1.1 Background

The following informations were developed at AMAA in 2003, the seventh international conference on advanced microsystems for automotive applications, by Dr J Valldort et. al. 2003.

Both military and commercial technologies increasingly look to micro-systems to insert intelligence into cars or planes. Safety improvement is particularly concerned with this trend: acceleration sensors for airbags, tire pressure monitoring and collision avoidance radar systems. However, despite all safety breakthroughs of this last decade, drivers still face potential hazards under conditions of darkness or obscured visibility resulting from such weather elements as fog, heavy rain or snow. A current challenging concern is to improve safety in such adverse conditions with the operation of front-hazard warning devices and a reliable collision avoidance system.

One of the major issues of such safety systems largely deals with the availability of adequate sensors that would allow for early and reliable

detection of an obstacle in front of a vehicle. Infrared thermal imaging is particularly suited for this purpose as it provides an effective night-time viewing system that could tackle the inefficiency of the usual sensors and fulfil the night operations safety requirements.

Thermal imaging systems detect the electromagnetic radiation emitted by any object at room temperature whether natural or artificial illumination. As a result, infrared sensors intrinsically offer significant advantages in comparison to alternative sensors working in the visible spectrum or in the millimetric wavelength range such as radars do.

Unlike visible vision, infrared enhances the range of visibility resolution because of its long wavelength. Radar, unfortunately, provides limited information regarding the shape of the detected object in comparison to infrared imaging. For various technological and financial reasons, infrared imaging has been developed primarily for military applications. At present it is used extensively for both military and civilian purposes, with applications that include target acquisition, surveillance, night vision, homing, tracking, thermal efficiency analysis, remote temperature sensing, and weather foreseeing. The aerospace and automobile industries are the most concerned with this micro-technology.

The major drivers for the aerospace industries are as follows:

- the need to reduce the size of the components cost-effectively but without compromising the real-life performance;
- the need for high resolution, high performance sensors for the aerospace industry;
- the need for improved environmental changes with specific reference to the high and low temperature ranges;
- the need to enable the industry and training intuitions to use the equipment in limited available space within the platform (examples include the use of sensors in cameras, night vision equipment and cellular phones);

- the need for medical applications such as thermal conditioning;
- the need for reduced performance low cost sensors in the security industry locally and internationally;
- the need for sensors for the aerospace industry supporting large export contracts and government bilateral agreements; and
- the need for security forces for day and night observation requirements including law and order.

In automobile industries, the drivers include sensors to improve safe driving as the sensor will assist drivers to see objects in time to take the required action, preventing accidents as follows:

- installing head-up display in the car's front console enabling the driver to see objects in time during day and night driving;
- applying brakes automatically when objects are in front of vehicle;
- applying brakes automatically if objects are behind vehicle when reversing; and
- installing room temperature IR sensors for the automotive industry.

1.2 Objectives

The primary objective of this study is to determine the sensitivity of the bolometer membranes that are un-cooled thermal imagers working with heat transfer, radiation in this case, between the device and the object to be detected.

The objectives of this study are therefore described as follows:

- To study the deformation behaviours of 13 bolometer pixel membranes subjected to varying thermal loads applied;
- To determine the Thermal Conductance of 13 bolometer pixel membranes (i.e. $G \text{ (W/K)} = \text{Change in applied heat} / \text{Change in temperature caused by the applied heat} = \Delta W / \Delta T$);

- To determine the Thermal Capacity of 13 bolometer pixel membranes, (i.e. $H \text{ (J/K)} = \tau \times G$, where τ , is the time constant for heating and cooling of the membranes and G is described above as well as the thermal time constant).
- To compare the behaviours of 13 bolometer pixel membranes while being subjected to similar thermal inputs and then determine their classification for commercial or military applications.

1.3 Methodology

This project forms part of a consortium project that includes contributions from the University of Pretoria, Denel Dynamics, Solid State Technologies and CPUT. This research focuses on the second prototype bolometer membrane that includes both metal (titanium) bolometer and vanadium oxide bolometer.

As part of the MEMS project, the finite element based MEMS analysis software, ConvertorWare, was used to identify solid models of the bolometer membranes and perform numerical investigations and simulations. Final results are compared to practical results obtained by the University of Pretoria and Denel Dynamics.

To determine the sensitivity of the bolometer, thermal-mechanical analysis was conducted, so it worked conveniently to use the electro-thermal analogy to find the thermal equivalent of electrical quantities. The first step in the building of the electro-thermal analogy was stating that electric charge and thermal energy are equivalent so that the amount of charge that will pass through the bolometer's section area per unit of time and the thermal equivalent which is the energy per unit of time, (i.e. power) is defined.

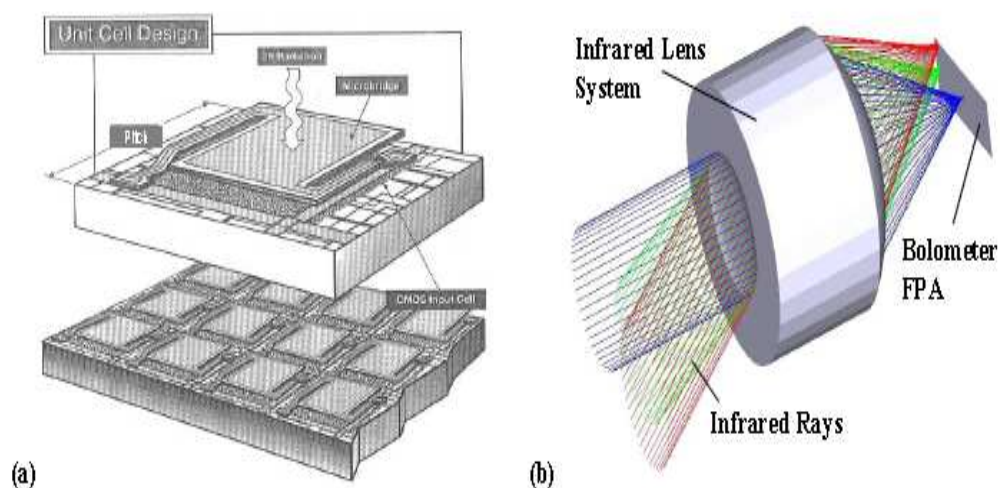


Figure 1-1: (a) Schematic drawing of monolithically integrated infrared bolometer focal plane array (FPA) and (b) placement of a focal plane array with an infrared lens system (Niklaus F, 2007, 2)

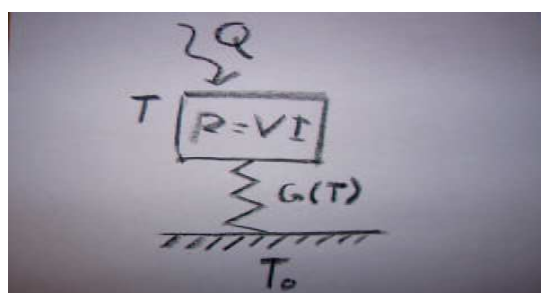


Figure 1-2: Ideal bolometer schematic

The figures above show simplified bolometer structures. An absorber is linked to a heat sink through a low thermal conductance (a), absorbs an incident radiant flux, the temperature increases (b). By measuring the resistance of a thermostat placed on the absorber, the amount of absorber radiant flux can be calculated.

The solid models determined by the use of ConvertorWare and other drawing software such as SolidWorks and CAD were done by importing different layers and packages defined by the University of Pretoria (UP). All thirteen pixel bolometer membranes were modelled using six masks name as given in Table 1.1 below.

Table 1-1 Bolometer masks (UP 2010)

Masks' name
Cavity
Metal
Gold
Vanadium oxide
Contact
Nitride

For the metal vanadium oxide sheet resistances, Greek cross layout was used for their determination, and the contact between the vanadium oxide and the Titanium has been measured using the Kelvin cross (UP 2010, 4).

A good sensitivity of the bolometer means that the device has a short time response, so this study determined the thermal conductance, thermal capacitance and time constant, which are the principal parameters for this purpose. For the completion of this research the reliance upon various subjects like Heat Transfer, Structural Mechanics, Physics, Mathematics and Electronics was critical.

To arrive at the thermal conductance, we have firstly determined the **heat flux** or **thermal flux**, also referred to occasionally as **heat flux density** or **heat flow rate intensity** which is a flow of energy per unit of area per unit of time in SI units, measured in $[W.m^{-2}]$. It has both a direction and magnitude so it is a vector quantity. To define the heat flux at a certain point in space, one takes the limiting case where the size of the surface becomes infinitesimally small. (Heat flux is often denoted, the subscript q specifying *heat* flux, as opposed to *mass* or *momentum* flux). The most important appearance of heat flux in physics is in Fourier's law describing heat conductance. If we know the loss due to the distance between the object and the device, then the amount of heat reaching the device surface will be the heat flow minus the lost.

Thermal load is specified for static analyses that vary from 500 – 10 000 $pW/\mu m^2$, then the thermal boundary conditions for static analyses. Using those parameters, we were able to determine the thermal conductance given by the heat flow and the surface area of the bolometer and the thermal

capacitance which characterises the ability of the device to convert the incoming radiation into an electrical signal that is proportional to the change in temperature. Using dynamic analyses, we determined then the time constant (τ) given by the thermal resistance (inverse of thermal conductance), and thermal capacitance an important parameter and determine the amount of energy required to change the temperature (www.wikipedia.org/wiki/heat-capacity) so that it shows how fast and good bolometers respond.

1.4 Thesis outline

This dissertation presents several chapters that provide a background of information concerning the manner in which the work was conducted.

Chapter 1 presents the introduction of the research thesis

Chapter 2 presents a literature survey pertaining to MEMS technology and uncooled infrared radiation.

Chapter 3 introduces the structure of the microbolometer. The objective is to develop the fabrication process of the devices in order to produce the solid model and prepare them for thermal analysis by defining thermal and mechanical properties of selected materials.

Chapter 4 deals with thermo-mechanical static analyses. These analyses result in the thermal conductance, first step of the determination of thermal parameters.

Chapter 5 presents calculations and transient analysis of the determined thermal capacitance and thermal time constant. These thermal parameters define the sensitivity of the bolometer.

Chapter 6 presents conclusions and recommendations for future work relating to un-cooled infrared technology.

Chapter Two

2. Literature Review

2.1 Introduction

This chapter presents a brief theory of Micro-Electro-Mechanical Systems (MEMS) and the importance of the MEMS technology, as well as the theory of infrared radiation.

2.2 MEMS Technology

Micro-Electro-Mechanical Systems (MEMS) is the integration of mechanical elements, sensors, actuators and electronics on a common silicon substrate through micro-fabrication technology. While the electronics are fabricated using Integrated Circuit (IC) process sequences (CMOS, Bipolar, or BICMOS process, for example), the micromechanical components are fabricated using compatible 'micromachining' processes that selectively etch away parts of the silicon wafer or add new structural layers to form the mechanical and electromechanical devices (Sun B, 2006, 4).

MEMS Technology has a unique ability to collect information, process it, determine a course of action, and then act as a trigger by communicating through an electronic interface. These capabilities allow MEMS to provide advanced applications for smart device technology such as collision avoidance systems and wireless handsets (Sun B, 2006, 4).

MEMS technology has revolutionised nearly every product category by bringing together silicon-based microelectronics with micromachining technology, making possible the realisation of complete systems-on-chip. MEMS is allowing the development of smart products, augmenting the computational ability of microelectronics with the perception and control capabilities of micro-sensors and micro-actuators, and expanding the space of possible designs and applications. As a result, MEMS is seen as a cost-effective candidate for the next generation solution across multiple markets (www.memsnet.com).

2.3 MEMS Applications and Markets

Figures 2.1 and 2.2 show the market of MEMS technology for different applications while Figure 2.3 shows the top 20 of the MEMS high value suppliers in millions of US dollars (Bouchaud J., 2011:4).

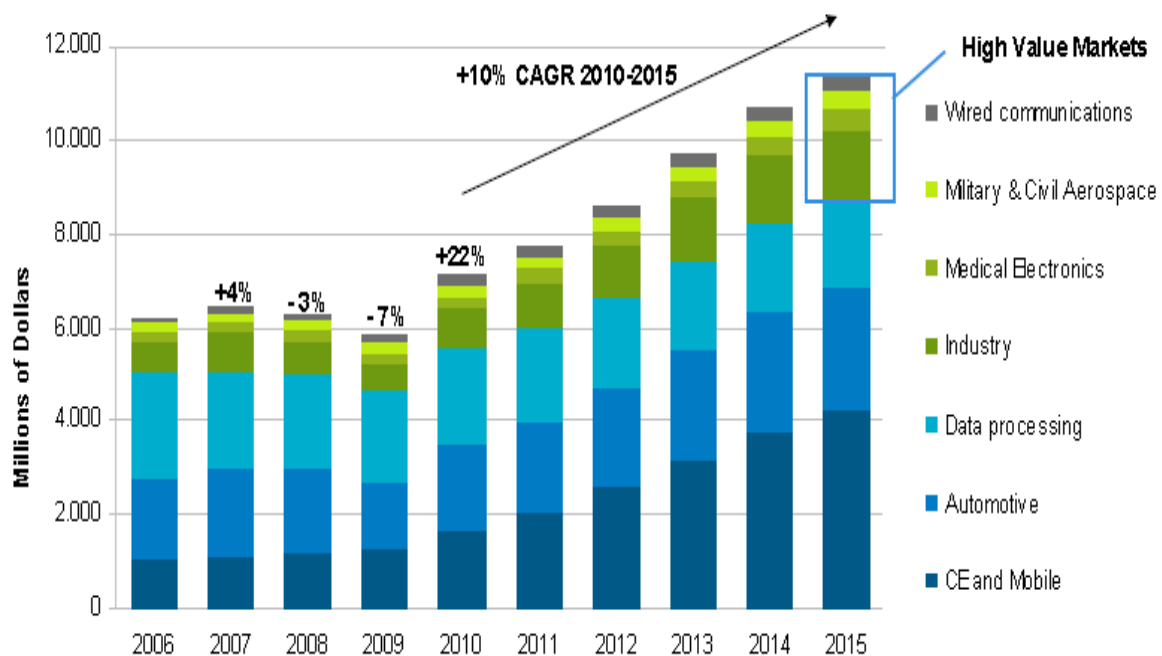


Figure 2-1 MEMS Market trucker (Bouchaud J., 2011:4)

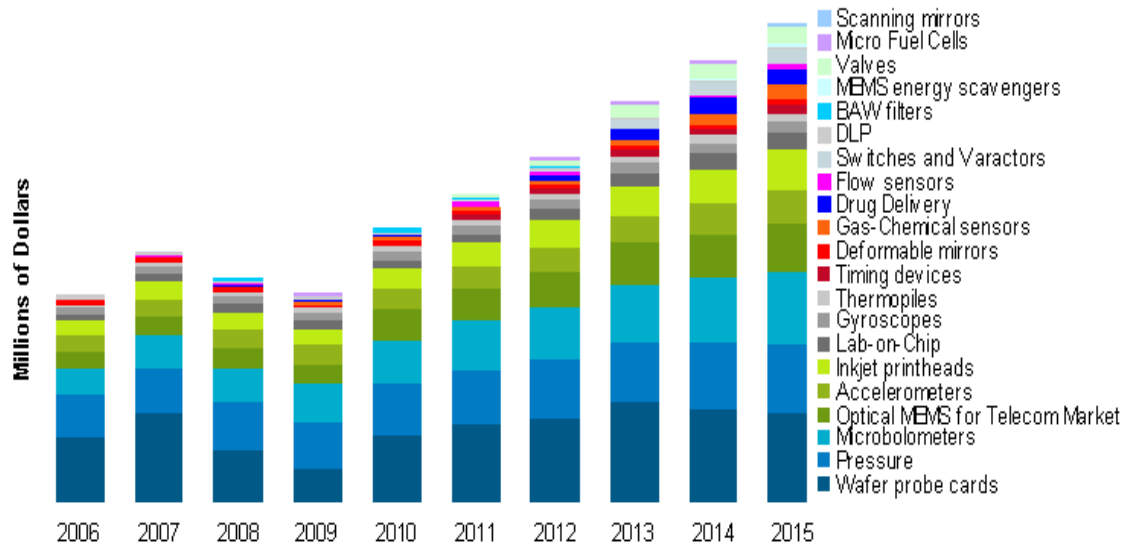


Figure 2-2: High value of MEMS devices (Bouchaud J., 2011:4)

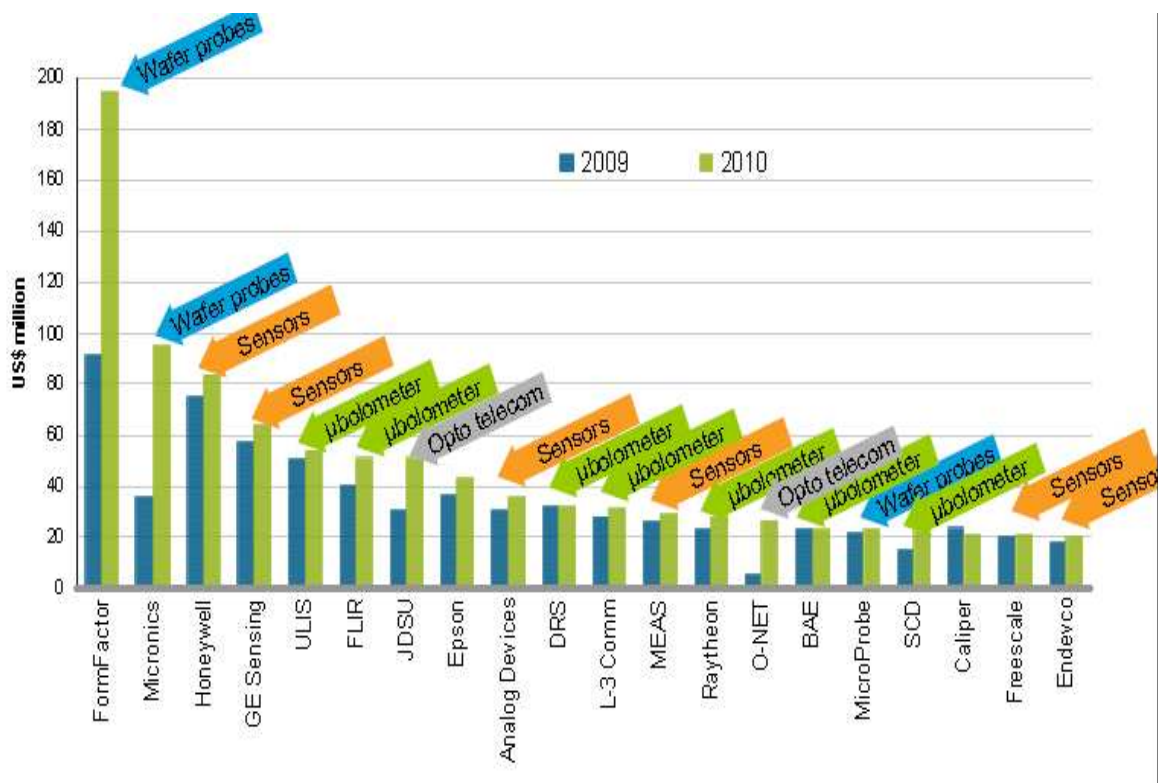


Figure 2-3: Top 20 MEMS suppliers' high value (Bouchaud J., 2011:4)

There are several applications for MEMS technology. As a breakthrough technology, allowing unparalleled synergy between previously unrelated fields

such as biology and microelectronics, many new MEMS applications will soon emerge, expanding beyond that which is currently identified or known.

Here are a few applications of current interest:

2.3.1 Automotive

Automotive application has assumed a large role in the field of MEMS technology. MEMS accelerometers are quickly replacing conventional accelerometers for crash air-bag deployment systems in automobiles. Small-sized and high performance acceleration sensors are fabricated using MEMS cantilever technology and equivalent electrical circuit techniques. This technology has made it possible to integrate the accelerometer and electronics onto one single silicon chip at lower cost, thereby being more functional, lighter, and more reliable and allowing for production for a fraction of the cost of the conventional macro-scale accelerometer elements (Yon JJ, 2003, 1).

2.3.2 Communication

High frequency circuits will benefit considerably from the advent of RF-MEMS technology. Electrical components such as inductors and tuneable capacitors can be improved significantly compared to their integrated counterparts if they are constructed using MEMS technology. With the integration of such components, the performance of communication circuits will improve, while the total circuit area, power consumption and cost will be reduced. In addition, the mechanical switch, as developed by several research groups, is a key component with huge potential in various microwave circuits. The demonstrated samples of mechanical switches have quality factors much higher than anything previously available (www.memsnet.com).

Reliability and packaging of RF-MEMS components seem to be the two critical issues that need to be solved before they receive wider acceptance by the market.

The telecommunication application has not taken a large role compared to medical application, though this is predicted to increase slightly in the coming years as clearly demonstrated by Figure 2.3. (Bouchaud J., 2011:4)

2.3.3 Biotechnology

MEMS technology is enabling new discoveries in science and engineering such as the Polymerase Chain Reaction (PCR) micro-systems for DNA amplification and identification, micro-machined Scanning Tunnelling Microscopes (STMs), biochips for detection of hazardous chemical and biological agents, and micro-systems for high-throughput drug screening and selection (Bouchaud J., 2011:4). This field of application has increased significantly as shown in Figure 2.4.

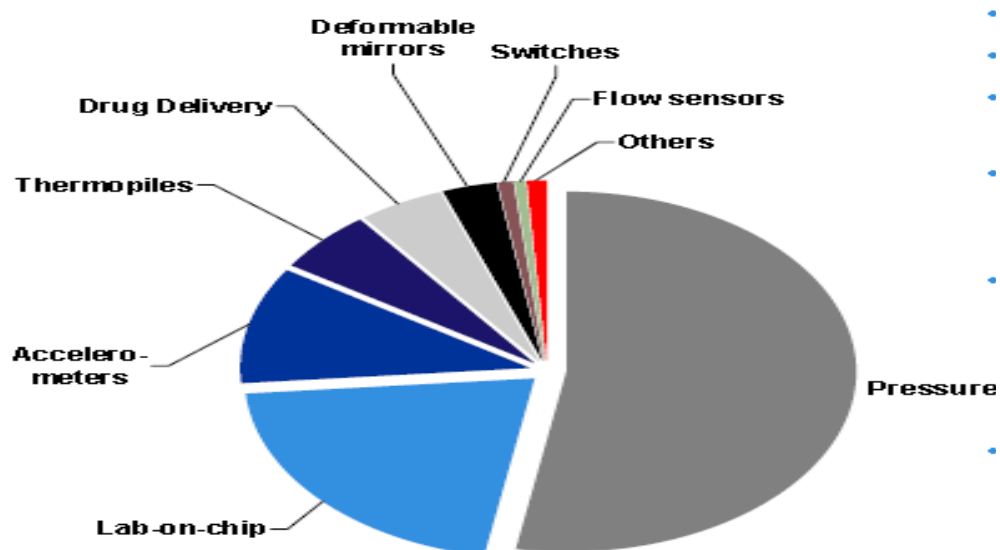


Figure 2-4: 2010 MEMS market (Bouchaud J., 2011:4)

2.4 Advantages of MEMS

MEMS devices are extremely small—for example, MEMS has made possible electrically-driven motors smaller than the diameter of a human hair—but MEMS technology is *not* primarily about size.

MEMS is also *not* about making things out of silicon, even though silicon possesses excellent material properties, making it an attractive choice for many high-performance mechanical applications; for example, the strength-to-weight ratio of silicon is higher than many other engineering materials, allowing for very high-bandwidth mechanical devices to be realised (www.memsnet.com).

Instead, the deep insight of MEMS is as a new manufacturing technology, a way of making complex electromechanical systems using batch fabrication techniques similar to those used for integrated circuits, and uniting these electromechanical elements together with electronics (www.memsnet.com).

2.4.1 Advantage of MEMS manufacturing

First, MEMS is an extremely diverse technology that could significantly affect every category of commercial and military product. MEMS are already used for tasks ranging from in-dwelling blood pressure monitoring to active suspension systems for automobiles. The nature of MEMS technology and its diversity of useful applications make it potentially a far more pervasive technology than even integrated circuit microchips (inems.com, 2007).

Second, MEMS blurs the distinction between complex mechanical systems and integrated circuit electronics. Historically, sensors and actuators are the most costly and unreliable part of a macro-scale sensor-actuator-electronics system. MEMS technology allows these complex electromechanical systems to be manufactured using batch fabrication techniques, increasing the reliability of the sensors and actuators to equal that of integrated circuits (inems.com, 2007).

Finally, even though the performance of MEMS devices and systems is expected to be superior to macro-scale components and systems, the price is predicted to be much lower (inems.com, 2007).

2.4.2 Challenges facing MEMS

The following information literatures are issued from www.memsnet.org; MEMS technology is currently used in low-volume or medium-volume applications.

Some of the obstacles preventing its wider adoption are as follows:

Limited Options: Most companies who wish to explore the potential of MEMS technology have very limited options for prototyping or manufacturing devices, and have no capability or expertise in micro-fabrication technology. Few companies will build their own fabrication facilities because of the excessive cost. A mechanism giving smaller organisations responsive and affordable access to MEMS fabrication is essential.

Packaging: The packaging of MEMS devices and systems needs to improve considerably from its current primitive state. MEMS packaging is more challenging than IC packaging due to the diversity of MEMS devices and the requirement that many of these devices are in contact with their environment. Currently, almost all MEMS development efforts must aim toward a new and specialised package for each new device. Most companies find that packaging is the single most expensive and time consuming task in their overall MEMS product development programme. As for the components themselves, numerical modelling and simulation tools for MEMS packaging are virtually non-existent. Approaches which allow designers to select from a catalogue of existing standardised packages for a new MEMS device without compromising performance would unarguably be beneficial.

Fabrication Knowledge Required: Currently, the designer of a MEMS device requires a high level of fabrication knowledge in order to create a successful design. Often the development of even the most mundane MEMS device requires a dedicated research effort to find a suitable process sequence for its fabrication. MEMS device design needs to be separated from the complexities of the process sequence.

2.5 Brief theory of infrared radiation

All bodies above zero absolute temperature (-273°C) emit infrared radiation in the form of waves which pass through space and are partly absorbed by bodies they strike. This radiation forms part of the electromagnetic spectrum and has the strongest heating effect of all. The nature of the radiation is the same in essence as that of x-rays, ultraviolet, visible light and radio waves ([www. Noblelightnews.com/200707.html](http://www.Noblelightnews.com/200707.html)).

The electromagnetic energy that is emitted from the surface of a heated body is called thermal radiation, and consists of a continuous spectrum of frequencies extending over a wide range. The spectral distribution and the amount of energy radiated depend chiefly on the temperature of the emitting surface ([www. Noblelightnews.com/200707.html](http://www.Noblelightnews.com/200707.html)).

2.5.1 Introduction

The term *infrared* covers the range of the electromagnetic spectrum longer than the visible wavelength, between 0.78 and 1000 μm . In the context of infrared spectroscopy, wavelength is measured in 'wavenumbers', which have the unit cm^{-1} .

$$\text{Wavenumber} = 1 / \text{wavelength in centimetres}$$

It is useful to divide the infrared region into three sections: *near*, *mid* and *far* infrared, as it is demonstrated in teaching.shu.ac.uk/hwb/chemistry/tutorials,

therefore all the theories of infrared radiation to follow are developed in this document.

Region	Wavelength range (μm)	Wavenumber range (cm^{-1})
Near	0.78 - 2.5	12800 – 4000
Middle	2.5 - 50	4000 - 200
Far	50 -1000	200 – 10

The most useful IR region lies between 4000 – 670 cm^{-1} (www.Noblelightnews.com/200707.html).

2.5.2 Theory of infrared (IR) absorption

Absorption of IR is restricted to compounds with small energy differences in the possible vibrational and rotational states.

For a molecule to absorb IR, the vibrations or rotations within a molecule must cause a net change in the dipole moment of the molecule. The alternating electrical field of the radiation (remember that electromagnetic radiation consists of an oscillating electrical field and an oscillating magnetic field, perpendicular to each other) interacts with fluctuations in the dipole moment of the molecule. If the frequency of the radiation matches the vibrational frequency of the molecule then radiation will be absorbed, causing a change in the amplitude of molecular vibration (www.Noblelightnews.com/200707.html).

2.5.3 Molecular rotations

Rotational transitions are of little use to the spectroscopic. Rotational levels are quantised, and absorption of IR by gas yields line spectra. However, in liquids or solids, these lines broaden into a continuum due to molecular collisions and other interactions (teaching.shu.ac.uk/hwb/chemistry/tutorials).

2.5.4 Molecular vibrations

The positions of atoms in a molecule are not fixed; they are subject to a number of different vibrations. Vibrations fall into the two main categories of stretching and bending (teaching.shu.ac.uk/hwb/chemistry/tutorials).

Stretching: Change in inter-atomic distance along bond axis

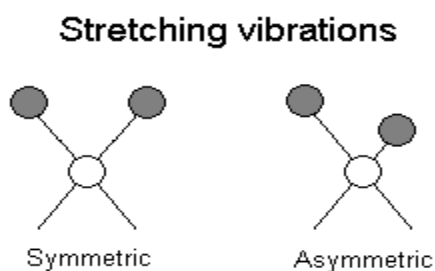


Figure 2-5: Stretching vibrations (teaching.shu.ac.uk/hwb/chemistry/tutorials)

Bending: Change in angle between two bonds. There are four types of bends:

- Rocking
- Scissoring
- Wagging
- Twisting

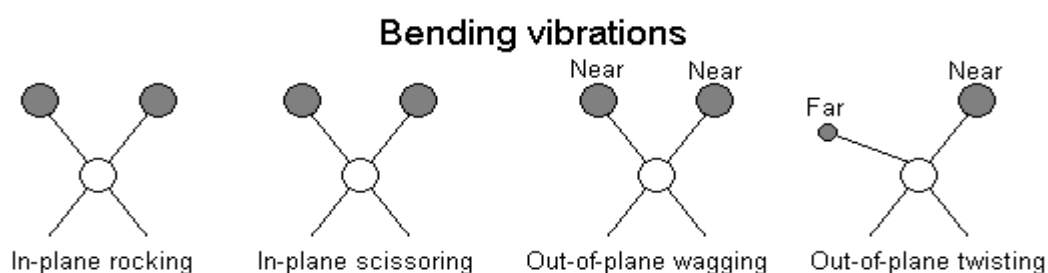


Figure 2-6: Bending vibrations (teaching.shu.ac.uk/hwb/chemistry/tutorials)

Figure 2.6 shows the bending vibrations of the IR spectroscopy. Each ball is moving away or sometimes can move toward from the other ball along the line of the spring and represent a stretching vibration that can either be symmetric or asymmetric. A molecule with three or more atoms can experience a bending vibration, a vibrational

mode where the angle between atoms changes
(www.chem.ucla.edu/harding/notes_14C_IR.pdf).

2.5.5 Vibrational coupling

In addition to the vibrations mentioned above, interaction between vibrations can occur (*coupling*) if the vibrating bonds are joined to a single, central atom. Vibrational coupling is influenced by a number of factors (teaching.shu.ac.uk/hwb/chemistry/tutorials):

- strong coupling of stretching vibrations occurs when there is a common atom between the two vibrating bonds;
- coupling of bending vibrations occurs when there is a common bond between vibrating groups;
- coupling between a stretching vibration and a bending vibration occurs if the stretching bond is one side of an angle varied by bending vibration;
- coupling is greatest when the coupled groups have approximately equal energies; and
- no coupling is seen between groups separated by two or more bonds.

2.5.6 Laws of radiation and definitions

Turning now to the oscillatory nature, the radiation passes through successive identical states at precise time intervals measured in seconds. The rate at which the states recur, or frequency, is measured in cycles per second so that frequency is equal to the reciprocal of time. The velocity of propagation (in a vacuum) for all radiation is 3×10^8 meters per second: the speed of light. From this we can deduce that the distance between successive identical states—the wavelength—is the product of velocity and time. This is shown in Figure 2.7 (Pol VDE, 2012, 1).

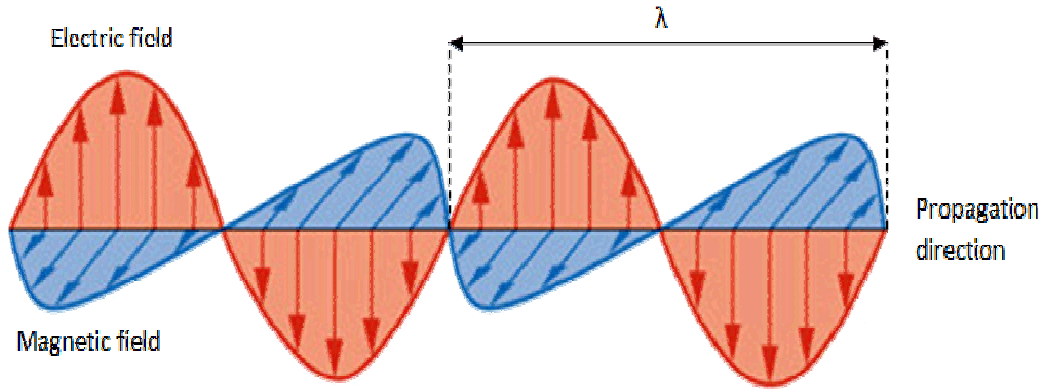


Figure 2-7: A schematic representation of electromagnetic radiation. The wavelength represented by λ (Pol, VDE, 2012, 1)

Expressing these statements mathematically, we find equations 2.1-2, as presented below;

$$f = \frac{1}{t} \quad (2.1)$$

$$\lambda = vt = \frac{V}{f} \quad (2.2)$$

t = time interval in seconds which separates the passage of radiation through two successive identical states

f = frequency in cycles per second

λ = wavelength in meters per second

V = speed of light in meters per second

Infrared and visible wavelengths are normally expressed in microns (or micrometers), the unit being one millionth of a meter. Radiation visible of the human eye occurs over a very narrow band, from 0.4 to 0.76 microns. The broad region occupied by infrared extends from 0.76 microns (that is just beyond the red end of the visible end of the spectrum) to 400 microns. However, the radiation used for process heating occurs between wavelengths of 1 and 5 microns in order to obtain adequate source temperatures. This represents a temperature range of 2200 °C to 300°C (wiki.answers .com/Q/IR).

Continuing well beyond the infrared or thermal region to much longer wavelengths of the order of centimetres and metres, the spectrum is occupied

by microwave, radar, and television and radio communications equipment (wiki.answers.com/Q/IR).

2.5.7 Definitions

Radiant power: the rate of the flow of electromagnetic energy, i.e. radiant energy.

- Radiant power is usually expressed in watts (Watts), ie., Joules per second
- The modifier is often dropped and “power” is used to mean “radiant power” ϕ (watts)

Radiant emittance: radiant power emitted into a full sphere, i.e. 4 sr (steradians), by a unit area of a source, expressed in watts per square meter. Synonyms: radiant existence, flux, radiant flux. M or E (watts/m²).

Radiance: radiant power, in a given direction, per unit solid angle per unit of projected area of the source, as viewed from the given direction. Radiance is usually expressed in watts per steradian per square meter. L (watts/m².sr) = M/π .

Irradiance: radiant power incident per unit area upon a surface. Irradiance is usually expressed in watts per square meter, but may also be expressed in Joules per square meter. Synonyms: power density, flux, radiant flux. R (watts/m²). (Cassanova J-L, 2007, 5).

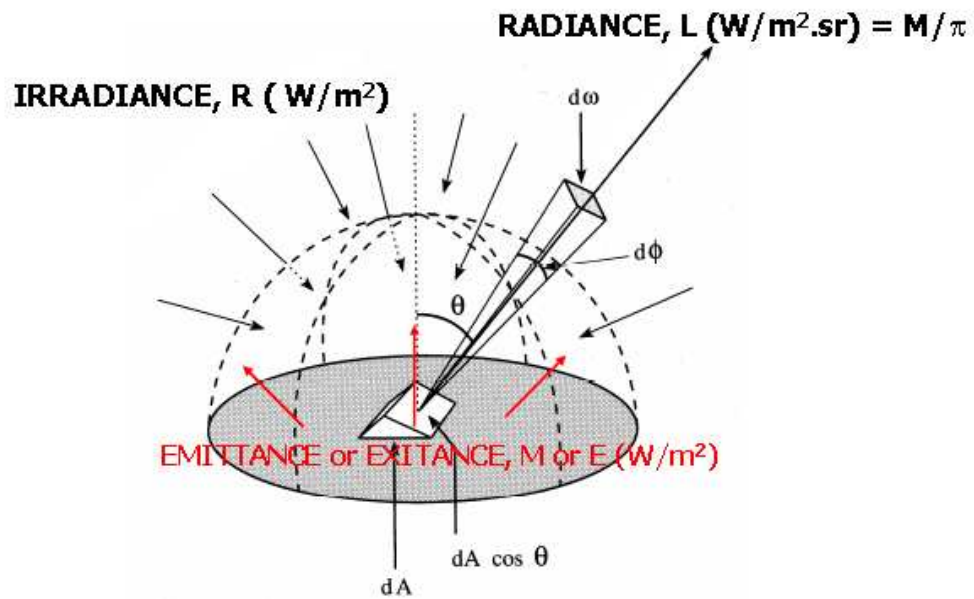


Figure 2-8: Graphical representation of radiance, irradiance and emittance (Cassanova J-L, 2007, 6)

2.5.8 Spectral magnitudes

All these magnitudes are usually expressed as spectral magnitudes, meaning they refer to wavelength:

- Radiant power: φ_λ (watts/ μm) or (watts. cm^{-1})
- Radiant emittance: R_λ (watts / $\text{m}^2.\mu\text{m}$) or (watts. $\text{cm}^{-1}/\text{m}^2$)
- Radiance: L_λ (watts/ $\text{m}^2.\text{sr}.\mu\text{m}$) or (watts. $\text{cm}^{-1}/\text{m}^2$).

cm^{-1} = number of wavelengths by cm = 10000.(1/ λ μm)

The simplest theory to express the thermal emission is based on the black body concept. A black body is an object that absorbs all electromagnetic radiation that passes through it and none is reflected. Despite the name, black bodies are not actually black as they radiate energy as well. How much electromagnetic radiation they give off depends on the temperature, and is expressed by the Planck's Law given in formula 2.3 and 2.4:

$$M_\lambda = \pi L_\lambda = \frac{\pi 2hc^2 \lambda^{-5}}{\exp\left(\frac{hc}{k\lambda T}\right) - 1} \quad (2.3)$$

$$M_{\lambda} = \frac{k_1 \lambda^{-5}}{\exp\left(\frac{k_2}{\lambda T}\right) - 1} \quad (2.4)$$

$$c = 3 \times 10^8 \text{ m/s}$$

$$k = 1,38 \times 10^{-23} \text{ J.K}^{-1}$$

$$h = 6,62 \times 10^{-34} \text{ J.s}$$

The consequences of Planck's Law are the Stefan-Boltzman's Law given below:

$$M = \int_0^{\infty} M_{\lambda} d\lambda = \frac{2\pi^5 k^4 T^4}{15c^2 h^3} = \sigma T^4 \quad (2.5)$$

The total emittance from the black body, including all wavelengths, is directly proportional to the fourth power of its temperature. This temperature is called 'Brightness Temperature' (BT) and is what we directly obtain from satellite signal. Mathematically it is expressed by Wien's law as shown in formula 2.6

$$\lambda_{max} = p_1 / T M_{\lambda max} = p_2 T^5 \quad (2.6)$$

$$p_1 = 2,898 \times 10^{-3} \text{ m.K}$$

$$p_2 = 1,2862 \times 10^{-5} \text{ m.K}$$

$$k_1 = 3,74 \times 10^{-16} \text{ W.m}^2$$

$$k_2 = 1,44 \times 10^{-2} \text{ m.K}$$

$$\sigma = 5,67 \times 10^{-8} \text{ W.m}^{-2} \text{.K}^{-4}$$

The maximum spectral emittance is proportional to the fifth power of the temperature, and it corresponds to a peak wavelength, λ_{max} , which is inversely proportional to the temperature.

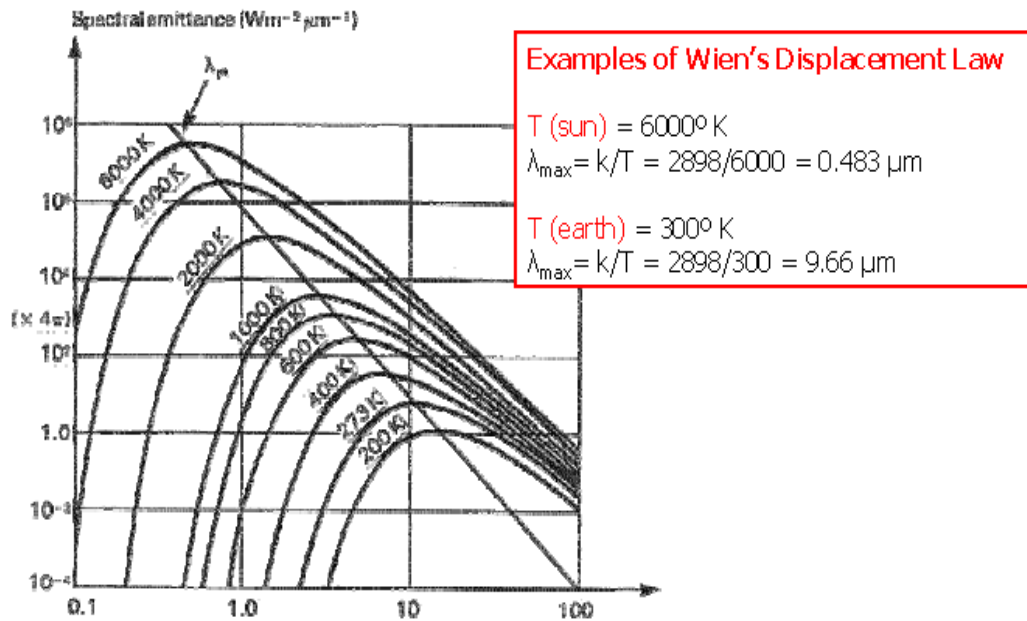


Figure 2-9: Wavelength and the λ_{\max} displacement from the law of Wien (Cassanova J-L, 2007, 12)

2.5.9 The emissivity

The real bodies are not black bodies, (BBs). Their emittance is always lower than that of the black bodies. So we need to introduce a factor call “emissivity”, ϵ , being $\epsilon < 1$, to obtain their emittance. Then they are called “grey bodies” (GBs).

$$M_{GB} = \epsilon \cdot \sigma \cdot T_{GB}^4 ; \epsilon < 1 \quad (2.7a)$$

We can imagine a BB with the same emittance as that of the GB

$$M_{BB} = M_{GB} = \sigma \cdot T_{BB}^4 \text{ (Brightness)} \quad (2.7b)$$

To have the same emittance of a GB, this BB has to be at the temperature T_{BB}

$$T_{BB, \text{brightness}} = \epsilon^{1/4} \cdot T_{GB} \quad (2.7c)$$

2.5.9.1 Factors that concern the emissivity ε

- the type of surface: vegetation, sand, snow, water;
- the colour (the obscure colours absorb/ emit better);
- the roughness of the surface (more roughness, more emission/ absorption);
- the content of humidity (more humidity, more emission/ absorption);
- the compactation (the emission/ absorption is proportional to the density);
- the wavelength of the radiation; and
- the angle of the vision.

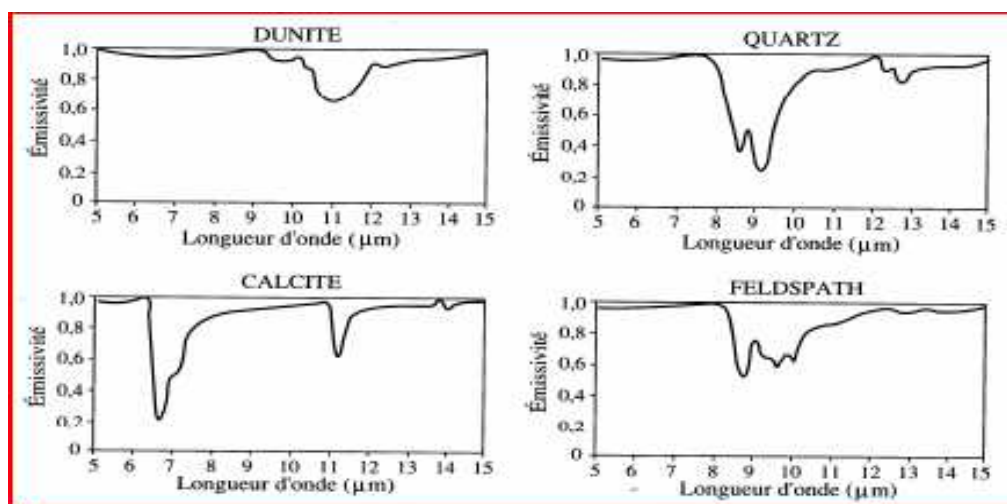


Figure 2-10: Emissivity of different materials (Cassanova J-L, 2007, 14)

$$\alpha_{\lambda} = (W/m^2 \text{ absorbed}) / (W/m^2 \text{ incidents}) = A_{\lambda} / I_{\lambda} = 1$$

$$\rho_{\lambda} = (W/m^2 \text{ reflected}) / (W/m^2 \text{ incidents}) = R_{\lambda} / I_{\lambda} = 0$$

$$\alpha_{\lambda} + \rho_{\lambda} = 1 \quad \Rightarrow \quad \text{BLACK BODY}$$

By definition of black body : $A_{\lambda} = I_{\lambda} = M_{\lambda}$

GREY BODY

$$\alpha'_{\lambda} = (W/m^2 \text{ absorbed}) / (W/m^2 \text{ incidents}) = A'_{\lambda} / I_{\lambda} < 1$$

$$\rho'_{\lambda} = (W/m^2 \text{ reflected}) / (W/m^2 \text{ incidents}) = R'_{\lambda} / I_{\lambda} > 0$$

$$\alpha'_{\lambda} + \rho'_{\lambda} < 1 \quad (2.8a)$$

As the body is thermal balance: $A'_{\lambda} = M'_{\lambda} = \alpha'_{\lambda} I_{\lambda}$

$$M'_{\lambda} / \alpha'_{\lambda} = I_{\lambda} = M_{\lambda} \Rightarrow \text{GREY BODY}$$

$$M'_{\lambda} = \epsilon_{\lambda} \cdot M_{\lambda} = \epsilon_{\lambda} \cdot M'_{\lambda} / \alpha'_{\lambda} \Rightarrow \epsilon_{\lambda} = \alpha'_{\lambda} \Rightarrow \epsilon_{\lambda} = 1 - \rho'_{\lambda} \quad (2.8b)$$

2.6 Un-cooled Infrared Imaging

Uncooled infrared (IR) imaging arrays have numerous applications in which low power consumption and high levels of integration are critical. Recent applications range from night vision for automobiles to satellites attitude control systems. One particular advantage of uncooled IR imagers is their potential for integration with conventional readout electronics, to yield single-chip sensor systems (Hornsey R et al, 2000, 2).

Major advances in complementary metal-oxide-semiconductor (CMOS) technology, driven mainly by the computer market, have resulted in substantial increases in on-chip functionality. This trend has also benefited the development of integrated sensors (Hornsey R et al, 2000, 2).

2.7 Summary

Chapter 2 presents an introduction of the MEMS technology and a brief overview of the theory of infrared radiation. Bolometers are part of the application and markets of the MEMS system that uses infrared radiation to detect objects; therefore, this chapter discusses the importance and application of MEMS, as well as an introduction to the infrared field.

Chapter Three

3. Principles and Fabrication of Uncooled Microbolometer Devices Analysed

3.1 Introduction

Uncooled infrared detectors have in recent years gained wide spread attention for infrared imaging applications, mainly because of their numerous advantages such as low cost, low weight, low power, large spectral response and long term operation. One of the most popular approaches for uncooled infrared imaging is to use microbolometer structures where infrared radiation increases the temperature of a material, causing a change in its resistance (Tezcan et al. 1999; 1).

There are efforts to implement microbolometers using many different materials. The most widely recognised material is vanadium oxide (VO_x), due to its high temperature coefficient of resistance (-TCR of about 2 to 3%/K) and its low temperature process (Tezcan et al. 1999; 1).

The main drawback of VO_x, however, is that it is not a standard material in IC fabrication processes. An IC compatible microbolometer material is the amorphous silicon carbide (SiC), which has a high TCR value of around 4-6%/K. However, the amorphous SiC requires high temperature annealing to achieve stability of microstructures, which is not suitable for post-CMOS processing; therefore, it is difficult to merge it with a CMOS process for monolithic implementation with readout circuitry (Tezcan et al. 1999; 1).

Another IC compatible microbolometer material is the polycrystalline silicon germanium (Poly SiGe), which has a TCR value of 2-3%/K, but its process temperature is also high for post-CMOS processing. A low temperature and IC compatible approach is to implement microbolometers using metal films such as platinum (Pt), but metals have very low TCR in general, limiting their performance (Tezcan et al. 1999; 1).

3.2 Ideal model of a microbolometer

3.2.1 Uncooled thermal detector structure

The schematic structure of an uncooled thermal detector is shown in Figure 3.1. As a general rule, these detectors measure the temperature rise due to IR radiation absorption by a thermally insulated element. Therefore, thermal detectors are mainly composed of an infrared absorber embedded in close contact with a thermometer element. The thermometer element senses incoming IR induced temperature rise and converts it into an electric signal. The most common detection mechanism is the resistive bolometer whose resistance changes with temperature. Considering a two-dimensional array of detectors, a Readout Integrated Circuit (ROIC) is generally designed to measure the resistance of each bolometer and to format the results into a single data stream for video imaging purposes. Finally, due to the strong correlation between thermal insulation and sensitivity, the high performance uncooled IR detector must be operated under vacuum – typically 10^{-2} mTorr – in a specific package supplied with an infrared window (Yon JJ et Al., 2003:2).

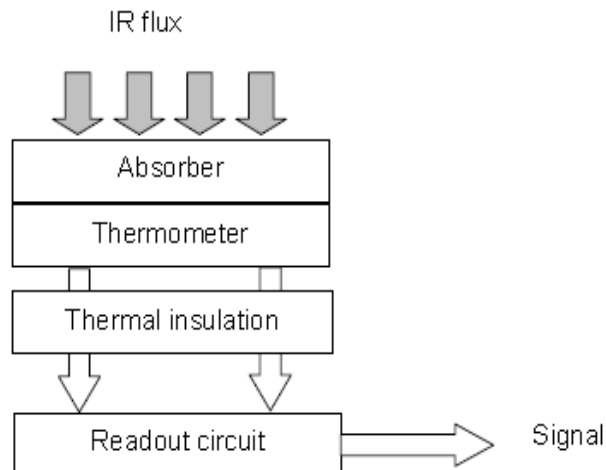


Figure 3-1: Schematic structure of thermal detector (Yon JJ)

3.2.2 Microbolometer principles

In the footsteps of MEMS devices, microbolometer sensors have benefitted from the latest advances in silicon technology. Previous high resolution thermal sensors required exotic and expensive cooling methods including Stirling cycle coolers and liquid nitrogen coolers. These methods of cooling made early thermal imagers expensive to operate and unwieldy to move (Yon JJ et Al., 2003:2).

A microbolometer consists of an array of pixels, each pixel being made up of several layers. Figure 3.2 below provides a generalised view of a pixel.

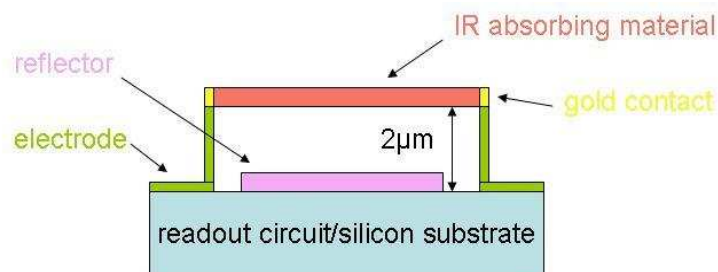


Figure 3-2: Cross sectional view of a microbolometer

3.2.3 Vanadium oxide and metal titanium bolometer analysed processing

3.2.3.1. Bolometer geometries

Thirteen thermally isolated bolometer devices were designed. These devices are all of suspended membranes of a two legs variety as shown in Figures 3.3 – 3.4 below. Both Titanium metal resistance bolometers and Vanadium oxide resistance bolometers were designed. Their dimensions are provided in Tables 3.1 – 3.3 below, with three metal and ten Vanadium oxide bolometers respectively:

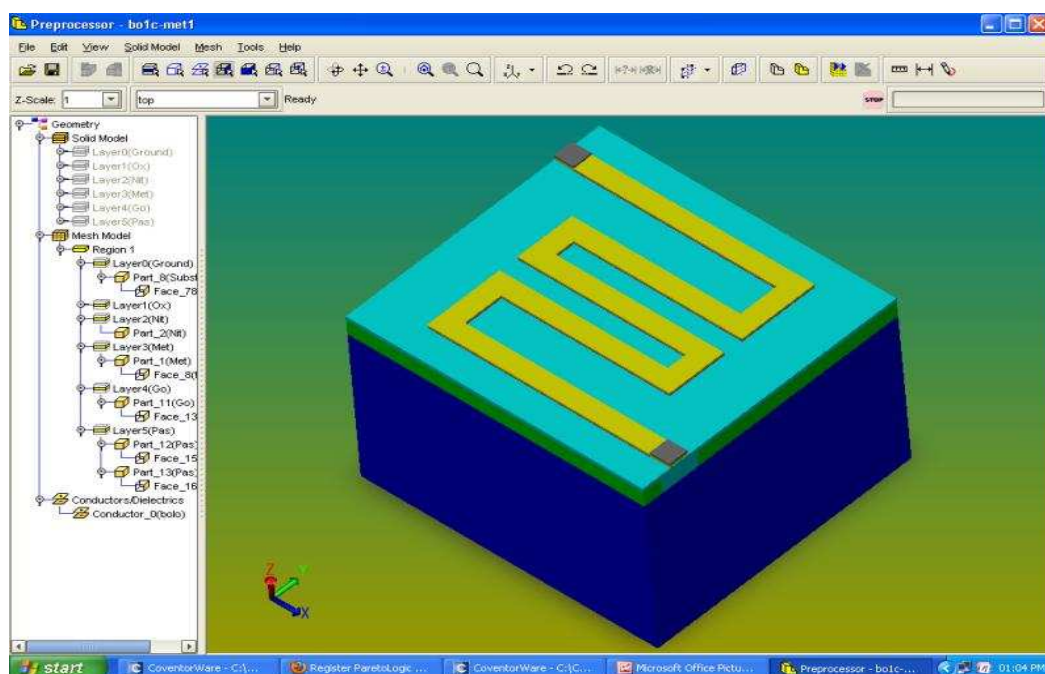


Figure 3-3: Metal bolometer solid model design built in Coventorware

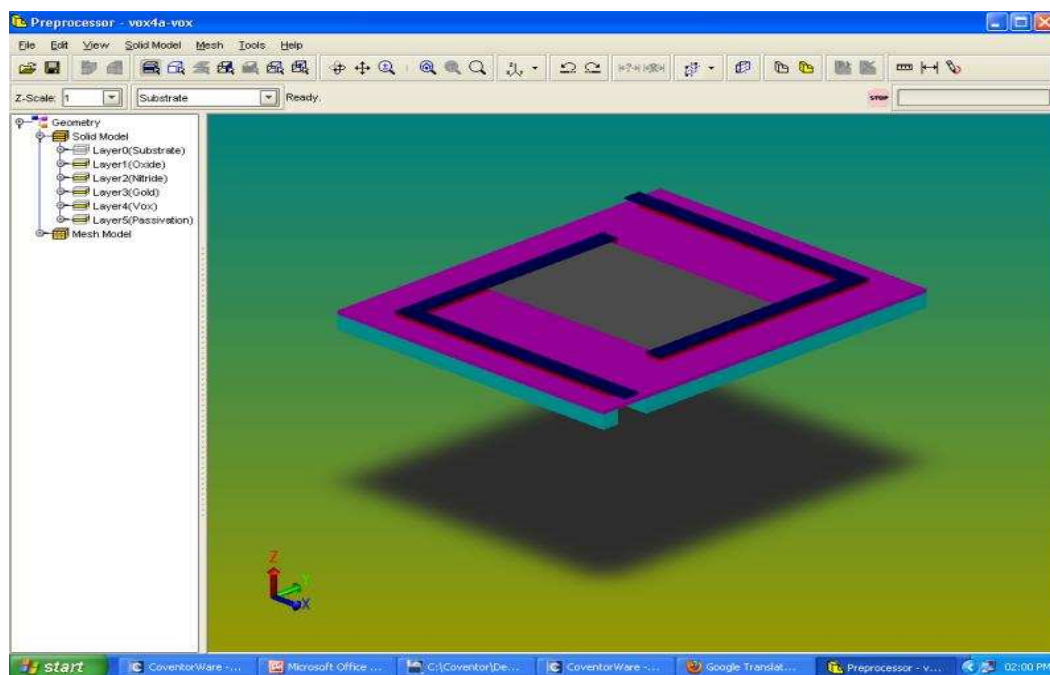


Figure 3-4: Vanadium Oxide bolometer membrane solid model of the VOx bolometer prototype

To determine the solid models of these devices, ConvertorWare was used with different layers and packages defined in collaboration with University of Pretoria partners. These bolometer membranes were designed with six masks as given in Table 1.1 and shown in Figures 3.5 – 3.6.

3.2.3.2. Device analysis and methodology

The device detail analysis was segmented into three main categories:

a. Metal (titanium) bolometer devices

Three metal membrane bolometers types were analysed:

- MET2
- MET3
- MET4

The MET range design detail (geometrics) is shown in Figure 3.5 below. This is more of the actual device details and these were modified as with type change. The MET type reflects optimisations to the metal titanium support leg

width. As part of this exercise, the support leg width was designed at set intervals of 3 μm i.e. 4 μm , 7 μm and 10 μm as shown in Table 3.1.

Table 3-1: Metal (titanium) bolometer geometry dimensions

Devices	d (μm)	w (μm)	l (μm)	lm (μm)	a (μm)	b (μm)	e (μm)	f (μm)	Nf	Am (μm^2)	Al (μm^2)	NI
MET2	2	28	21	15	2	30	2	4	7	588	256	7.6
MET3	3	31	25	15	3	34	3	7	5	775	518	4.8
MET4	4	33	26	19	4	37	4	10	3	858	820	3.7

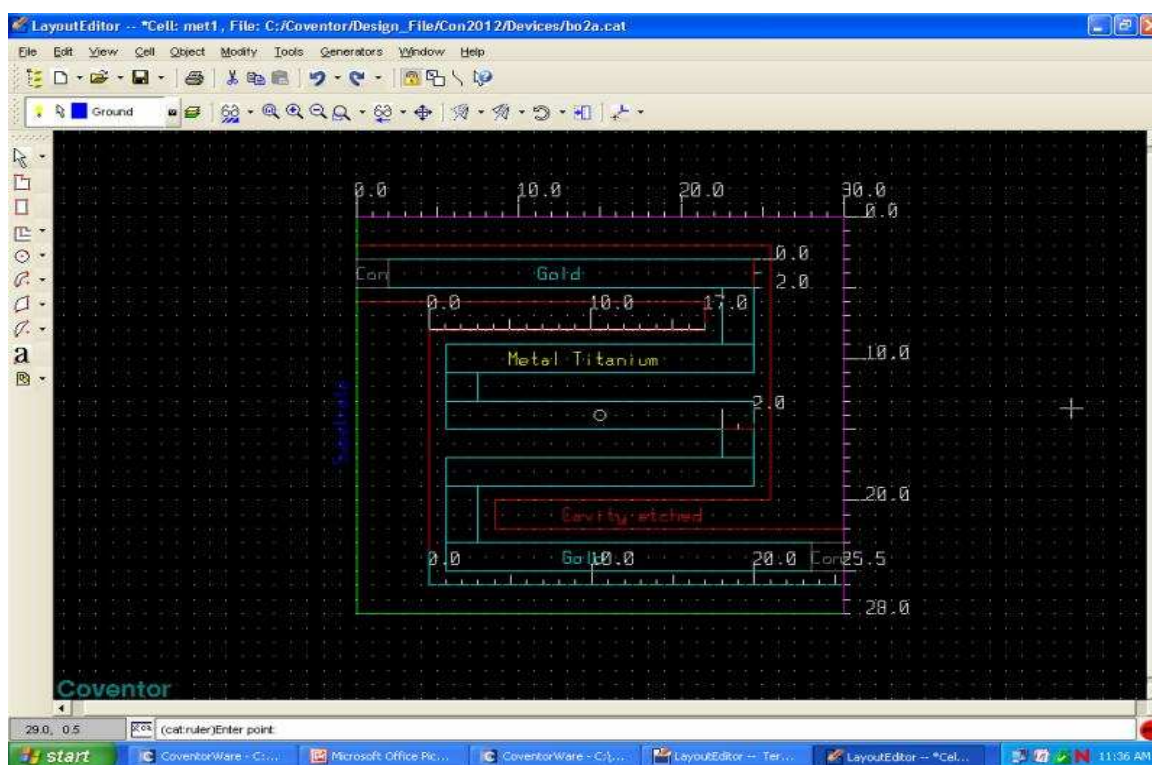


Figure 3-5: Typical metal titanium bolometer layout

The purpose of this exercise was to establish whether the use of big support leg widths was necessary or not. The Results section dwells extensively on the findings.

b. Vanadium oxide (VOx) bolometer devices

Several vanadium oxide bolometers were also designed. A typical vanadium oxide layout representing different masks is shown in Figure 3.6.

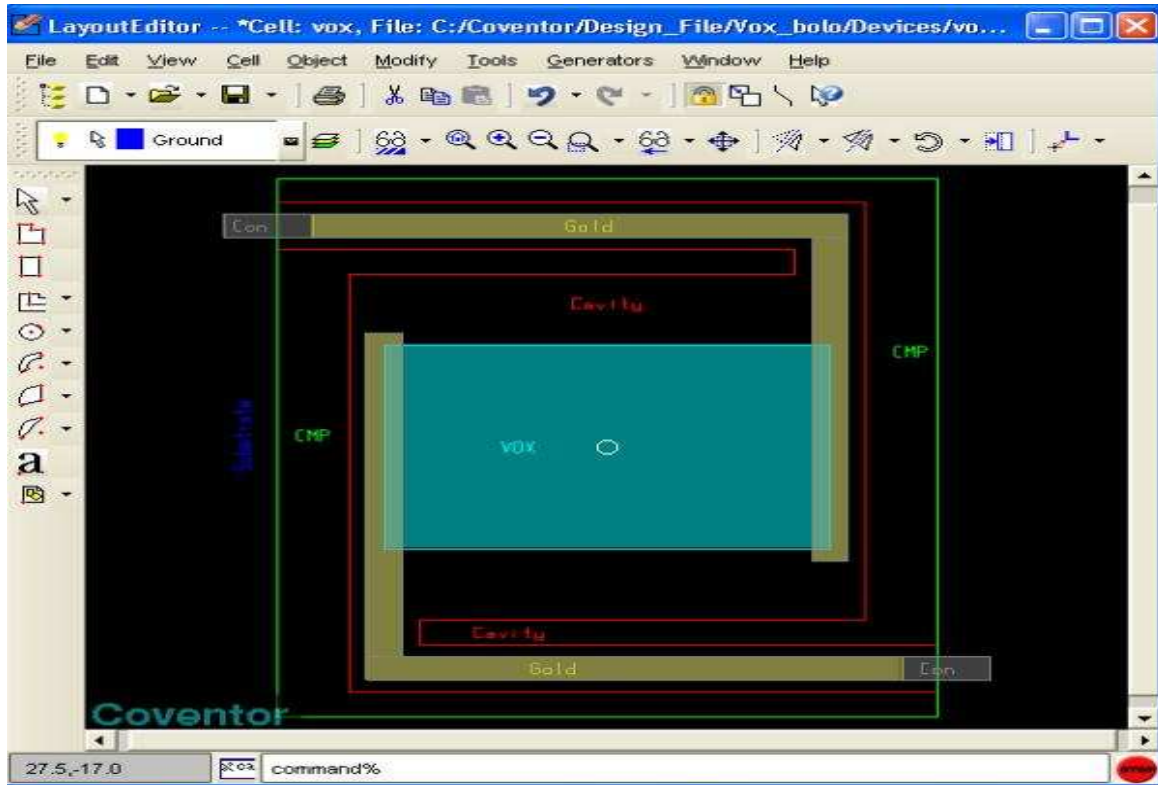


Figure 3-6: Typical Vanadium oxide bolometer layout

Three vanadium oxide bolometers were designed, utilising 2, 3 and 4 micron design rules respectively as minimum dimensions. Dimensions of the vanadium oxide bolometers are defined in Table 3.2. These three bolometers are named VOX2, VOX3 and VOX4.

Table 3-2: Vanadium oxide (VOx) bolometer geometry dimensions

Devices	d (μm)	w (μm)	l (μm)	lv (μm)	a (μm)	b (μm)	e (μm)	f (μm)	Wv (μm)	Am (μm ²)	Al (μm ²)	Nf
VOX2	2	28	21	23	2	30	2	4	17	609	264	7.8
VOX3	3	31	25	21	3	34	3	7	17	775	518	4.8
VOX4	4	33	26	19	4	37	4	10	16	858	820	3.7

To improve the modelling capabilities of the thermal properties, a range of vanadium oxide bolometers with varying membrane areas and varying suspended leg lengths were designed. These devices are described in Table 3.3. From that table it can be seen that devices VOXA, VOXB, VOXC and VOXD all have the same leg thermal parameters, but different membrane areas. Also, devices VOXC, VOXE, VOXF and VOXG have the same membrane areas, but different leg thermal values.

The purpose of this is to determine the behaviour of thermal conductance under vacuum conditions even further, and atmospheric pressure of vanadium oxide with different lengths of leg folding around the membrane.

Table 3-3: VOx (second set) bolometer geometry dimensions

Devices	d (μm)	w (μm)	l (μm)	lv (μm)	a (μm)	b (μm)	e (μm)	f (μm)	Wv (μm)	Am (μm^2)	Al (μm^2)	Nf
VOXA	2	28	21	23	2	30	2	4	17	609	264	7.8
VOXB	3	31	25	21	3	34	3	7	17	775	518	4.8
VOXC	4	33	26	19	4	37	4	10	16	858	820	3.7
VOXD	3	50	25	15	3	28	3	7	42	1250	434	4.0
VOXE	3	37	25	15	3	28	3	7	29	925	434	4.0
VOXF	3	25	25	15	3	28	3	7	17	625	434	4.0
VOXG	2	25	25	19	2	28	2	4	19	240	625	3.7

3.3 Material selection

The two most commonly used infrared radiation detecting materials in microbolometers are amorphous silicon ($\alpha\text{-Si}$) and vanadium oxide (VOx). Much research has been conducted to test the feasibility of other materials to be employed as detecting material.

A range of other materials that have already been investigated include the following: Ti, YBaCuO, GeSiO, poly SiGe, BiLaSrMnO and a protein-based cytochrome C and bovine serum albumin (Infrared imaging news, vol14; 2008, 5).

A microbolometer is a specific type of resistor used as a detector in thermal imaging devices. It is a tiny vanadium oxide (VOx) or amorphous silicon (α -Si) resistor with a large temperature coefficient on a silicon element with large surface area, low heat capacity and good thermal isolation. Infrared radiation from a specific range of wavelengths strikes the vanadium oxide or amorphous silicon and changes its electrical resistance. Changes in scene temperature cause changes in the bolometer temperature which are then converted to electrical signals and processed into an image (Infrared imaging news, vol14; 2008, 5).

Amorphous silicon (α -Si) works well mainly because it can easily be integrated into the CMOS fabrication process. Amorphous silicon (α -Si) is extensively described and used in a large variety of products such as active layer in thin-film transistors for liquid crystal displays, small area solar powered photovoltaic devices for consumer products and large area power solar cells (Infrared imaging news, vol14; 2008, 6).

The hydrogenated amorphous silicon (α -Si) microbolometer arrays take advantage of the high TCR, relatively high optical absorption coefficient and the further advantage that they can be manufactured using silicon fabrication compatible processes TCR up to about 3 %/K at room temperature (Infrared imaging news, vol14; 2008, 6).

Bolometers made of α -Si can consist of very thin membranes, allowing for a low thermal mass and consequently, for bolometers with a low thermal conductance, while maintaining a fixed bolometer time constant (Infrared imaging news, vol14; 2008, 6).

The vanadium oxide thin films that are used have TCR in the range 2 %/K and 3 %/K at room temperature (C. Chen, X. Yi, J. Zhang et al, pp.54, 2001) and are used today in a variety of bolometer products. There are many phases in vanadium oxides, such as VO_2 , V_2O_5 and V_2O_3 . These undergo transition from an insulator or semiconductor to a metal phase at a specific temperature. Single crystal VO_2 and V_2O_5 have TCR above 4 %/K, but are difficult to make. Commonly used thin film deposition techniques such as evaporation and sputtering will give amorphous or polycrystalline films. V_2O_5 can be formed by ion beam from vanadium metal target in high O_2 partial pressure, but its resistance at room temperature is very high. V_2O_3 has low formation energy and undergoes a transition from semiconductor to metal phase at low temperature, so its resistance is very low at room temperature. Because high electrical resistance of a device results in a high level of noise, the use of the V_2O_3 phase showing low resistance is important to the fabrication of low-noise microbolometers (Chen S et Al, Vol.16, 2007, 696-700).

Vanadium oxide films can be prepared by a variety of methods, including the annealing and oxidation of evaporated vanadium under controlled conditions, reactive RF sputtering (Chen S et Al, Vol.16, 2007, 696-700) and pulsed laser deposition (Han Y.H et. al. Vol.86, 2005, 254101-3).

A wide range of materials were used for the simulation process as presented in Table 1.1.

Silicon

Silicon is very popular in the sensing industry due to its characteristics, availability and manufacturing costs. Amorphous silicon, otherwise known as either a-Si or α -Si, is the non-crystalline allotropic form of silicon, meaning this type can be deposited in thin films at very low temperatures onto a variety of substrates, offering some unique capabilities in a variety of electronics. It is basically a chemical element which has the symbol Si and atomic number 14.

A tetravalent metalloid, silicon is less reactive than its chemical analogue, carbon. Metalloid or semi-metal is a term used in chemistry when classifying the elements. All these terms had to be understood by a mechanical engineer to fully understand the complexity of this exercise (Ram RS et Al, 1998, 341-352).

On the basis of their general physical and chemical properties, nearly every element in the periodic table can be termed either a *metal* or a *non-metal*. However, a few elements with intermediate properties are referred to as *metalloids* (from the Greek *metallon* = "metal" and *eidōs* = "sort") (Ram RS et Al, 1998, 341-352).

Silicon has many industrial uses: it is the principal component of most semiconductor devices, most importantly, integrated circuits or *microchips*. Silicon is widely used in semiconductors because it remains a semiconductor at higher temperatures than the semiconductor germanium and because its native oxide is easily grown in a furnace and forms a better semiconductor/dielectric interface than any other material (Ram RS et Al, 1998, 341-352).

Titanium

Titanium is a chemical element with the symbol Ti and atomic number 22. Some scientist still call titanium a "space age metal" because it has a low density and is a strong, lustrous, corrosion-resistant (including sea water, aqua regia and chlorine) transition metal with a silver colour (Donochie JM, 1988, 6).

Titanium can be alloyed with iron, aluminium, vanadium, and molybdenum among other elements to produce strong lightweight alloys for many industries and products:

- aerospace (jet engines, missiles, and spacecraft),
- military

- industrial processes (chemicals and petro-chemicals, desalination plants, pulp, and paper)
- automotive
- agri-food
- medical prostheses
- orthopaedic implants (ironically, a close friend of the author had to undergo this surgery in July of 2009 and only then did it 'click' that this material could also be used for this type of application)
- dental and endodontic instruments and files
- dental implants
- sporting goods
- jewellery
- and mobile phones

The two most useful properties of the metal form are corrosion resistance and the highest strength-to-weight ratio of any metal. In its unalloyed condition, titanium is as strong as some steels, but 45% lighter. Table 3.6 below presents some useful data collected on this particular material to indicate its electrical resistivity capabilities (Donochie JM, 1988, 6).

Table 3.1: Titanium physical properties

Electrical Properties		Conditions	
		Temp. K	Note
Electrical resistivity	4.200×10^{-7} W-m	293.15	n/a
Thermal properties		Conditions	
		Temp. (K)	Pressure (Pa)
Melting temperature	n/a	1941	101325
Fusion enthalpy	295 J/g	0	101325
Heat capacity	523 J/kg-K	298.15 more...	100000
Thermal conductivity	21.9 W/m-K	300 more...	101325

The table above speaks volumes of what this material *could* potentially do.

Gold

Gold's physical quantities and thermal properties

- Density: 19,300 kg per cubic metre.
- Melting point: 1337.33 K (1064.18 °C).

- Boiling point: 3129 K (2856 °C).
- Atomic number: 79.
- Nucleic protons: 79.
- Atomic weight: 197.
- Nucleic neutrons (normal): 118.
- Thermal conductivity: 320 W/m.K
- Coefficient of linear thermal expansion at 20°C: $14.2 \times 10^{-6} /m$

Gold's chemical qualities

Gold is a chemical element so it can only be mined, not manufactured. It is largely inert, which means: (i) It is almost totally immune to decay, (ii) it is not very useful in any industrial/chemical processes which use it up, and (iii) it is easy to store cheaply for long periods.

Gold is remarkable for its rarity, density, softness, and its electrical conductivity.

Gold finds a small number of industrial uses arising from its physical qualities. For example, it is used in dentistry and in the manufacture of some electronics which require high quality non-corrosive contacts as it is shown in jagenergy.com.au, 1.

Silicon nitride

Silicon nitride (Si_3N_4) is a chemical compound of silicon and nitrogen. It is a hard ceramic with high strength over a broad temperature range, moderate thermal conductivity, low coefficient of thermal expansion, moderately high elastic modulus, and unusually high fracture toughness for a ceramic. This combination of properties leads to excellent thermal shock resistance, the ability to withstand high structural loads to high temperature, and superior wear resistance. Silicon nitride is mostly used in high-endurance and high-temperature applications such as gas turbines, car engine parts, bearings, metal working and cutting tools. Silicon nitride bearings are used in the main engines of NASA's space shuttles. Thin silicon nitride films are a popular

insulating layer in silicon-based electronics and silicon nitride (NASA, Retrieved 2009-06-06).

Silicon nitride is often used as an insulator and a chemical barrier in manufacturing integrated circuits to electrically isolate different structures or as an etch mask in bulk micromachining. As a passivation layer for microchips, it is superior to silicon dioxide, as it is a significantly better diffusion barrier against water molecules and sodium ions, two major sources of corrosion and instability in microelectronics. It is also used as a dielectric between polysilicon layers in capacitors in analogue chips (NASA, Retrieved 2009-06-06).

VO_x

Vanadium (V) oxide (*vanadia*) is the chemical compound with the formula V_2O_5 . Commonly known as vanadium pentoxide, this brownish yellow solid is the most stable and common compound of vanadium. Upon heating, it reversibly loses oxygen. Related to this ability, V_2O_5 catalyses several useful aerobic oxidation reactions, the largest scale of which underpins the production of sulphuric acid from sulphur dioxide. It is a poisonous brownish yellow solid which, because of its high oxidation state, is both an amphoteric oxide and an oxidising agent. Unlike most metal oxides, it dissolves slightly in water to give a pale yellow, acidic solution. When this compound is formed by precipitation from aqueous solution, then its colour becomes a deep orange (www.wikipedia.org/Vanadium).

Vanadium oxide physical constants

Table 3-2 Vanadium oxide physical properties

Molecular weight (g/mol)	181.9
Density(g/cm ³)	4.571
Specific gravity	3.36
Specific heat @ 25°C (cal/g°C)	0.485
Melting point (°C)	690
Boiling / Flash Point (°C)	1750
Vapour density	6.3
Solubility in water	0.10 g/100 ml
HS Code	2825.30
Colour	Yellow-orange

3.4 Manufacturing process

3.4.1 CoventorWare

Simulation software specially developed for the design and analyses of micro devices, CoventorWare was used in this study and works to the exact micrometre. CoventorWare offers a consolidated range of tools for MEMS design that allows an almost immediate flexibility of both the loading conditions and operational conditions. The programme in its entirety introduces the designer to a more practical response of the device being examined, allowing for the collection of as much data as possible for analysis purposes. This will form a significant part of this research: understanding the loading conditions and mathematical methods of analysing such conditions. Part of this research will also entail learning about and offering suggestions pertaining to the loading conditions to arrive at certain results which will be debated extensively (<http://www.scribd.com/doc/14464450/MEMS-Report>).

CoventorWare is an interlinked connection of software flow charts, a tool offering a multi-domain, multi-technology simulation environment well-suited

for designing and analysing complex Microsystems as explained above. CoventorWare is routinely used for design and analysis of devices such as inertial sensors employed in the automotive sector, micro-mirrors for DLP, heads for ink-jet-printers, and RF switches for telecommunication and aerospace applications (<http://www.scribd.com/doc/14464450/MEMS-Report>). For this research, this tool was used extensively for the design optimisations and later simulations of the optimised design, as it is capable of creating designs, generating) simulation models, analysing system performance, reviewing performance sensitivities, studying component stresses, and creating virtual prototypes.

The methodology followed is shown below. Briefly, the first stage is to draw an architectural layout, following that with a device design. This is where the device design is given geometrical inputs. Conditions of analysis are also set in this stage. Once the parameters and material properties are updated, the next stage is usually the initiation of analysis.

3.5 Fabrication process

3.5.1 Fabrication technologies

The three characteristic features of MEMS fabrication technologies are miniaturisation, multiplicity and microelectronics. Miniaturisation enables the production of compact, quick-response devices. Multiplicity refers to the batch fabrication inherent in semiconductor processing which allows thousands or even millions of components to be easily and concurrently fabricated. Microelectronics provides the intelligence for MEMS and allows the monolithic merger of sensors, actuators, and logic to build closed-loop feedback components and systems. The successful miniaturisation and multiplicity of traditional electronics systems would not have been possible without IC fabrication technology. Therefore, IC fabrication technology, or 'microfabrication', has so far been the primary enabling technology for the development of MEMS. Microfabrication provides a powerful tool for batch

processing and miniaturisation of mechanical systems into a dimensional domain not accessible by conventional (machining) techniques. Furthermore, microfabrication provides an opportunity for integration of mechanical systems with electronics to develop high-performance closed-loop-controlled MEMS.

Advances in IC technology in the last decade have brought about corresponding progress in MEMS fabrication processes. Manufacturing processes allow for the monolithic integration of MicroElectroMechanical structures with driving, controlling and signal-processing electronics. This integration promises to improve performance of micromechanical devices, as well as reduce the cost of manufacturing, packaging and instrumenting these devices (<http://www.scribd.com/doc/14464450/MEMS-Report>).

Integrated circuit (IC) fabrication

Any discussion of MEMS requires a basic understanding of IC fabrication technology, or 'microfabrication', the primary enabling technology for the development of MEMS. The major steps in IC fabrication technology are film growth, doping, lithography, etching, dicing and packaging (<http://www.csa.com/discoveryguide/mems/overview.php>).

Film growth: Usually a polished Si wafer is used as the substrate on which a thin film is grown. The film, which may be epitaxial Si, SiO₂, silicon nitride (Si₃N₄), polycrystalline Si (polysilicon), or metal, is used to build both active or passive components and interconnections between circuits.

Doping: To modulate the properties of the device layer, a low and controllable level of an atomic impurity may be introduced into the layer by thermal diffusion or ion implantation.

Lithography: A pattern on a mask is then transferred to the film by means of a photosensitive (i.e., light sensitive) chemical known as a 'photoresist'. The process of pattern generation and transfer is called 'photolithography'. A typical mask consists of a glass plate coated with a patterned chromium (Cr) film.

Etching: Next is the selective removal of unwanted regions of a film or substrate for pattern delineation. Wet chemical etching or dry etching may be used. Etch-mask materials are used at various stages in the removal process to selectively prevent those portions of the material from being etched. These materials include SiO₂, Si₃N₄, and hard-baked photoresist.

Dicing: The finished wafer is sawed or machined into small squares, or dice, from which electronic components can be made.

Packaging: The individual sections are then packaged, a process that involves physically locating, connecting and protecting a device or component. MEMS design is strongly coupled to the packaging requirements, which in turn are dictated by the application environment (<http://www.csa.com/discoveryguide/mems/overview.php>).

3.5.2 Bolometer process sequence for the prototype model

This process sequence has been decided by the consortium and will be completed through different technics and organisations as mentioned bellow:

Oxide deposition: Deposit a 2 micron thick silicon dioxide layer on the silicon substrate using LPCVD technology. This process step was performed at SAMES.

Cavity definition: Using the first mask CAVITY, a photolithography step followed by an oxide etch is performed to define the cavity. This process step will be done at DETEK.

Sacrificial layer: After defining the cavity regions, a 2.5 micron thick aluminium sacrificial layer is deposited.

Wafer polishing: The aluminium layer was deposited thicker than the original oxide layer to ensure a planar surface after CMP polishing of the aluminium.

Nitride deposition: A 0.5 micron layer LPCVD silicon nitride is deposited on top of the planar surface. Process steps 3 to 5 will be done in Scotland.

All the following steps will be performed at DETEK:

Metal deposition: A 100 nm thick Ti and 300 nm thick Au metal double layer is deposited directly after the nitride deposition. Using lift-off techniques, the second mask METAL will define the areas where the metal lines are deposited.

Gold definition: Since the thin Ti layer may experience step coverage problems at the cavity edges, it was decided to allow the thicker Au layer to extend slightly (couple of micron) into the cavity region. This can be achieved by using the third mask GOLD to etch the Au and define the Ti metal resistance and contact.

VOX deposition: the vanadium oxide layer is deposited and ohmic contact is made to the Ti layer. The VO_x thickness will be in order of 100 nm. The fourth mask VO_x will be used to photolithographically define the vanadium oxide bolometer resistance.

Oxide passivation: After the definition of the vanadium oxide resistance, a 250 nm thick silicon dioxide layer is deposited to passivate the vanadium oxide and to protect the structure during the sacrificial layer etching.

Contact definition: The fifth mask, CON, is used to define the areas where the Au layer will be made thicker. This will be a lift-off process after the etching through the oxide layer was performed to expose the thinner Au metal layer. The thicker Au will have a thickness approaching one micron and will reduce series resistance and facilitate wire bonding.

Nitride etch: The sixth and final mask, NITRIDE, will be used to define the areas where the covering silicon dioxide and underlying silicon nitride layers will be removed by etching to expose the underlying sacrificial layer filling the cavity.

Sacrificial layer etch: After defining the nitride layer openings, the aluminium sacrificial layer within the cavity can be fully removed by wet etching. It is a self-stopping etch. The process, sequences and final bolometer structure after the sacrificial etch and drying cycle are shown in different steps of Figure 3.9.

The MEMS processing were conducted in 12 steps as defined and input in the process editor (see Figure 4.1- 4.4).

Step 1: substrate deposition;

Steps 2 & 3: straight cut defining the first mask, cavity;

Steps 4 & 5: deposition of sacrificial layer followed by a planar polishing of the sacrificial layer

Step 6: planar LPCVD deposition of nitride Si₃N₄;

Steps 7 & 8: straight cut positive to define second mask, metal (titanium);

Step 9: straight cut positive for third mask, gold;

Steps 10 & 11: planar deposition and straight cut positive for fourth and fifth mask (Con and Nitride);

Step 12: remove sacrificial layer.

The above shown MEMS procedure is merely the initial stage of the entire analysis. This phase is known as the 'MEMS processor' where the device is being characterised with different segments of material to be used during the analysis process.

The next phase is where the design gets drawn and a solid model is produced in the CoventorWare pre-processor.

The figures below show different views of the devices and a typical solid model developed through the process for both Titanium bolometer and Vanadium oxide bolometer.

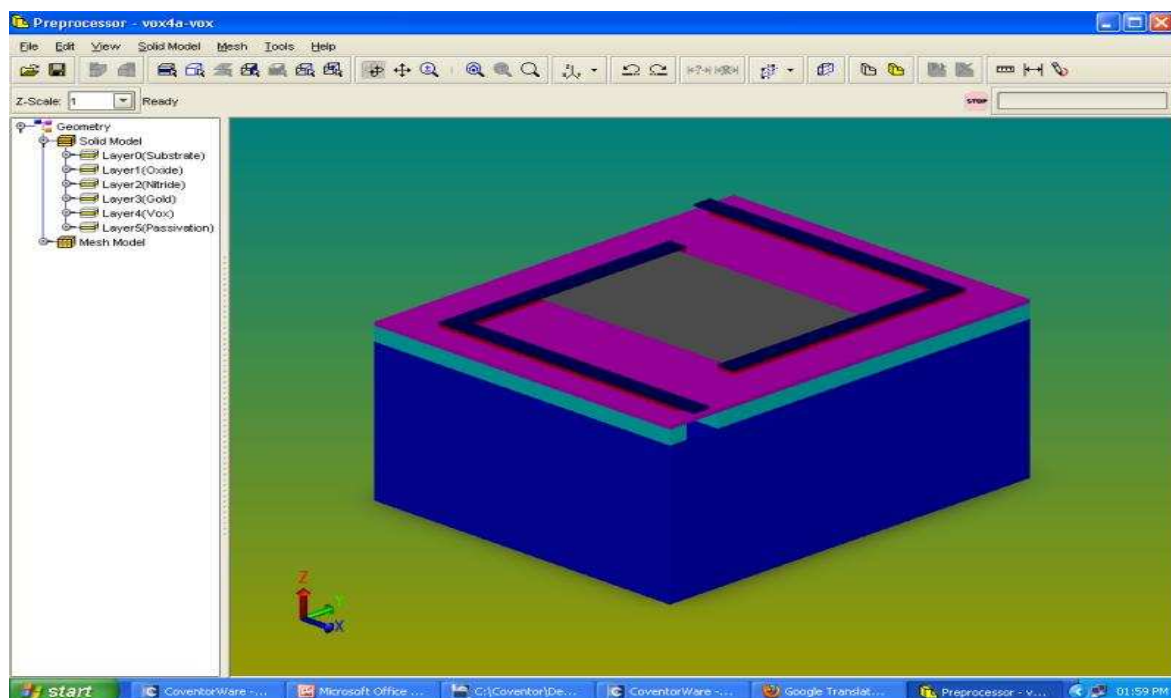


Figure 3-7: Vanadium oxide solid model with different layers shown in the tree (top left)

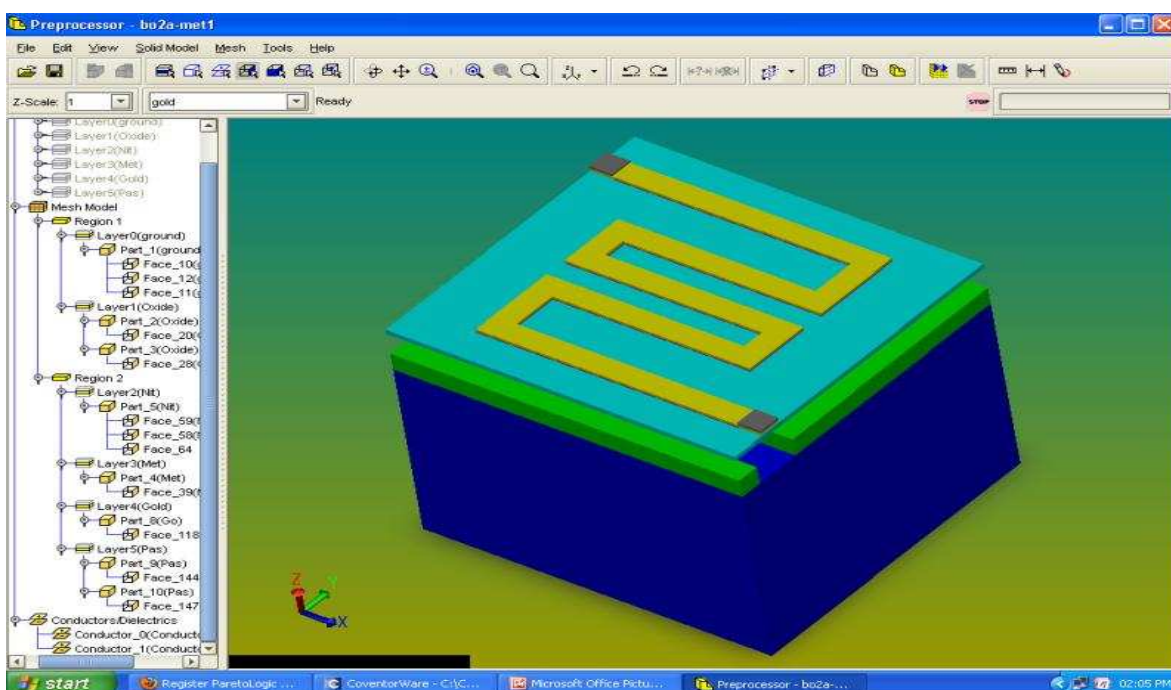


Figure 3-8: Metal (Ti) bolometer solid model with expended tree showing different layers, faces and edges

In order to perform analyses, the solid model tool uses the 2-D layout and process characterisation information to build a solid model. Once the 3-D model is created, the next step in physical design is mesh generation.

ConventorWare uses finite element and boundary element techniques for solving the different equations of each physical domain in the problem. The parabolic tetrahedron (Figure 3.9) mesh type was selected due to its ability to completely disintegrate any shape or geometry of an object being analysed.

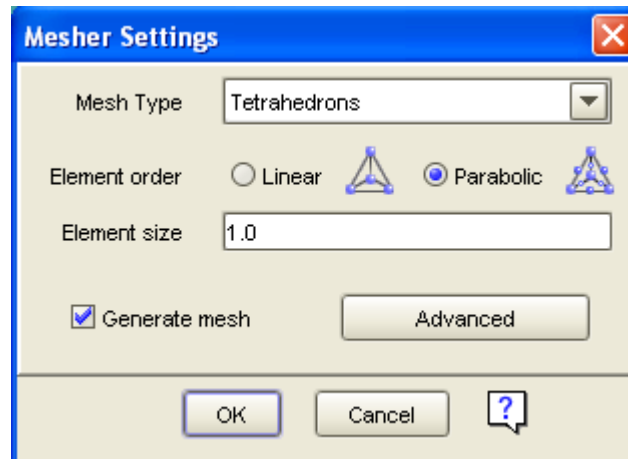


Figure 3-9: Mesher settings

Figure 3.9 and Figure 3.10 below show the generation of mesh of the devices solid model.

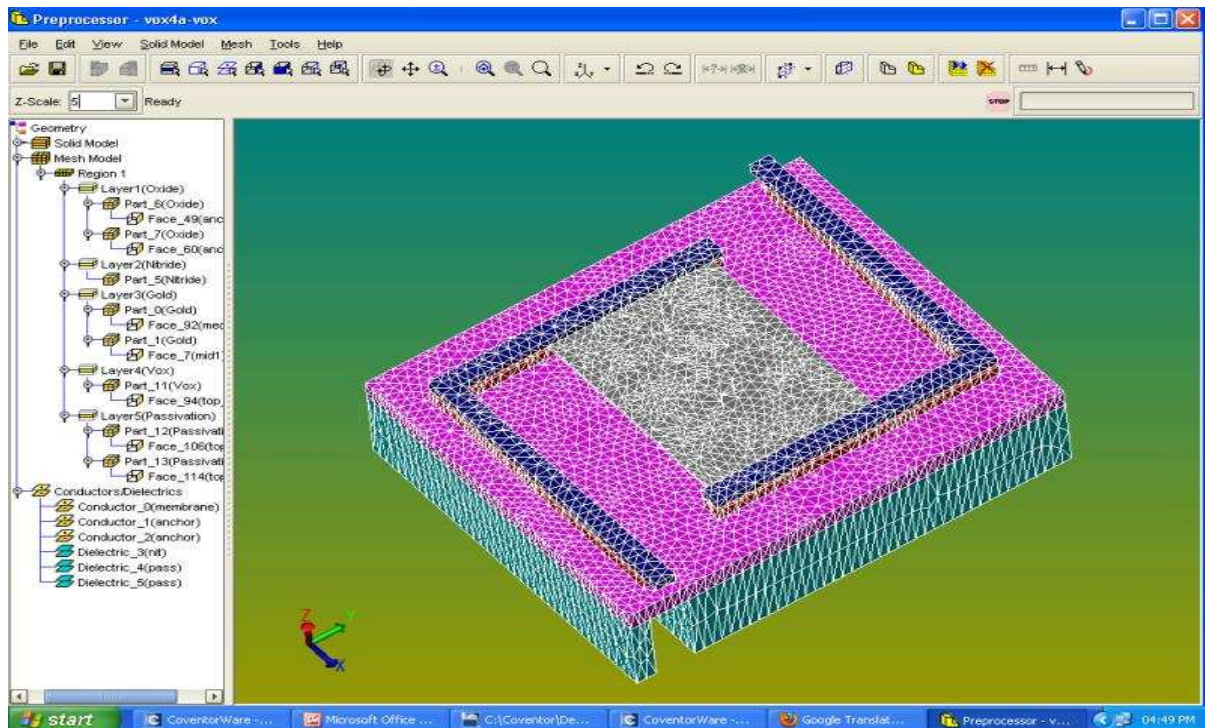


Figure 3-9: Top view of the meshed Vanadium oxide (VOXA) solid model ready for analysis

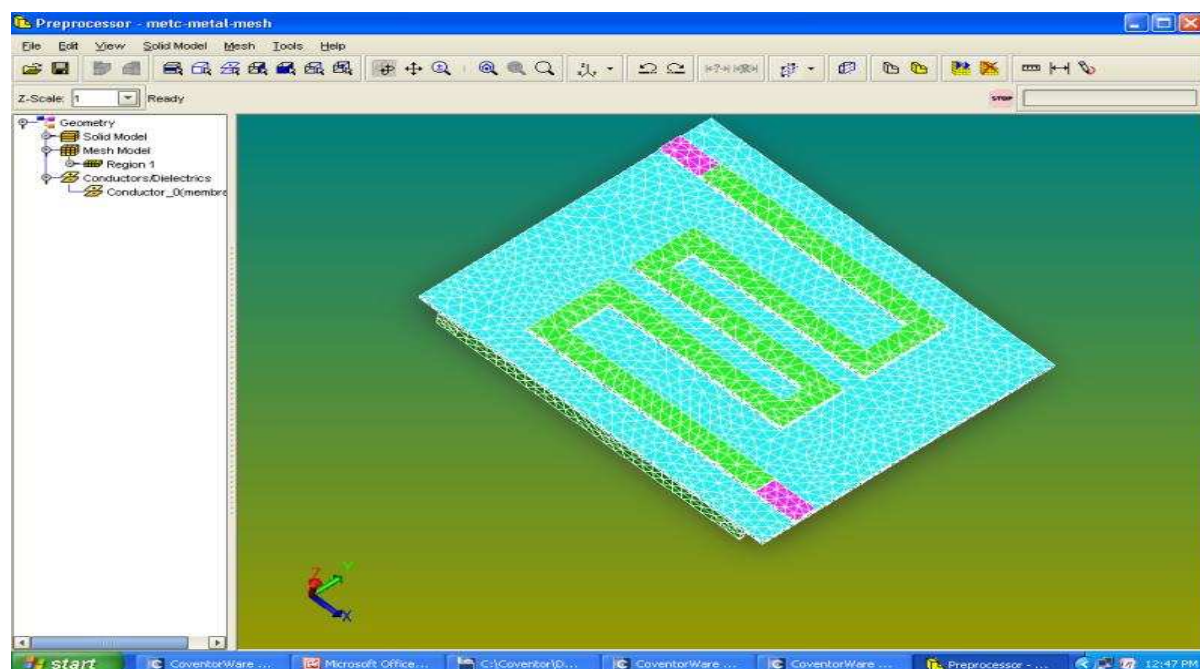


Figure 3-10: Top view of the meshed Metal bolometer (MET2) solid model

3.6 Summary

Chapter 3 is based on the building of solid models for all 13 membrane bolometers. This was done through the FEA pack CoventorWare with thermal and physic properties fixed for all materials used before proceeding in the processor. Then solid models were prepared for analysis through tetrahedron meshing and parabolic element.

Chapter Four

4. Results and Discussions of Static Analysis

4.1 MEMS Processing and Virtual Fabrication

The actual fabrication process of both bolometer pixel devices are described in the previous Chapter. In this Chapter, CoventorWare is used to develop the 13 virtual devices for Fabrication, Solid Modelling, and Numerical Analyses. Figure 4.1 and 4.2 shows the virtual MEMS fabrication steps developed for both Ti and VOX devices.

Number	Step Name	Layer Name	Material Name	Thickness	Mask Name	Photoresist	Depth	Mask Offset	Sidewall Angle	Comments
0	Substrate	Substrate	SILICON	50	SubstrateMask					
1	Stack Material	Oxide	SILICON_OXIDE	2						
2	Straight Cut				Cavity	+	0	0		
3	Conformal Shell	Layer 1	ALUMINUM	2.5						
4	Straight Cut				CMP	-	0	0		
5	Planar Fill	Nitride	Si3N4	0.5						
6	Stack Material	Metal	TITANIUM	0.1						
7	Straight Cut				Metal	+	0	0		
8	Stack Material	Gold	GOLD	0.3						
9	Straight Cut				Gold	+	0	0		
10	Stack Material	Passivation	SILICON_OXIDE	0.25						
11	Straight Cut				Con	+	0	0		
12	Delete		ALUMINUM							

Figure 4-1: Metal bolometer process editor

Number	Step Name	Layer Name	Material Name	Thickness	Mask Name	Photoresist	Depth	Mask Offset	Sidewall Angle	Comments
0	Substrate	Substrate	SILICON_100	20	Ground					
1	Stack Material	Oxide	SILICON_OXIDE	2						
2	Straight Cut				Cavity	+	0	0		
3	Conformal Shell	Sacrifice	ALUMINUM(FILM)	2.5						
4	Straight Cut				CMP	-	0	0		
5	Stack Material	Nitride	Si3N4	0.5						
6	Stack Material	Gold	GOLD	0.3						
7	Straight Cut				GOLD	+	0	0		
8	Stack Material	Vox	Vox	0.1						
9	Straight Cut				VOX	+	0	0		
10	Stack Material	Passivation	SILICON_OXIDE	0.25						
11	Straight Cut				CON	+	0	0		
12	Delete		ALUMINUM(FILM)							

Figure 4-2: VOx bolometer process editor

Figures 4.3 and 4.4 diagrammatically describes the virtual fabrication process as used in CoventorWare. The virtual fabrication process for the MET devices consist of 12 steps while that of the VOX devices consist of 13 steps. The processes for both devices are similar up to step 6. After this step the processing changes to accommodate the different sensor materials.



Figure 4-3: Metal bolometer virtual fabrication used CoventorWare



Figure 4-4: VOX bolometer virtual fabrication as used in CoventorWare

The diagrams and tables below shows the dimensions of the 13 devices

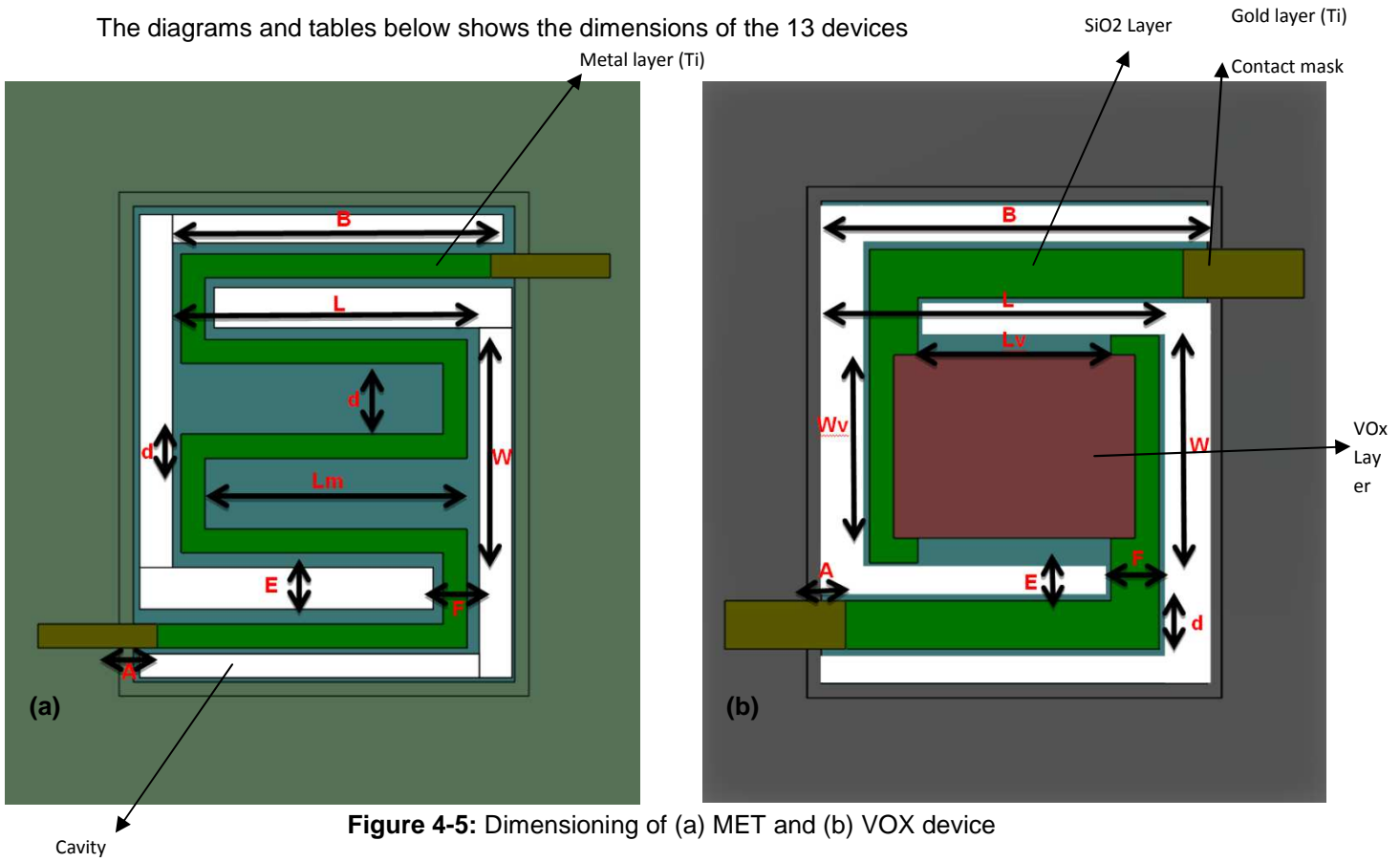


Figure 4-5: Dimensioning of (a) MET and (b) VOX device

Table 4-1: Metal (titanium) bolometer geometry dimensions

Devices	d (μm)	w (μm)	l (μm)	lm (μm)	a (μm)	b (μm)	e (μm)	f (μm)	Nf	Am (μm ²)	Al (μm ²)	NI
MET2	2	28	21	15	2	30	2	4	7	588	256	7.6
MET3	3	31	25	15	3	34	3	7	5	775	518	4.8
MET4	4	33	26	19	4	37	4	10	3	858	820	3.7

Table 4-2: Vanadium oxide (VOx) bolometer geometry dimensions

Devices	d (μm)	w (μm)	l (μm)	lv (μm)	a (μm)	b (μm)	e (μm)	f (μm)	Wv (μm)	Am (μm ²)	Al (μm ²)	Nf
VOX2	2	28	21	23	2	30	2	4	17	609	264	7.8
VOX3	3	31	25	21	3	34	3	7	17	775	518	4.8
VOX4	4	33	26	19	4	37	4	10	16	858	820	3.7

Table 4-3: VOx (second set) bolometer geometry dimensions

Devices	d (μm)	w (μm)	l (μm)	lv (μm)	a (μm)	b (μm)	e (μm)	f (μm)	Wv (μm)	Am (μm^2)	Al (μm^2)	Nf
VOXA	2	28	21	23	2	30	2	4	17	609	264	7.8
VOXB	3	31	25	21	3	34	3	7	17	775	518	4.8
VOXC	4	33	26	19	4	37	4	10	16	858	820	3.7
VOXD	3	50	25	15	3	28	3	7	42	1250	434	4.0
VOXE	3	37	25	15	3	28	3	7	29	925	434	4.0
VOXF	3	25	25	15	3	28	3	7	17	625	434	4.0
VOXG	2	25	25	19	2	28	2	4	19	240	625	3.7

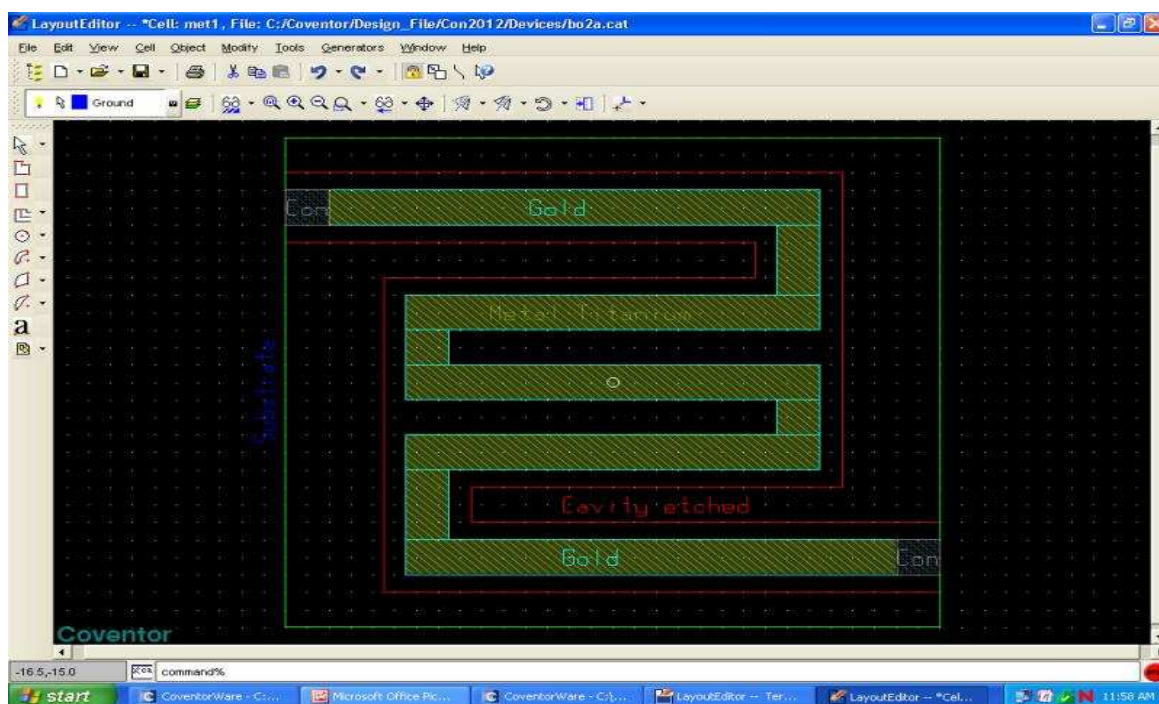
The above tables present the geometric properties of bolometer membranes, Titanium and VOx, whose characteristics are explained below:

- w : width of membrane bolometer
- l : the length of membrane
- lm : the length of metal line
- d : width of metal layer / spacing between metal fingers
- a : length of gold overlap with capacity
- b : length of isolated interconnect finger
- f : width of leg
- e : width of cavity etch
- Nf : number of fingers

To determine the solid models of these devices, ConvertorWare was used with different layers and packages defined in collaboration with University of Pretoria partners. These bolometer membranes were designed with six masks as given in Table 3.4 and shown in Figures 3.5 – 3.6.

Table 4-4: Mask definitions of bolometers analysed

Layer name	Description
Cavity	Define regions of sacrificial layer
Metal	Define lift-off mask for metal deposition
Gold	Define where gold will be etched to leave titanium as bolometer material
Vanadium oxide	Define regions where vanadium oxide bolometer resistors will be formed
Contact	Define regions where gold will be thickened for wire bonding and lower series resistance
Nitride	Define the etch of sacrificial layer

**Figure 4-6:** Metal bolometer masks layout

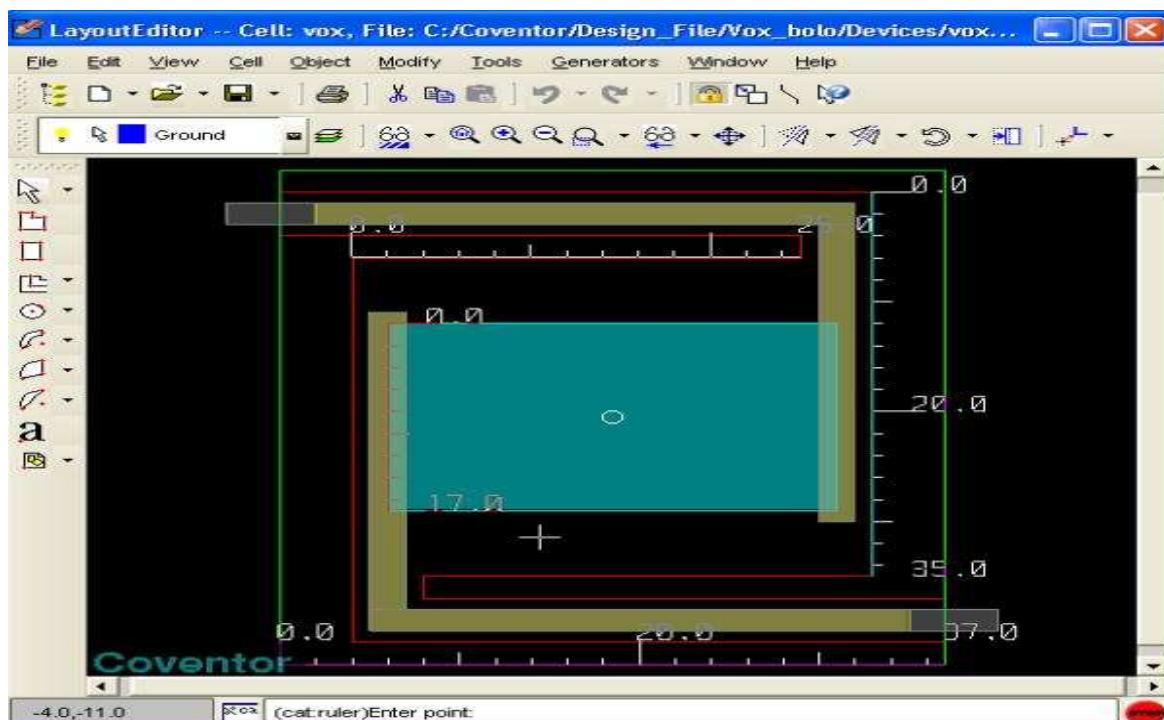


Figure 4-7: VOx bolometer masks layout

4.2 Numerical analyses

Static Thermo-Mechanical Analyses was chosen as the solution type for the 13 bolometer pixel devices, i.e. a solution of the thermal field generated by the applied heat source is first calculated; these results are then used to determine mechanical deformations caused by the change in temperature of the structure. A total of **1144** static analyses were conducted in order to determine the thermal conductance.

Dynamic Thermo-Mechanical Analyses was chosen as the solution type, i.e. a solution of the thermal field generated by the applied heat source over a period of time. The results of these analyses were used to determine the change in temperature of the chosen bolometer membrane design. A total of **5** dynamic thermal analyses were conducted in order to achieve the third objective.

4.2.1 Thermal Loading for Static Analyses

Thermal Loads simulating thermal radiation given off by human beings were applied to the top surface of the Bolometer Membranes. These loads varied from 500 – 10 000 pW/ μm^2 with increments of 500 pW/ μm^2 for the two first and 1000 pW/ μm^2 for the rest of loads.

4.2.1.1 Thermal Boundary Conditions for Static Analyses

The substrate temperature was varied from 263 – 303K, (i.e. -10 – 30⁰C) with increments of 5K.

4.2.1.2 Mechanical Boundary Conditions

The anchor/feet are assumed to be fixed in all directions, i.e. U_x , U_y , and $U_z = 0.0$. All other nodes are free to move in all directions.

4.2.2 Thermal Loading for Dynamic Analyses

5 Different dynamic analyses were performed on bolometer membranes MET2, MET3, VOX3, VOXA and VOXF.

4.2.2.1 Thermal Boundary Conditions for Dynamic Analyses

The substrate temperature was kept at 300K.

4.2.2.2 Mechanical Boundary Conditions

The anchor/feet are assumed to be fixed in all directions, i.e. U_x , U_y , and $U_z = 0.0$. All other nodes are free to move in all directions.

4.2.2.3 Dynamic analyses

In the first analysis, a thermal load of 0.0 to 10 000 pW/ μm^2 was applied to the top surface of the membrane of MET2 over a time period of 0.0 to 4.0 μs . It then drops from 10 000 to 0.0 pW/ μm^2 in 0.1 μs (see the graph in figure 5.1; Chapter 5). The objective of this was to observe how sensitive devices are in a very short period of time as it reflects on the importance of deformation of membrane bolometers.

In the second analysis a thermal load was applied to the top surface of the membrane of MET3 i.e. 0.0 to 10 000 pW/ μm^2 – 0.0 to 3.0 μs , then it drops from 10 000 to 0.0 pW/ μm^2 in 0.1 μs (see the graph in figure 5.5, Chapter 5).

In the third analysis a thermal load of 0.0 to 10 000 pW/ μm^2 was applied to the top surface of the membrane of VOX3. The initial ramping of the load, i.e. from 0.0 to 10 000 pW/ μm^2 occurred over a period of 3.0 μs . the load was then held at 10 000 pW/ μm^2 for a further 32.0 μs . the entire analysis time was thus 35 μs (see the graph in figure 5.9; Chapter 5).

The fourth and fifth analyses are similar to the third, i.e. a thermal load of 0.0 to 10 000 pW/ μm^2 was applied to the top surface of the membrane (VOXA and VOXF) over a total time period of 0.0 to 35.0 μs .

4.3 Static Analyses and data treatment

Static analysis: to assess the sensitivity of the material being used. The object was subjected to a range of heat fluxes to also establish the sensitivity range. And how much does the material change its temperature due to it being subjected to the heat flux

After running analyses as stated in Chapter 3, the results collected from CoventorWare are shown in the figures below:

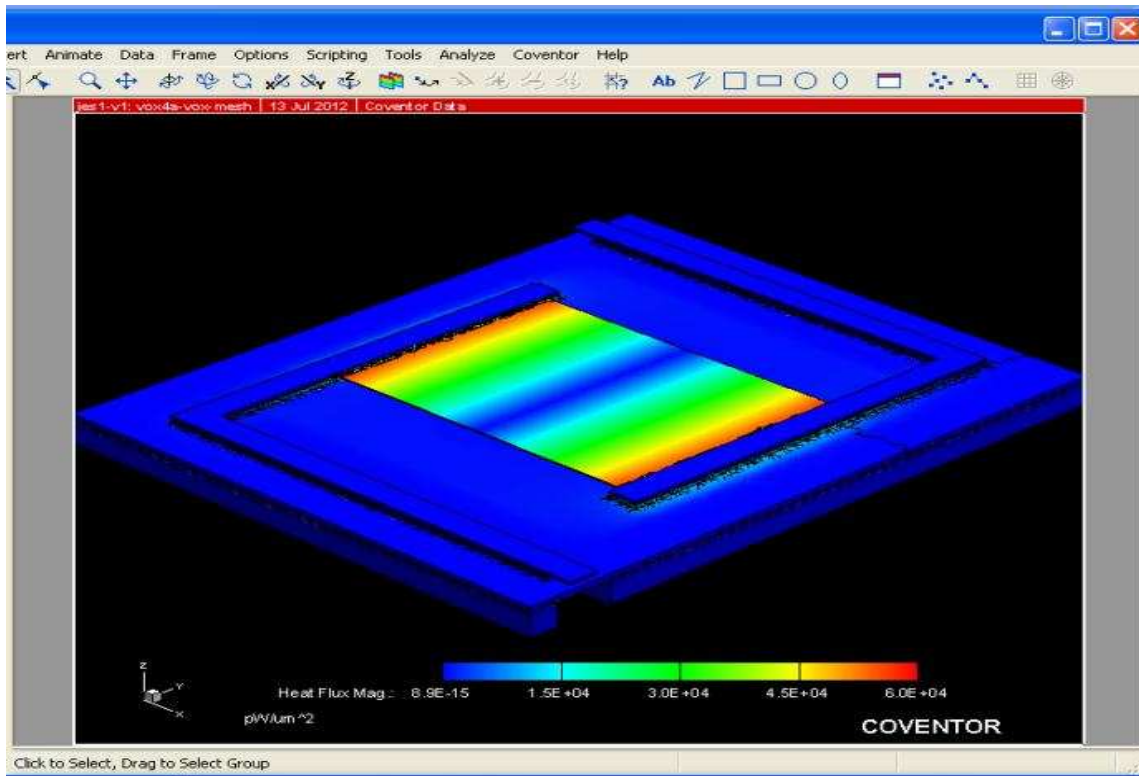


Figure 4-8: VOx bolometer heat flux variation at 300K

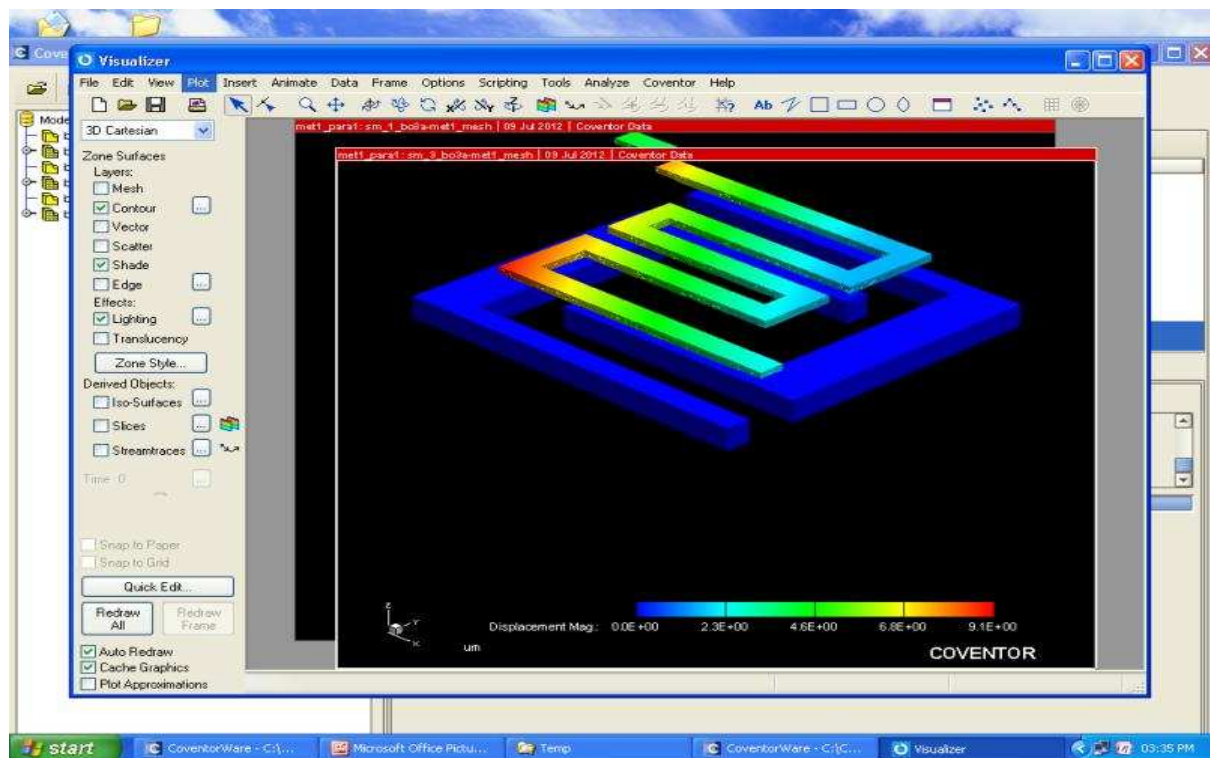


Figure 4-9: Titanium bolometer displacement at a heat flux of 10000 pW/μm²

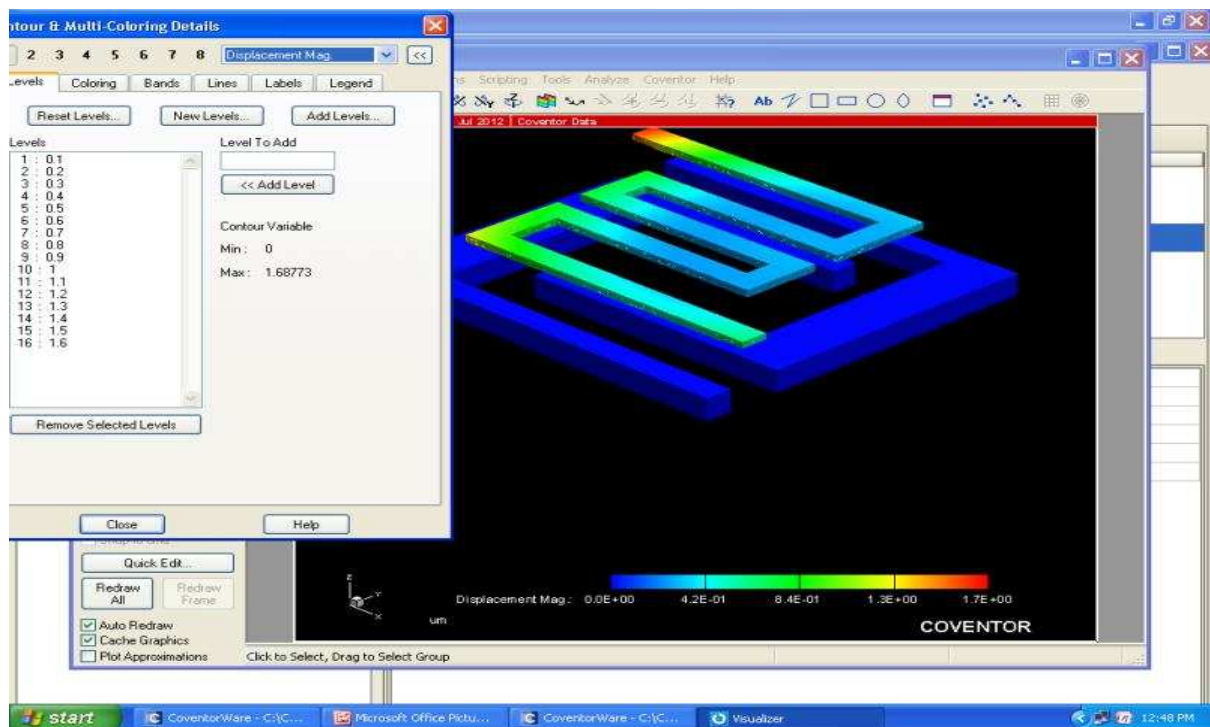


Figure 4-10: Titanium bolometer at 1000 pW/μm²

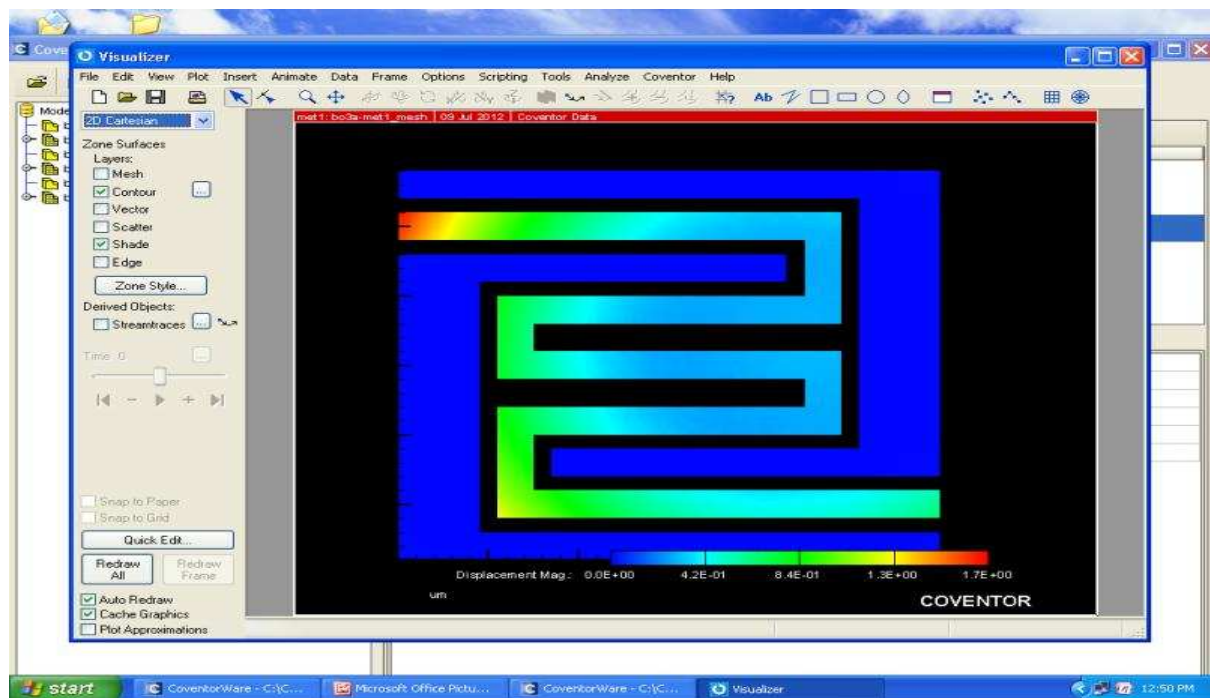


Figure 4-11: Metal titanium thermomechanical layout

The process editor of all type was set up as shown above. The above clip is purely to describe the fabrication process. The main objective of these exercises was to monitor behavioural changes to the beam when subjected to different heat flux in pico watts per square area ($\text{pW}/\mu\text{m}^2$).

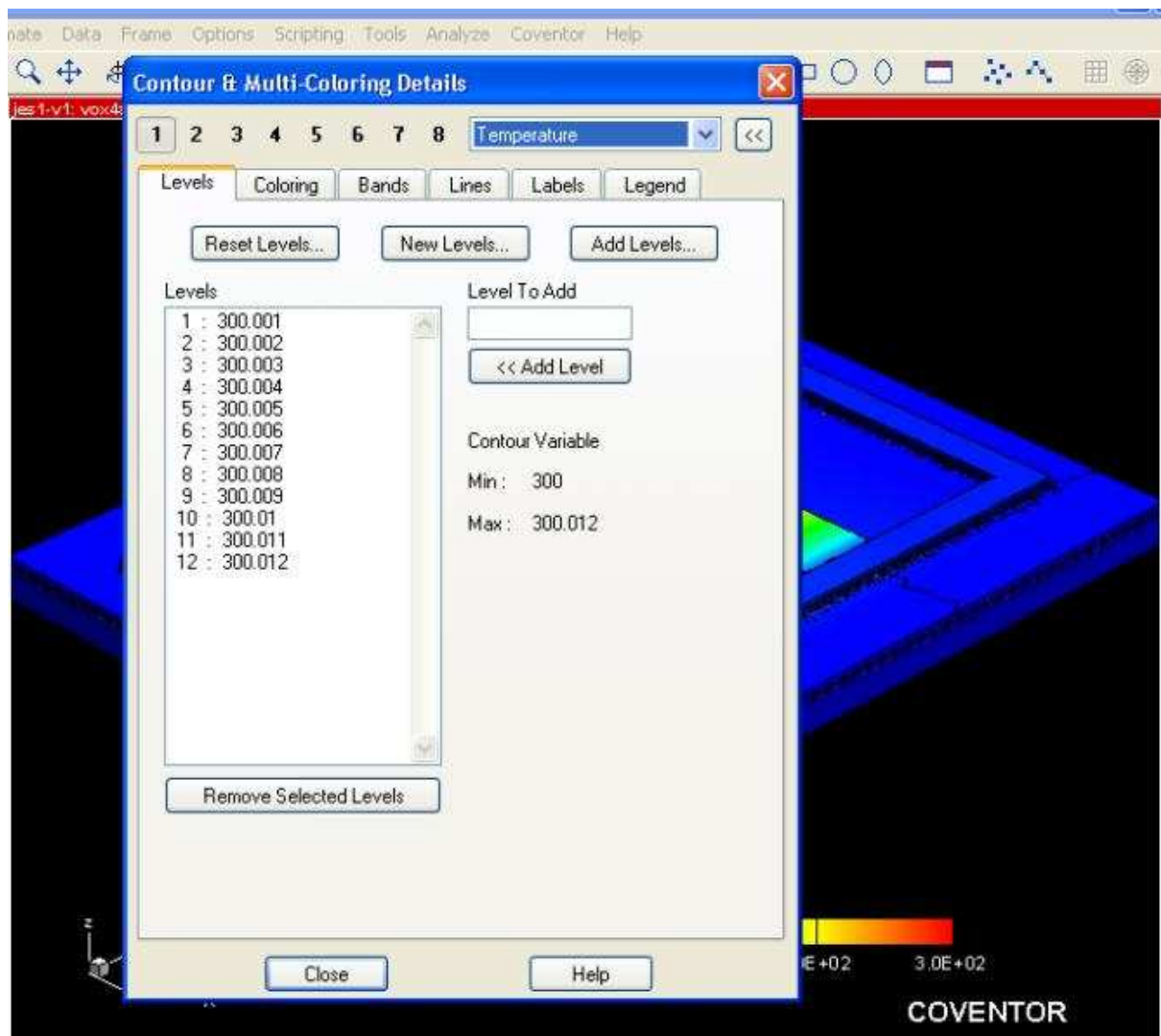


Figure 4-12: ConventorWare data collection of VOX2 at 300K

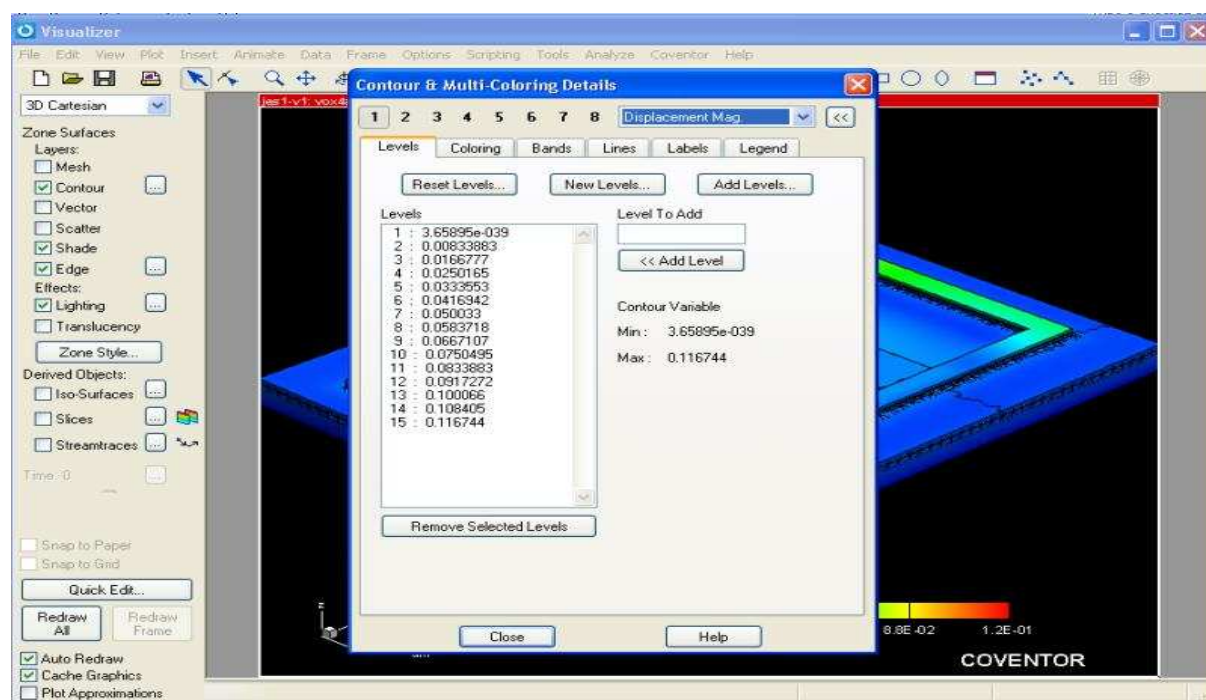


Figure 4-13: Displacement data collected of VOX2 at 300K

Table 4-5 Data collection from CoventorWare

Heat flux	Node Temp_Max	Node Temp_Min	Heat flux (W/microm)	DT= $T_{MAX} - T_{MIN}$	Displacement (m)	DW (Power)
500	300.001	300	5E-10	0.001	0.00833883	4.16942E-12
1000	300.002	300	1E-09	0.002	0.02501650	2.50165E-11
2000	300.003	300	2E-09	0.003	0.0416942	8.33884E-11
3000	300.004	300	3E-09	0.004	0.0583718	1.75115E-10
4000	300.005	300	4E-09	0.005	0.0750495	3.00198E-10
5000	300.006	300	5E-09	0.006	0.0917272	4.58636E-10
6000	300.007	300	6E-09	0.007	0.108405	6.5043E-10
7000	300.008	300	7E-09	0.008	0.1250826	8.75578E-10
8000	300.009	300	8E-09	0.009	0.1417602	1.13408E-09
9000	300.010	300	9E-09	0.010	0.1584378	1.42594E-09
10000	300.011	300	0.0000001	0.011	0.1751154	1.75115E-09

Using data collected from CoventorWare we can determine the thermal conductance:

$$\Delta T = T_{Node Max} - T_{Node Min} \quad (4.1)$$

Equation 4.1 shows the variation of temperature of the device subjected to a thermal load in the form of an incident heat flux. The thermal conductance is found as shown in equation 4.2 below.

$$G = \frac{\Delta W}{\Delta T} \quad (4.2)$$

Where

- G is the thermal conductance in W/K (Watt per Kelvin)
- ΔT is the changing in temperature
- ΔW is the Heat flux

Results from calculations are shown in table 4.6

Table 4-6 Thermal conductance results of VOX2

Heat Flux Φ ($\mu\text{W}/\mu\text{m}$)	Max T (K)	Min T (K)	Φ (W/ μm)	ΔT	Displacement	ΔW	Thermal conductance G, (W/K)
500	300.001	300	5.00E-10	0.00104	0.00833883	4.17E-12	4.80769E-07
1000	300.0021	300	1.00E-09	0.00208	0.0250165	2.50165E-11	4.80769E-07
2000	300.0042	300	2.00E-09	0.00416	0.0416942	8.33884E-11	4.80769E-07
3000	300.0062	300	3.00E-09	0.00624	0.0583718	1.75115E-10	4.80769E-07
4000	300.0083	300	4.00E-09	0.00832	0.0750495	3.00198E-10	4.80769E-07
5000	300.0104	300	5.00E-09	0.0104	0.0917272	4.58636E-10	4.80769E-07
6000	300.0125	300	6.00E-09	0.01248	0.108405	6.5043E-10	4.80769E-07
7000	300.0146	300	7.00E-09	0.01456	0.1250826	8.75578E-10	4.80769E-07
8000	300.0166	300	8.00E-09	0.01664	0.1417602	1.13408E-09	4.80769E-07
9000	300.0187	300	9.00E-09	0.01872	0.1584378	1.42594E-09	4.80769E-07
10000	300.0208	300	1.00E-08	0.0208	0.1751154	1.75115E-09	4.80769E-07

From table 4-7, VOX2's thermal conductance is found with the value of 4.80769E-07 W/K or 0.480769 μW/K. Its equation is shown in figure

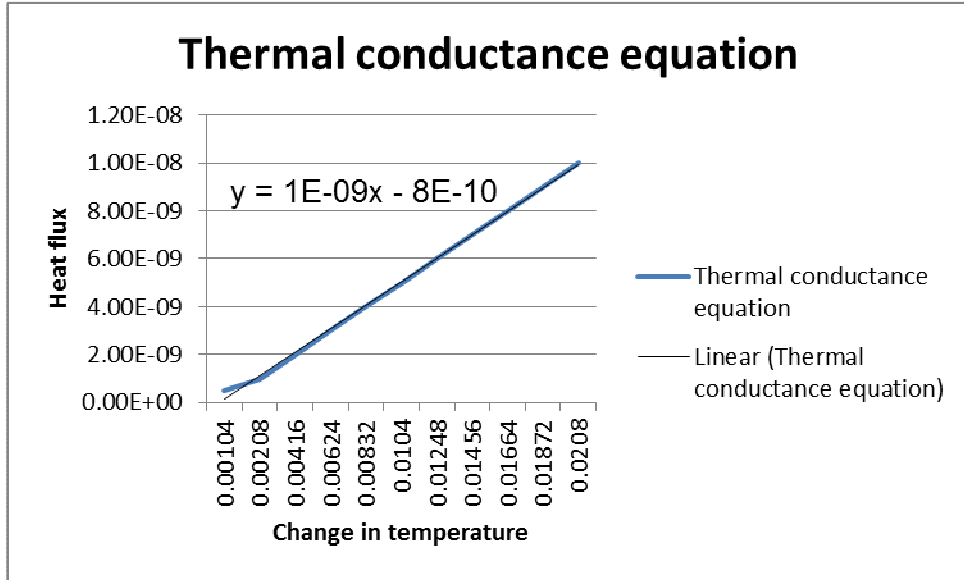


Figure 4-14: Thermal conductance equation of VOX2

Repeating the same process, for MET2:

Table 4-7: Thermal conductance results of MET2

Heat Flux Φ (pW/μm ²)	Max T (K)	Min T (K)	Φ (W/μm ²)	ΔT	Displacement (μm)	ΔW	Thermal conductance G, (W/K)
500	300.0011	300	5.00E-10	0.00107	0.00833883	4.16942E-12	4.6729E-07
1000	300.0021	300	1.00E-09	0.00214	0.0250165	2.50165E-11	4.6729E-07
2000	300.0043	300	2.00E-09	0.00428	0.0416942	8.33884E-11	4.6729E-07
3000	300.0064	300	3.00E-09	0.00642	0.0583718	1.75115E-10	4.6729E-07
4000	300.0085	300	4.00E-09	0.00856	0.0750495	3.00198E-10	4.6729E-07
5000	300.0106	299.9999	5.00E-09	0.0107	0.0917272	4.58636E-10	4.6729E-07
6000	300.0128	299.9999	6.00E-09	0.01284	0.108405	6.5043E-10	4.6729E-07
7000	300.0149	299.9999	7.00E-09	0.01498	0.1250826	8.75578E-10	4.6729E-07
8000	300.017	299.9999	8.00E-09	0.01712	0.1417602	1.13408E-09	4.6729E-07
9000	300.0191	299.9998	9.00E-09	0.01926	0.1584378	1.42594E-09	4.6729E-07
10000	300.0212	299.9998	1.00E-08	0.0214	0.1751154	1.75115E-09	4.6729E-07

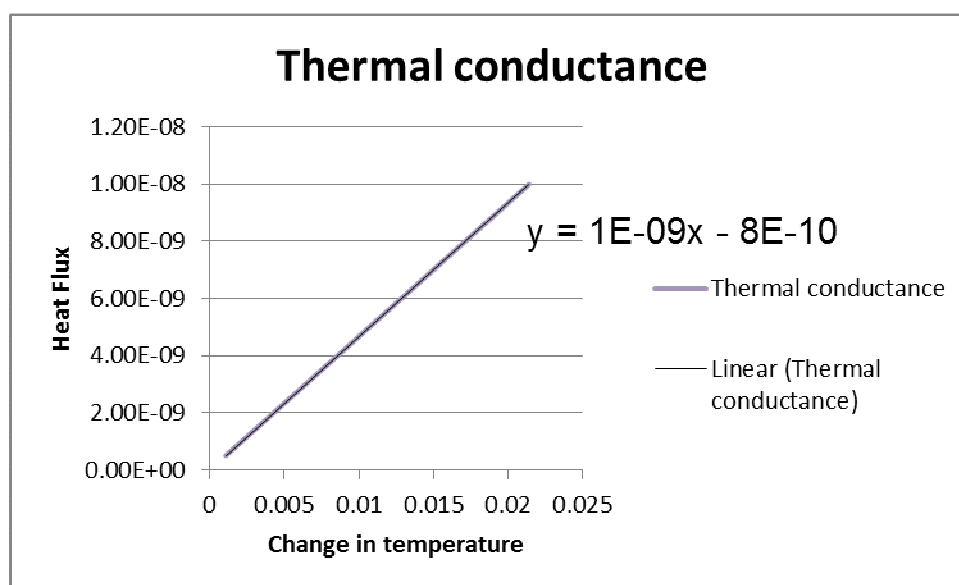


Figure 4-15: Thermal conductance equation of MET2@300K

From table 4-8, the thermal conductance for MET2 in vacuum is found with the value of $4.6729E-07$ W/K or 0.46729 μ W/K. The equation is shown in figure 4.15.

Tables 4-9:4-11 below present the thermal conductance determined for one pixel of one bolometer device. For each set of the three, one of devices analysed is represented in these tables i.e, MET3, VOX4 and VOXF.

Table 4-8: Thermal conductance results of MET3

Heat Flux Φ (μ W/ μ m)	Max T (K)	Min T (K)	Φ (W/ μ m)	ΔT	Displacement	ΔW	Thermal conductance G, (W/K)
500	300.0007	300	5.00E-10	0.000698	0.0104562	5.2281E-12	7.16332E-07
1000	300.0014	300	1.00E-09	0.001396	0.0209124	2.09124E-11	7.16332E-07
2000	300.0028	300	2.00E-09	0.002792	0.0418249	8.36498E-11	7.16332E-07
3000	300.0042	300	3.00E-09	0.004188	0.0627374	1.88212E-10	7.16332E-07
4000	300.0056	300	4.00E-09	0.005584	0.0836499	3.346E-10	7.16332E-07
5000	300.007	300	5.00E-09	0.00698	0.1045624	5.22812E-10	7.16332E-07
6000	300.0084	300	6.00E-09	0.008376	0.1254749	7.52849E-10	7.16332E-07
7000	300.0098	300	7.00E-09	0.009772	0.1463874	1.02471E-09	7.16332E-07
8000	300.0112	300	8.00E-09	0.011168	0.1672999	1.3384E-09	7.16332E-07
9000	300.0126	300	9.00E-09	0.012564	0.1882124	1.69391E-09	7.16332E-07
10000	300.014	300	1.00E-08	0.01396	0.2091249	2.09125E-09	7.16332E-07

From table 4-9, it is shown that the thermal conductance of MET3 is 0.716332 $\mu\text{W/K}$.

Table 4-9: VOX4 thermal conductance results in vacuum

Heat Flux Φ ($\mu\text{W}/\mu\text{m}$)	Max T (K)	Min T (K)	Φ ($\text{W}/\mu\text{m}$)	ΔT	Displacement	ΔW	Thermal conductance G, (W/K)
500	300.0005	300	5.00E-10	0.00049	0.104562	5.2281E-11	1.02041E-06
1000	300.001	300	1.00E-09	0.00098	0.24512	2.4512E-10	1.02041E-06
2000	300.002	300	2.00E-09	0.00196	0.385678	7.71356E-10	1.02041E-06
3000	300.0029	300	3.00E-09	0.00294	0.526236	1.57871E-09	1.02041E-06
4000	300.0039	300	4.00E-09	0.00392	0.63455	2.5382E-09	1.02041E-06
5000	300.0049	300	5.00E-09	0.0049	0.634551	3.17276E-09	1.02041E-06
6000	300.0059	300	6.00E-09	0.00588	0.634553	3.80732E-09	1.02041E-06
7000	300.0069	300	7.00E-09	0.00686	0.76431	5.35017E-09	1.02041E-06
8000	300.0078	300	8.00E-09	0.00784	0.894067	7.15254E-09	1.02041E-06
9000	300.0088	300	9.00E-09	0.00882	1.023824	9.21442E-09	1.02041E-06
10000	300.0098	300	1.00E-08	0.0098	1.153581	1.15358E-08	1.02041E-06

Table 4-10: VOXF thermal conductance results in vacuum

Heat Flux Φ ($\mu\text{W}/\mu\text{m}$)	Max T (K)	Min T (K)	Φ (W/ μm)	ΔT	Displacement	ΔW	Thermal conductance G, (W/K)
500	300.0009	300	5.00E-10	0.000895	0.0106523	5.32615E-12	5.58659E-07
1000	300.0018	300	1.00E-09	0.00179	0.0209323	2.09323E-11	5.58659E-07
2000	300.0036	300	2.00E-09	0.00358	0.0414923	8.29846E-11	5.58659E-07
3000	300.0054	300	3.00E-09	0.00537	0.0620523	1.86157E-10	5.58659E-07
4000	300.0072	300	4.00E-09	0.00716	0.0826123	3.30449E-10	5.58659E-07
5000	300.009	300	5.00E-09	0.00895	0.1031723	5.15862E-10	5.58659E-07
6000	300.0107	300	6.00E-09	0.01074	0.1237323	7.42394E-10	5.58659E-07
7000	300.0125	300	7.00E-09	0.01253	0.1442923	1.01005E-09	5.58659E-07
8000	300.0143	300	8.00E-09	0.01432	0.1648523	1.31882E-09	5.58659E-07
9000	300.0161	300	9.00E-09	0.01611	0.1854123	1.66871E-09	5.58659E-07
10000	300.0179	300	1.00E-08	0.0179	0.2059723	2.05972E-09	5.58659E-07

All the thermal conductance for all devices, metal bolometer and vanadium bolometer were determined the same way, results are given in table 4-7 and 4.8.

Table 4-11: thermal conductance of each device in W/K

Heat Flux Φ ($\mu\text{W}/\mu\text{m}$)	MET2 (G)	MET3 (G)	MET4 (G)	VOX2 (G)	VOX3 (G)	VOX4 (G)	VOX A (G)	VOX B (G)	VOX C (G)	VOX D (G)	VOX E (G)	VOX F (G)	VOX G (G)
500	4.6729E-07	7.16E-07	8.26E-07	4.81E-07	7.26E-07	1.02E-06	1.08E-06	1.09E-06	9.62E-07	4.78E-07	9.9E-07	5.59E-07	9.8E-07
1000	4.6729E-07	7.16E-07	8.26E-07	4.81E-07	7.26E-07	1.02E-06	1.08E-06	1.09E-06	9.62E-07	4.78E-07	9.9E-07	5.59E-07	9.8E-07
2000	4.6729E-07	7.16E-07	8.26E-07	4.81E-07	7.26E-07	1.02E-06	1.08E-06	1.09E-06	9.62E-07	4.78E-07	9.9E-07	5.59E-07	9.8E-07
3000	4.6729E-07	7.16E-07	8.26E-07	4.81E-07	7.26E-07	1.02E-06	1.08E-06	1.09E-06	9.62E-07	4.78E-07	9.9E-07	5.59E-07	9.8E-07
4000	4.6729E-07	7.16E-07	8.26E-07	4.81E-07	7.26E-07	1.02E-06	1.08E-06	1.09E-06	9.62E-07	4.78E-07	9.9E-07	5.59E-07	9.8E-07
5000	4.6729E-07	7.16E-07	8.26E-07	4.81E-07	7.26E-07	1.02E-06	1.08E-06	1.09E-06	9.62E-07	4.78E-07	9.9E-07	5.59E-07	9.8E-07
6000	4.6729E-07	7.16E-07	8.26E-07	4.81E-07	7.26E-07	1.02E-06	1.08E-06	1.09E-06	9.62E-07	4.78E-07	9.9E-07	5.59E-07	9.8E-07
7000	4.6729E-07	7.16E-07	8.26E-07	4.81E-07	7.26E-07	1.02E-06	1.08E-06	1.09E-06	9.62E-07	4.78E-07	9.9E-07	5.59E-07	9.8E-07
8000	4.6729E-07	7.16E-07	8.26E-07	4.81E-07	7.26E-07	1.02E-06	1.08E-06	1.09E-06	9.62E-07	4.78E-07	9.9E-07	5.59E-07	9.8E-07
9000	4.6729E-07	7.16E-07	8.26E-07	4.81E-07	7.26E-07	1.02E-06	1.08E-06	1.09E-06	9.62E-07	4.78E-07	9.9E-07	5.59E-07	9.8E-07
10000	4.6729E-07	7.16E-07	8.26E-07	4.81E-07	7.26E-07	1.02E-06	1.08E-06	1.09E-06	9.62E-07	4.78E-07	9.9E-07	5.59E-07	9.8E-07
G at 300K	4.6729E-07	7.16E-07	8.26E-07	4.81E-07	7.26E-07	1.02E-06	1.08E-06	1.09E-06	9.62E-07	4.78E-07	9.9E-07	5.59E-07	9.8E-07

Table 4-12 Bolometer devices' thermal conductance

Device	Thermal conductance G(W/K)
MET2	4.6729E-07
MET3	7.16E-07
MET4	8.26E-07
VOX2	4.81E-07
VOX3	7.26E-07
VOX4	1.02E-06
VOXA	1.08E-06
VOXB	1.09E-06
VOXC	9.62E-07
VOXD	4.78E-07
VOXE	9.9E-07
VOXF	5.59E-07
VOXG	9.8E-07

when comparing set by set their respective thermal conductance, it has been noticed different behaviors from pixel membrane bolometer devices as shown in figures 4.16 – 4.21.

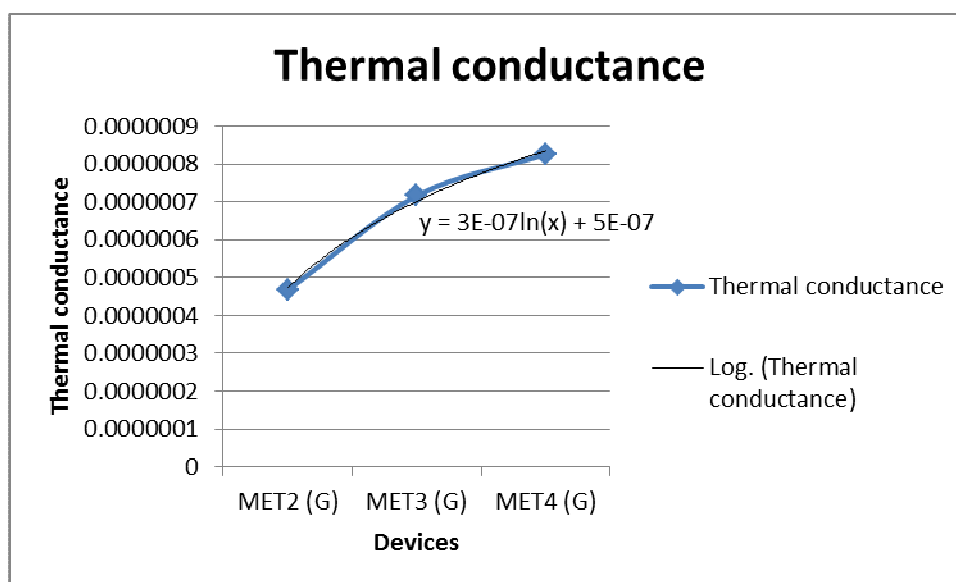


Figure 4-16: Titanium pixel bolometers' thermal conductance variations of three different metal titanium bolometer

In figure 4.16, a comparison is showed between respective thermal conductance of all the three MET devices and it is noticed that they increase following a logarithmic function. It is also presented in fig 4.17 that the width and length of membrane are increasing following the same function, therefore the thermal conductance is dependent of the two factors above mentioned (width and length) and vary accordingly. This means that a big device absorbs more heat than a small one.

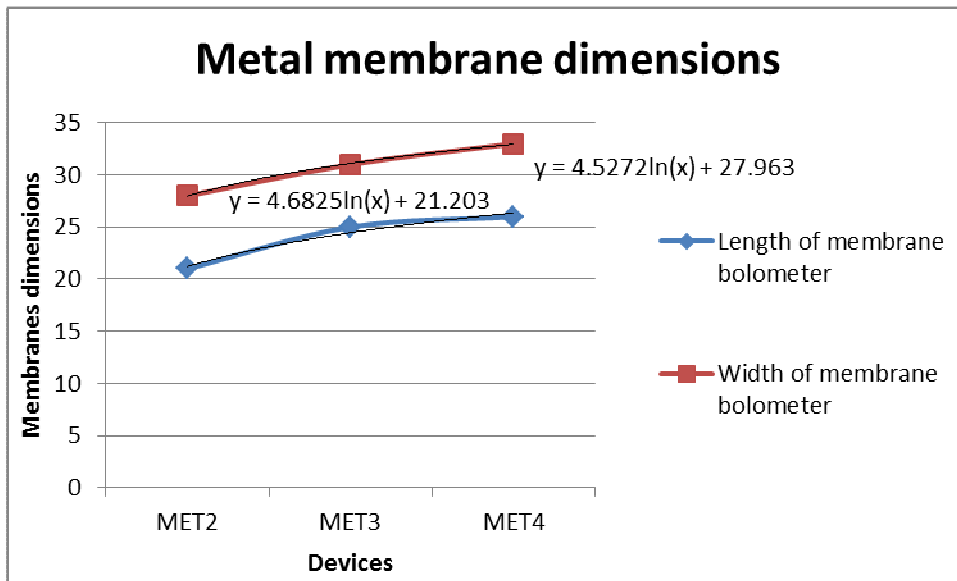


Figure 4-17: Length and width of bolometer membrane variation

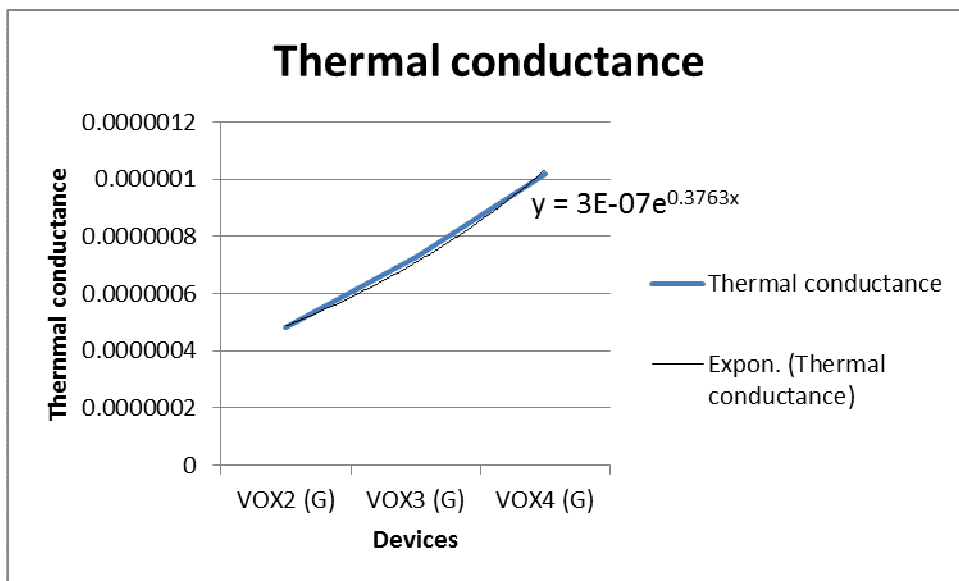


Figure 4-18: Vox devices thermal conductance

The first set of VOX devices varies their thermal conductance exponentially as shown in figure 4.18. They also depend on the variation of the length and width of membrane bolometer.

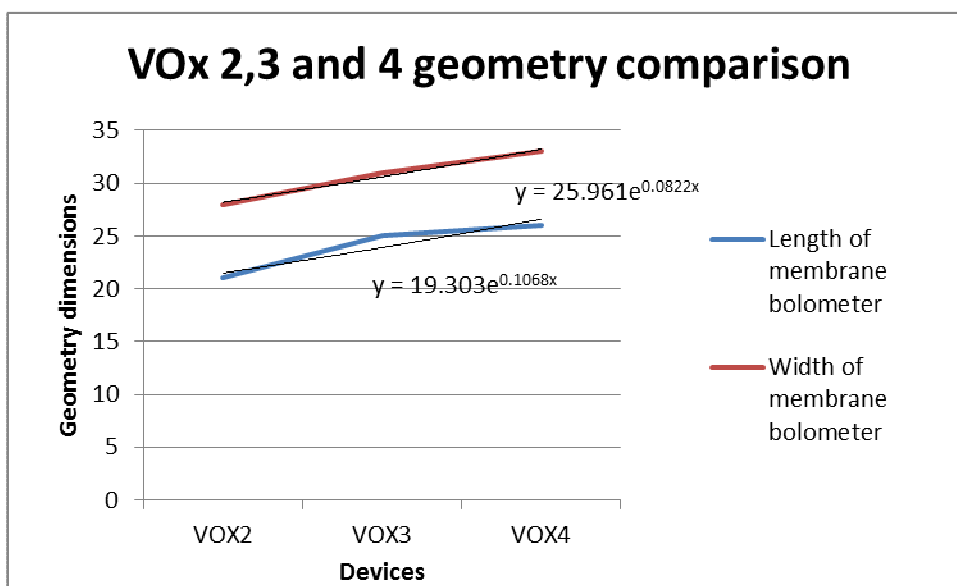


Figure 4-19: Length and width variation

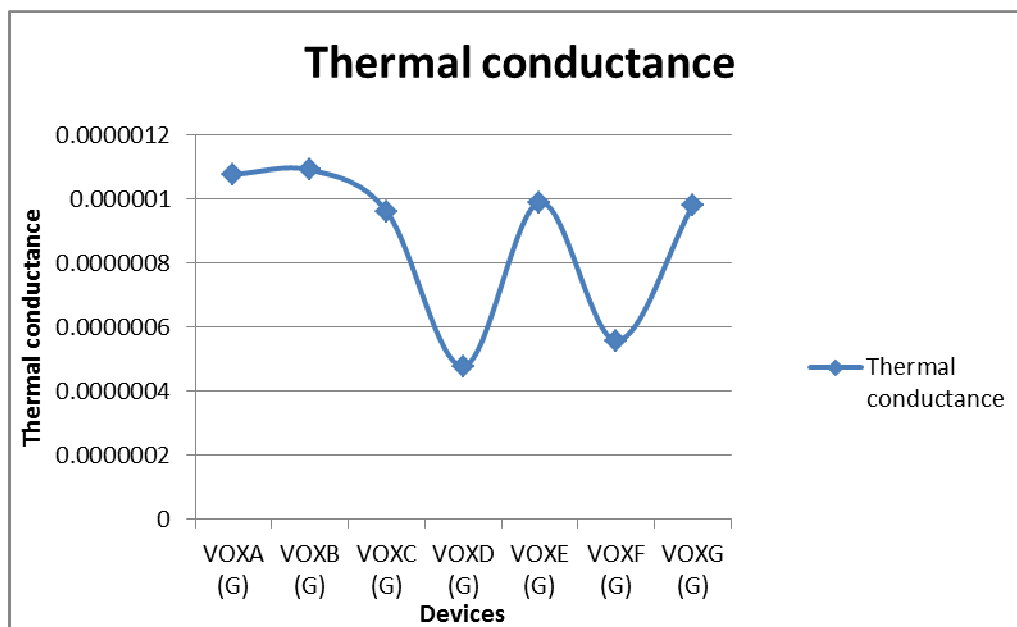


Figure 4-20: Vox devices (set 3) Thermal conductance

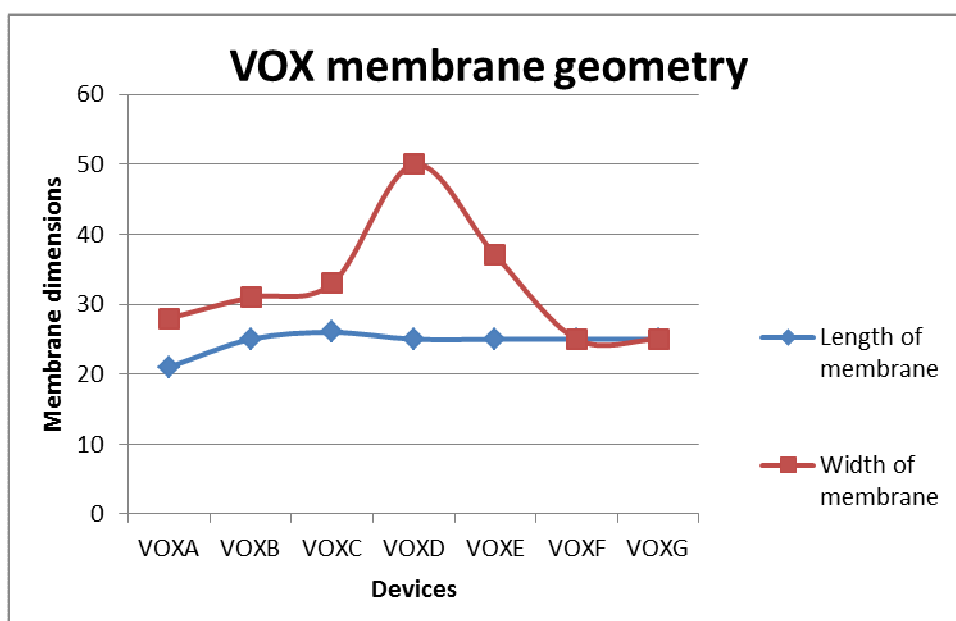


Figure 4-21: Length and width variation

4.4 Analysis approach

The first analyses were conducted in order to determine the change in temperature of the chosen bolometer membrane design. For a single bolometer pixel membrane, a heat flux was applied to the absorption surface area. This heat flux was varied from 500 - 10000pW/m², i.e. 11 analyses. Each of these analyses were conducted at initial temperatures ranging from 263 - 303K with increments of 5K resulting in 8 analyses per applied heat flux. The total static analyses performed to obtain the device thermal conductance are thus 88. For all thirteen devices, the number of analyses performed to determine their individual thermal conductance was 1144.

The dimensional ranges of the devices were as stipulated on the device details with changes to the support legs at increments of 3µm for the first six bolometer devices: MET2, MET3, MET4, VOX2, VOX3 and VOX4. Each geometrical change was exposed to a range of ambient temperature changes at increments of 5K. This increase in temperature produced maximum thermal

deformations in the Z-direction of all pixels. Deformations in the Y-direction appear unchanged for all pixels while a slight increase in deformation is observed in the X-direction as the pixel width is decreased. A graphical representation of these results is shown below. The maximum deformation occurs in the centre of beams for metal bolometer and on the edges of legs for the Vanadium oxide bolometer as shown in Figures 4.22 and 4.23.

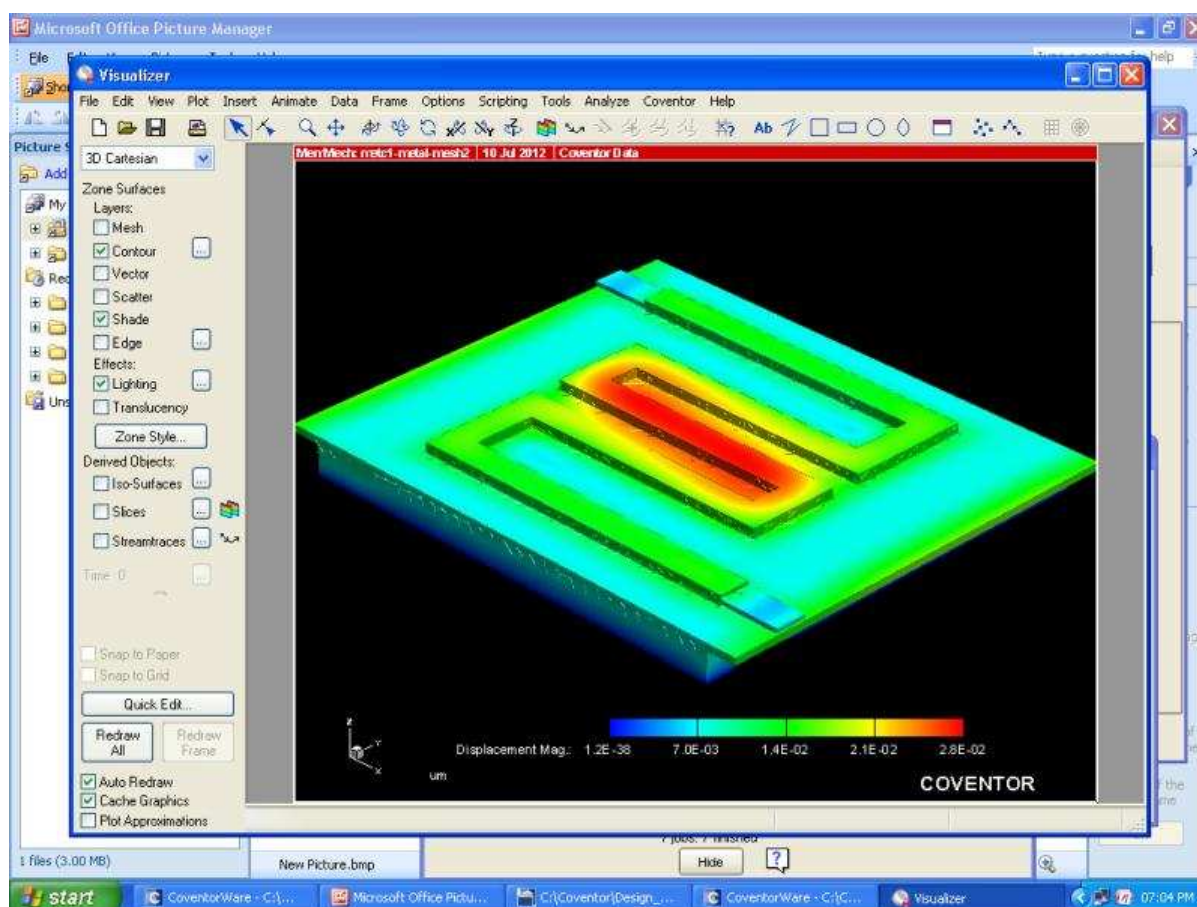


Figure 4-22: Titanium bolometer thermal deformations displacement

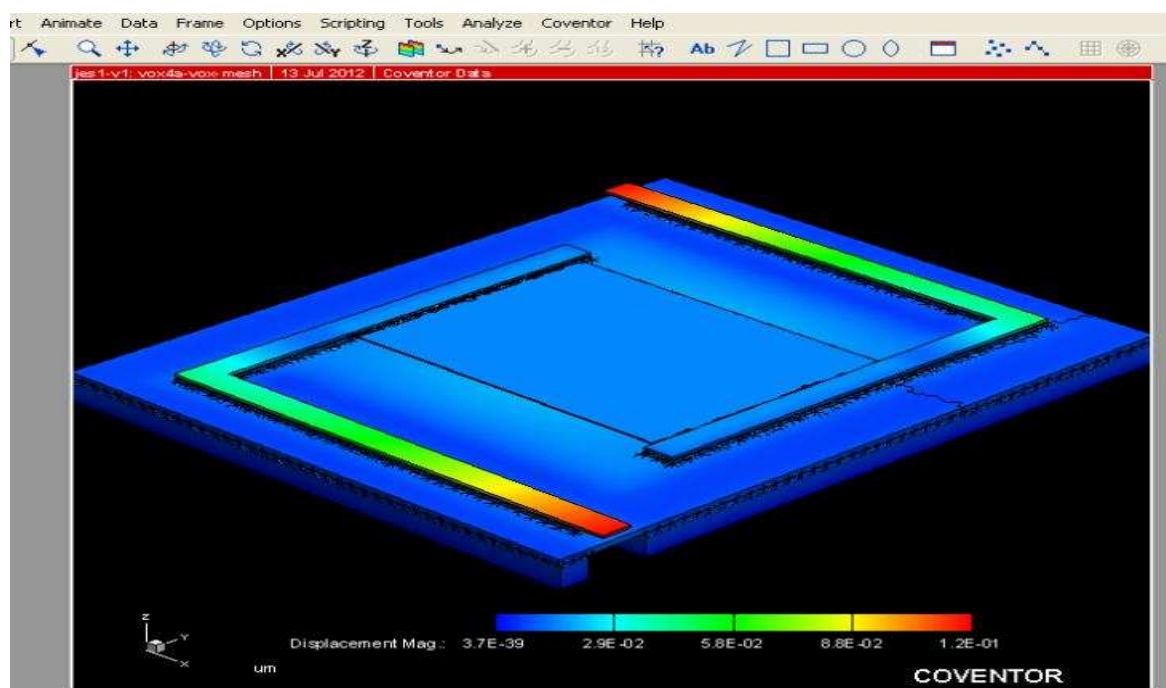


Figure 4-23: VOx bolometer thermal deformations displacement

Change in heat (W) vs. nodal displacement (L) for VOX2

At temperature of 300K with no changes to the geometrics, it was observed that the change in wattage is proportional to the device displacement. It was further noted that the more heat flux applied, the more signs of deformation became apparent. With the incremental increase of the heat flux at 500 – 10000, the nodal temperatures also increased in increments of 0.001 degrees Celsius. This resulted in a nodal displacement of $8.3388\text{E-}3\mu\text{m}$ as shown in Figure 4.24. The relationship between the changes in heat to that of the nodal changes is as shown graphically on an Y-X plot. The changes to the Y-direction can be mathematically derived by the following equation: $y = 0.0167x - 0.0083$ and the change in temperature by $y = 0.001x - 1\text{E-}14$.

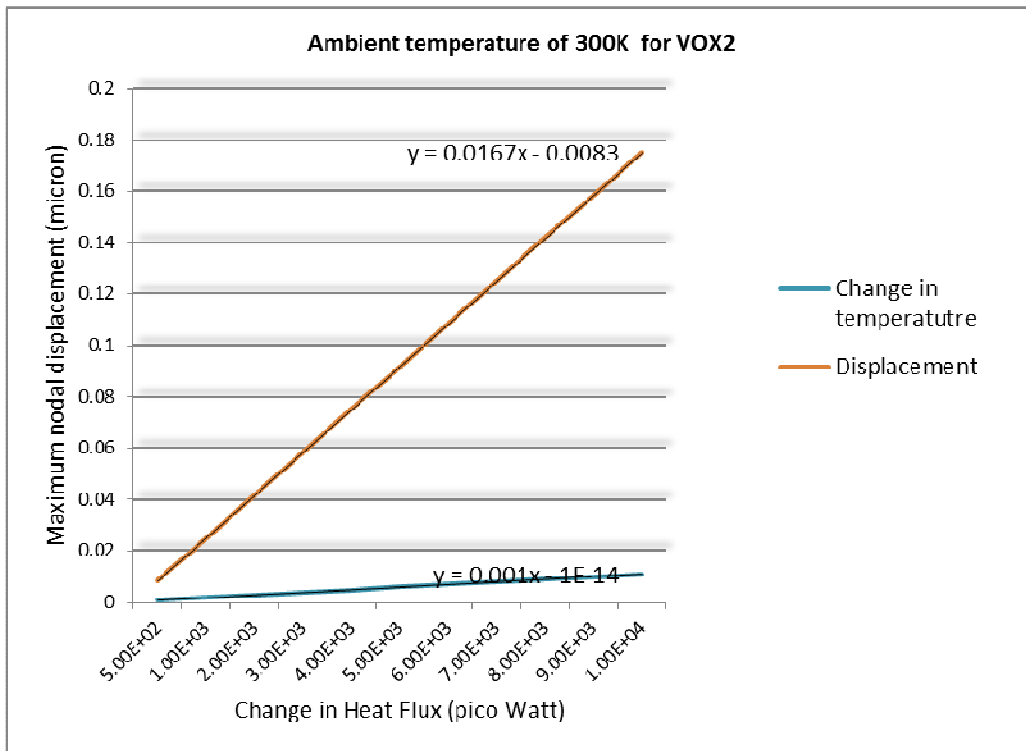


Figure 4-24: VOX2 L vs W at ambient temperature of 300K

The ‘VOX3’ range: VOX3: change in temperature (K) vs nodal displacement (L)

Temperature is a measurement of heat. The change in heat results will have the same effects to the device geometrics. As a result, the below graph of figure 4.25, depicts the same relationship to that of the L (displacement) vs W (heat).

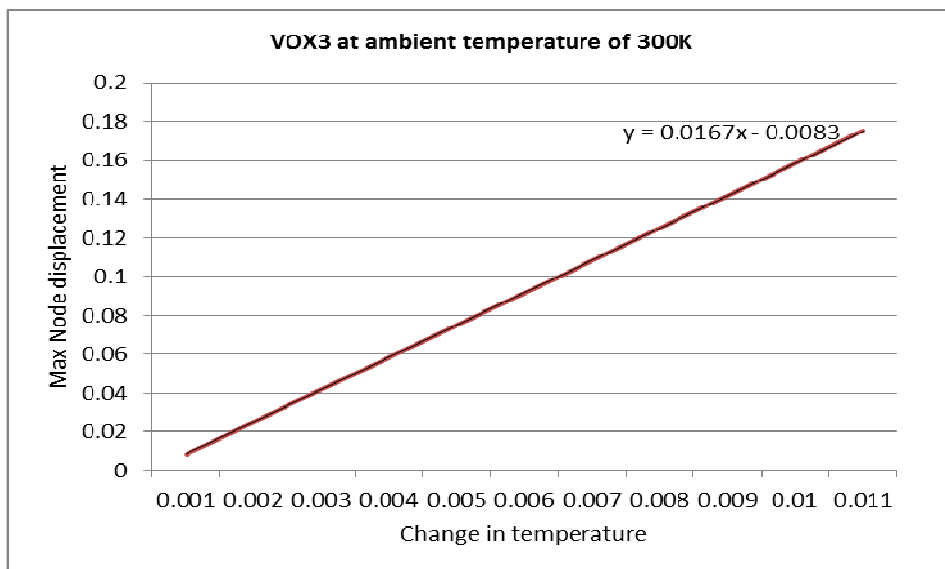


Figure 4-25: VOX3 L vs W at ambient temperature of 300K

Change in heat (W) vs. nodal displacement(L) for MET2

The changes to the Y-direction can be mathematically derived by the following equation: $y = 0.0167x - 0.0083$ which shows the same variation almost with VOX2 at the same temperature as shown in Figure 4.26.

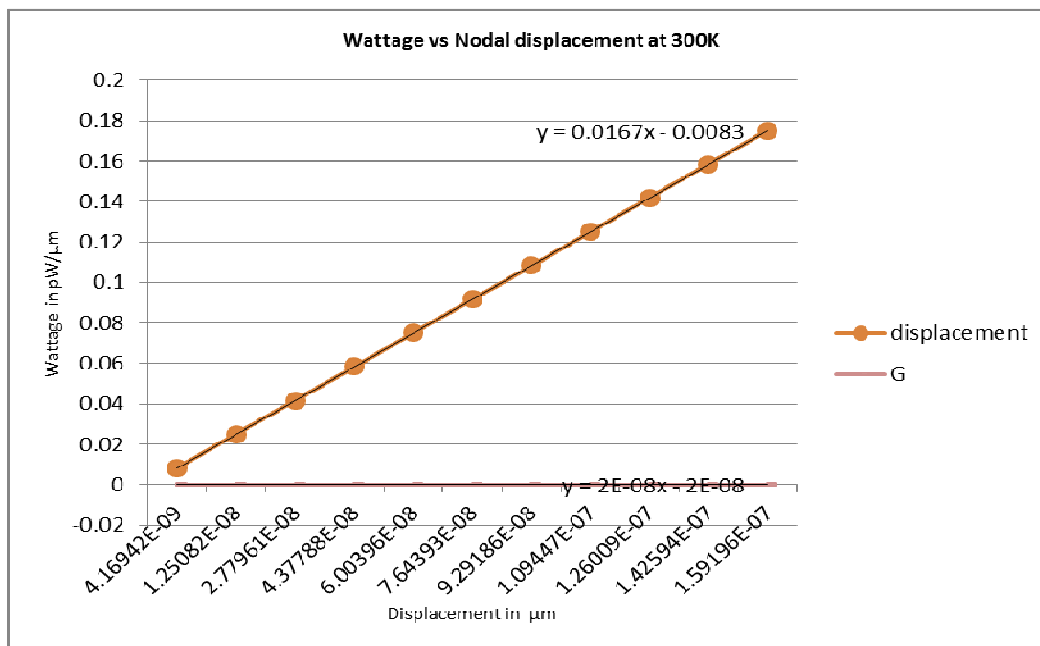


Figure 4-26: MET2 L vs W at ambient temperature of 300K

Change in heat (W) vs. nodal displacement(L) for VOX3

The change in heat is dependent on the change in temperature. Any increase in wattage has a direct influence on the increase in temperature as it is shown in figure 4.27. The changes to the Y-direction can be mathematically derived by the following equation: $y = 0.1298x + 0.5048$

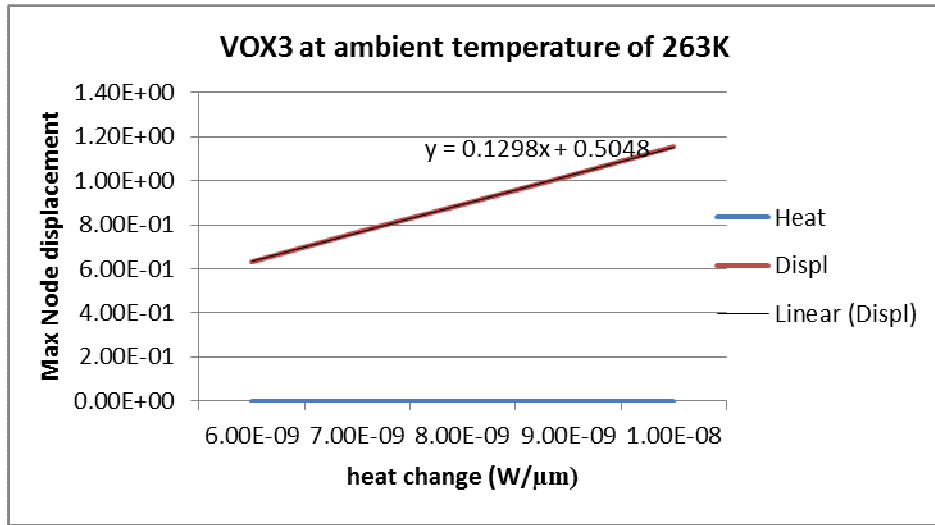


Figure 4-27: VOX3 L vs W at ambient temperature of 263K

The “MET4” range: MET4: change in heat (W) vs. displacement (L)

The change in heat is directly proportional to change in temperature. Any increase in wattage has a direct influence on the increase in temperature, Figure 4.13. $y = 0.0204x - 0.0171$.

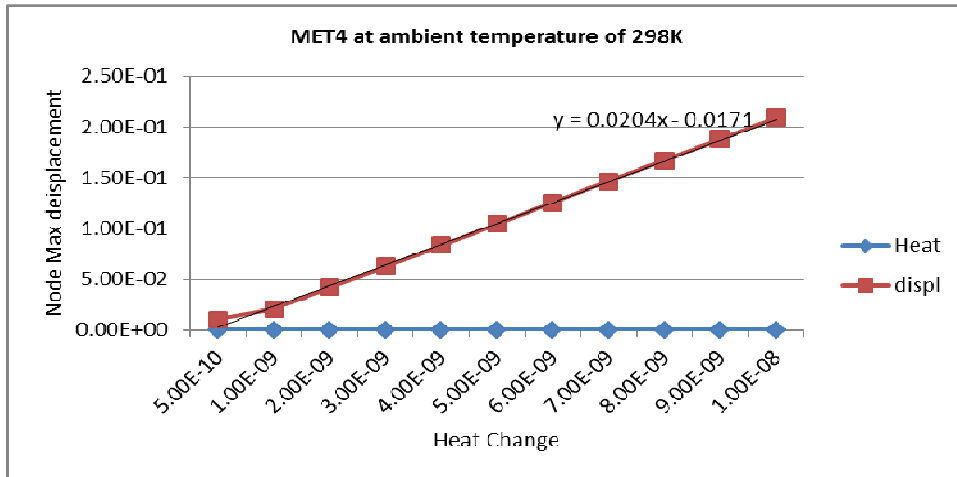


Figure 4-28: MET4 W vs L at ambient temperature of 298K

The 'VOXA' range @ 273K:VOXA: change in heat (W) vs. nodal displacement (L)

The following graph reflects a mixed reaction to the increase of heat flux. The graph initially reflects an inverse ratio relation between the change in heat and the change in nodal displacement. With an applied heat flux of 500, the change in heat is at 1.522282E-08 watts. This obviously changes the nodal displacement by 0.304563 μm . The y-changes are reflected as follows:

$$y = 0.0642x + 0.2487$$

This is an indication of some real movements on the membrane as it reacts under different loading conditions as it is presented in figure 4.29.

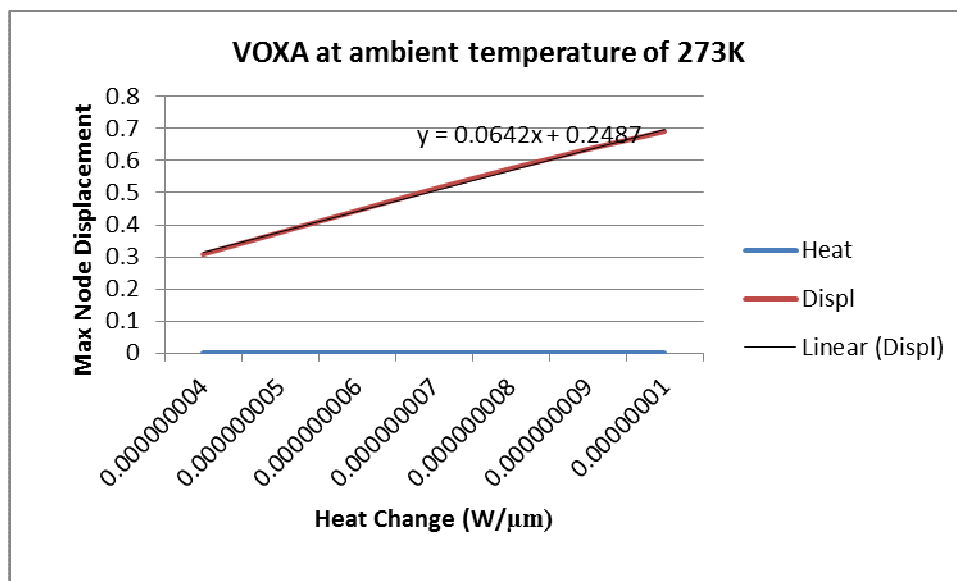


Figure 4-29: VOXA W vs L at ambient temperature of 273K

The 'VOXB' range @ 278K:VOXB: change in Heat (W) vs. Nodal Displacement (L)

The following graph reflects a mixed reaction to the increase of the heat flux as the previous graph for VOXA. The graph initially reflects a horizontal ratio relation between the change in heat and the change in nodal displacement from an applied heat flux of 500pW until 4000pW. In that interval the wattage

varies around $8\text{E-}08$ watts. This obviously changes the nodal displacement by around $0.29\mu\text{m}$. The y-changes are reflected as follows:

$$y = -0.0642x + 0.2487.$$

This is an indication of some real movements on the membrane as it reacts under different loading conditions, Figure 4.30.

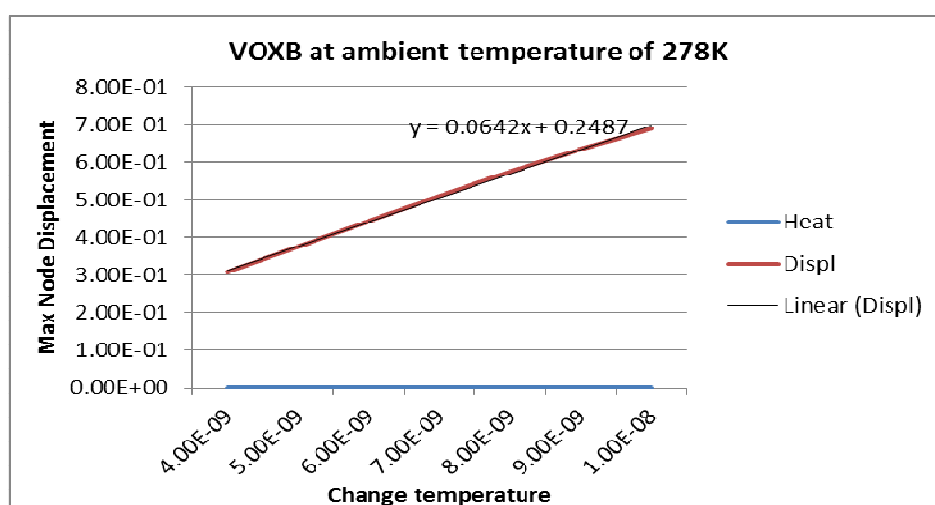


Figure 4-30: VOXB W vs L at ambient temperature of 278K

4.5 Static analysis at atmospheric pressure

Working at atmospheric the thermal conductance given in figure 4.4 will depend on the following:

- Conductance through the legs supporting the membrane called G_{leg}
- Conductance through surrounding gas, G_{gas}
- Conductance due to radiation G_{rad}

$$G_{total} = G_{leg} + G_{gas} + G_{rad} \quad (4.3)$$

Conductance through legs

This parameter is given by the equation below:

$$G_{leg} = \lambda_{leg} \frac{W_{leg} d_{leg}}{l_{leg}} = \lambda_{leg} \frac{d_{leg}}{N_L} \quad (4.4a)$$

Where

W_{leg} = width of supporting leg

d_{leg} = thickness of supporting leg

l_{leg} = length of supporting leg

λ_{leg} = thermal conductivity of supporting leg material

N_L = number of thermal squares per leg given by the equation below:

$$N_L = \frac{E}{F} + 0.56 + \frac{B - F}{F} \quad (4.4b)$$

Where B, E and F can be read in Tables 3:1 – 3:3.

In calculating G_{leg} , it is assumed that conduction is completely due to conduction through supporting legs, and conduction within the membrane plate is negligible.

Example of calculations for VOX2 and MET4

$$VOX2: N_L = \frac{2}{4} + 0.56 + \frac{31 - 4}{4} = 7.81$$

$$G_{leg} = 3.07 \times 10^{-5} \times \frac{2}{7.86} = 7.86 \times 10^{-6} W/K$$

$$MET4: N_L = \frac{4}{10} + 0.56 + \frac{37 - 10}{10} = 3.66$$

$$G_{leg} = 2.19 \times 10^{-5} \times \frac{4}{3.66} = 2.39 \times 10^{-5} W/K$$

Conductance through surrounding gas

This is found by the following formula

$$G_{gas} = \lambda_{gas} \frac{A_{mem}}{S} \quad (4.5)$$

Where

A_{mem} = membrane area

s = membrane to substrate separation

λ_{gas} = gas thermal conductivity

Thermal conductance through gas can be neglected under low pressure (10^{-3} to 10^{-4} mbar) conditions; therefore G_{leg} will be dominant thermal conductance.

Conductance due to radiation

This is determined through the formula below:

$$G_{\text{rad}} = 4\sigma\varepsilon A_{\text{mem}} T^3 \quad (4.6)$$

Where

σ = Boltzmann constant = 5.67×10^{-8} W/m²K

ε = effective emissivity \cong 0.88 for metal film bolometer with coating (J-S. Shie all. "Characterisation and modelling of metal-film microbolometer", Journal of microelectromechanical systems, Vol 5, No.4, pp 303, December 1996).

A_{mem} = membrane area

T = temperature

Calculated results for G_{leg} of all devices analysed are shown in Table 4.17 below:

Table 4-13 Calculated Thermal conductance at atmospheric conditions

Devices	G_{total} (W/K)
MET2	5.79E-06
MET3	1.36E-05
MET4	2.39E-05
VOX2	7.86E-06
VOX3	1.90E-05
VOX4	3.36E-05
VOXA	2.31E-05
VOXB	2.31E-05
VOXC	2.31E-05
VOXD	2.31E-05
VOXE	1.61E-05
VOXF	8.72E-06
VOXG	1.26E-05

4.6 Summary

Chapter 4 presents the results of thermomechanical analyses performed and the thermal conductance of the devices that was found, which is the first step in the determination of a bolometer's responsivity. Using the analytical model and static analyses, equations were presented and the behaviour of membranes' functions of changing temperatures have been noted and studied.

Tables 4-6:4-13 present different results of static analyses that provide devices' thermal conductance.

Table 4-13 shows thermal conductance of all thirteen pixel membrane bolometers determined at an ambient temperature of 300 K, from what vary behaviours have been noticed and challenged.

In the first set of pixels; MET2, 3 and 4, devices' thermal conductance vary following a logarithmic function as shown in figure 4.16, that is dependent to the length and width variations, see figure 4.17. It follows that devices' thermal

conductance depend on the two factors above mentioned, therefore MET4 has the highest thermal conductance because of its biggest width and the longest length while MET2 that has the lowest, has also the smallest thermal conductance.

In the second set of bolometer membranes the variation is following an exponential function for both the thermal conductance and the geometry properties; length and width.

The last set of VOX bolometer provides a different variation behaviour, which does not depend only with the width and length, but also with the membrane's support length. From this set VOXD has the lowest thermal conductance because of its small membrane pixel's width.

Table 4.13 provides results of analysis expressed in terms of thermal conductance that presents the thermal resistance (isolation) between the suspended plate (microbolometer pixel) and its substrate and surroundings, allowing the plate to respond to incident IR radiation by getting warmer or cooler. Comparing all FPA membrane bolometers analysed, it has seen that MET2 for Metal bolometer, VOX2 and VOXD for Vanadium oxide bolometer have the lowest thermal conductance, therefore they are preferred to the other because a low thermal conductance provides a required high thermal isolation as demonstrated by Honeywell USA on the compact portable uncooled IR cameras. Despite the fact that MET3 and VOX3 have the same geometric dimensions, the Titanium bolometer presents a lower thermal conductance than the vanadium, therefore Titanium is preferred to Vanadium oxide due to its low thermal conductance as presented by Frank Nikluas in pros. of SPIE Vol. 6836 68360D-15, in 2007.

It is also noticed that thermal conductance is smaller in vacuum than at atmospheric pressure, which allows the bolometer to perform better in vacuum, as the thermal isolation of the vacuum is higher than for air, this was demonstrated by M Zimmermann in 2001.

To conclude this chapter some observations of the devices are made and explained below;

The peak temperature of MET bolometers is reached at the highest thermal load applied; i.e. $10\ 000\text{pW}/\mu\text{m}^2$ when working with the ambient temperature of 288K, 293K, 298K, 300K and 303K.

In general the displacement of MET devices is proportional to the Heat load and varies with an increment that is of about $0.0166776\ \mu\text{m}$ for MET2 in particular. The displacement is proportional to the change in heat and change in temperature.

The peak temperature for VOX devices is also reached at $10\ 000\text{pW}/\mu\text{m}^2$ and at higher ambient temperature and the displacement increase following a fixed increment, with $0.0040291\ \mu\text{m}$ for VOX2 in particular.

It has also been noticed that VOXB, VOXD, VOXE and VOXF have the same displacement behaviour, increment and peak temperature, while they have different geometry properties. This can be understood in the way that even though their geometries differ, the combination of width, length and support legs put in almost the same range, that influences their thermal and physical properties.

Chapter Five

5. Results and Discussions of Dynamic Analyses

The objective of dynamic analyses was to determine Thermal Capacity of the bolometer membranes defined by equation 5.1 below:

$$H = \tau \times G \quad (5.1)$$

where H is the thermal capacity in Joule per Kelvin (J/K);

τ is the time constant for heating and cooling of the membrane in second (s);
and

G is the thermal conductance.

5.1 Thermal modelling

Thermal Capacity of the bolometer membranes can also be determined analytically knowing the thermal properties of membrane bolometers.

In general, the heat capacity is given by

$$H = V\rho c \quad (5.2)$$

Where V = volume of the detector membrane;

ρ = the density of the membrane material; and

c = the specific heat of the membrane material.

The thermal time constant is as shown in Equation 5.3 below:

$$\tau = \frac{H}{G} \quad (5.3)$$

where H is the thermal heat capacity, and

G is the thermal conductance.

And the volume is given by

$$V = (A_{\text{membrane}} + A_{\text{leg}}) \cdot d \quad (5.4)$$

where d is the width used in CoventorWare for all the devices. A_{membrane} is the membrane area of bolometers and A_{leg} is the area of their supporting legs.

For this matter $d = 1 \mu\text{m}$.

The performance of a bolometer detector is characterised by factors like temperature coefficient of resistance (TCR), responsivity (R_v), and detectivity (D) which is analysed in this research as thermal sensitivity defined by low thermal conductance, low heat capacitance and short thermal time constant as shown in equations 5.5 to 5.8.

$$TCR = \alpha = R^{-1} \frac{dR}{dT} \quad (5.5)$$

We assume that the vanadium oxide thin film that are used have TCR in the range of 2 %/K and 3 %/K at room temperature as C. Chen et al in 2001, which is today used in a variety of bolometer products. The α -Si microbolometer arrays have a TCR up to 3 %/K at ambient temperature as published by A.J. Syllaios et. al. in 2000. High TCR provides maximum sensitivity to thermal variation in the detector which is why metal films make

good bolometer detectors as demonstrated by V.K Jain et. al. in 1997. Therefore in this thesis a TCR of 3 %/K has been used.

$$R_v = \frac{I_b R \alpha \eta}{G \sqrt{1 + f^2 \tau^2}}$$

Where

I_b = bolometer bias current

R = bolometer resistance

$$R = R_0(1 + \alpha(T - T_0)) \quad (5.7)$$

$(1 + \alpha(T - T_0))$ = displacement (thermal expansion) due to changing in temperature

R_0 depends on the electrical resistivity of the bolometer material

f = modulation frequency

In this thesis we assumed a modulation frequency of 10Hz based on results got by A. Moftakharzadeh et. al. (EUCAS 2007), where they demonstrated that 10Hz was a good frequency and higher frequencies create more intense effect of thermal noise, reducing the responsivity.

P = bolometer bias power given by

$$P = I_b^2 \times R \quad (5.8)$$

A heated body gives off thermal radiation. From the Wien's displacement law, the Wavelength of the heat expelled from the human body is around 9500nm. Typically the Human body expels Heat of $P_{net}=95$ Joule/second or Watt (W).

Considering that a distance separates the body (object) to the device, we assumed that 5W is lost from the body over the distance which results to the amount of heat reaching the device's surface to be 90W. The resulting heat flux that is incident on the surface is approximately 10^4 pW/m².

η = absorptivity of IR sensitive film. It has been demonstrated experimentally that metal alloy films, porous metal, and metal blacks have an absorbance of 90% and presented by Y. Sui et. al. in 2012.

5.2 Determination of thermal properties

Table 5.1 below shows thermal and physical parameters required to determine thermal properties of the membrane bolometers.

Table 5-1 Thermal and physical parameters

Material	Specific heat (J/gK)	Density g/cm ³
Gold	0.129	19.3
Titanium	0.523	4.51
Vanadium oxide	0.39	3.36
CVD Silicon dioxide	1	2.22
CVD Silicon nitride	1.2	3.1

Using the values in Tables 5.1, 3.1, 3.2 and 3.3, and Equations 5.2 and 5.3, the thermal properties (heat capacity and thermal time constant) are found for both in vacuum and atmosphere as shown in Table 5.2 and 5.3 below:

Table 5-2 thermal parameters in vacuum

Devices	Thermal Heat Capacitance (J/K)	Thermal Conductance G (W/K)	Thermal time constant (Second)
MET2	2.33E-09	4.67E-07	4.99E-03
MET3	3.58E-09	7.16E-07	5.00E-03
MET4	4.64E-09	8.26E-07	5.61E-03
VOX2	2.11E-09	4.81E-07	4.39E-03
VOX3	3.12E-09	7.26E-07	4.30E-03
VOX4	4.06E-09	1.02E-06	3.98E-03
VOXA	4.07E-09	1.08E-06	3.78E-03
VOXB	3.28E-09	1.09E-06	3.00E-03
VOXC	2.56E-09	9.62E-07	2.66E-03
VOXD	1.83E-09	4.78E-07	3.82E-03
VOXE	2.97E-09	9.90E-07	3.00E-03
VOXF	2.34E-09	5.59E-07	4.19E-03
VOXG	2.09E-09	9.80E-07	2.13E-03

Table 5-3: Thermal parameters at atmospheric

Devices	Thermal Conductance G (W/K)	Thermal Heat Capacitance (J/K)	Thermal time constant (Second)
MET2	5.79E-06	2.33E-09	4.02E-04
MET3	1.36E-05	3.58E-09	2.63E-04
MET4	2.39E-05	4.64E-09	1.94E-04
VOX2	7.86E-06	2.11E-09	2.68E-04
VOX3	1.90E-05	3.12E-09	1.64E-04
VOX4	3.36E-05	4.06E-09	1.21E-04
VOXA	2.31E-05	4.07E-09	1.76E-04
VOXB	2.31E-05	3.28E-09	1.42E-04
VOXC	2.31E-05	2.56E-09	1.11E-04
VOXD	2.31E-05	1.83E-09	7.92E-05
VOXE	1.61E-05	2.97E-09	1.84E-04
VOXF	8.72E-06	2.34E-09	2.68E-04
VOXG	1.26E-05	2.09E-09	1.66E-04

Using tables 5.2 and 5.3 and equations 5.1 – 5.8, the thermal responsivity were also found for all thirteen pixel bolometers in vacuum and results are presented in table 5.4.

Table 5-4: Bolometer pixel thermal responsivity in vacuum

Device	Responsivity (V/W)
MET2	8.09E-02
MET3	5.18E-02
MET4	4.47E-02
VOX2	9.40E-02
VOX3	6.47E-02
VOX4	5.23E-02
VOXA	6.85E-02
VOXB	6.95E-02
VOXC	6.84E-02
VOXD	3.12E-02
VOXE	3.67E-02
VOXF	3.67E-02
VOXG	4.32E-02

Thermal load was applied as shown in figure 5.1. It has been applied from 0.0 to 10 000 pW/ μm^2 on MET2 over a time period of 4.0 μs , then it drops from 10 000 to 0.0 pW/ μm^2 in 0.1 μs . Thermal behaviour represented by the heating vs cooling curves is shown if figure 5.2.

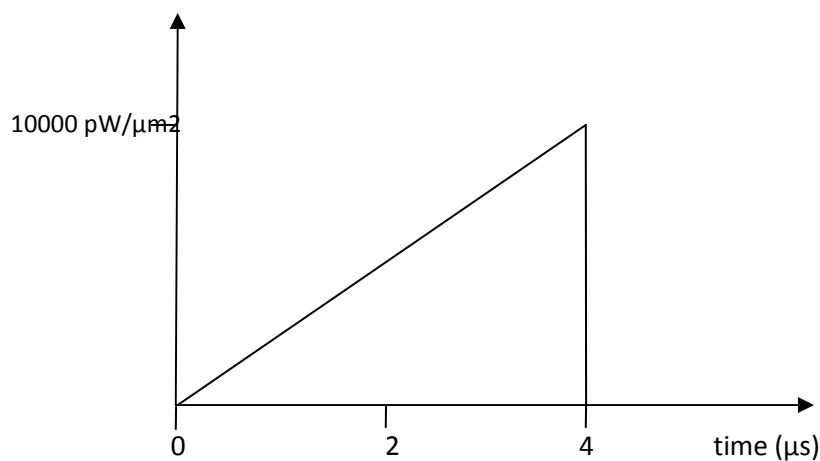


Figure 5-1: Applied heat on MET2 for 4 micron second

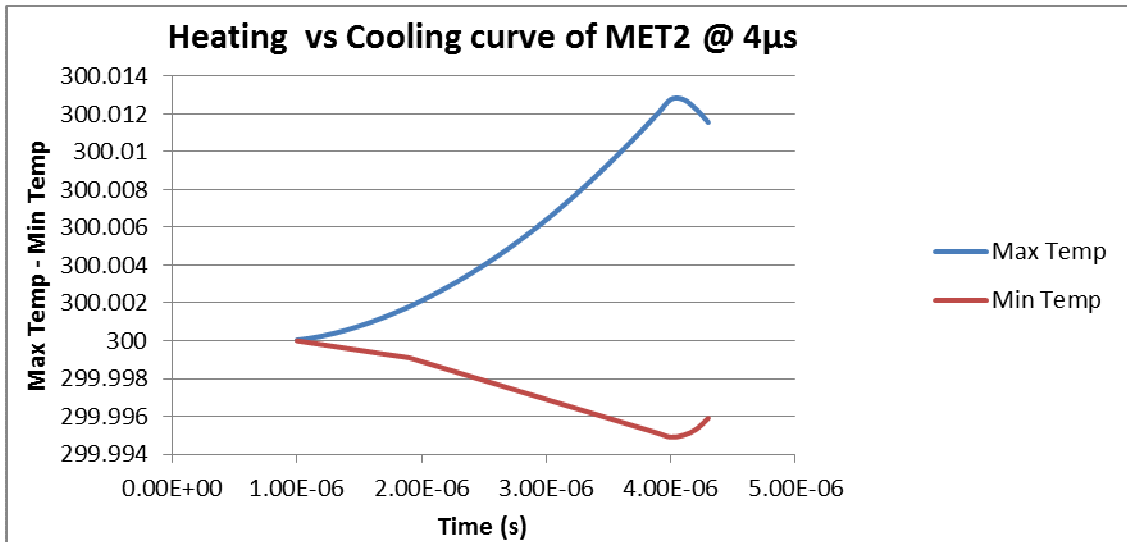


Figure 5-2: Heating vs Cooling curve of MET2 @ 4µs

In order to determine the thermal time constant, the maximum temperature Heating vs Cooling curve must be considered with the heating and cooling parts of the curve represented separately as shown in figures 5.3 – 4.

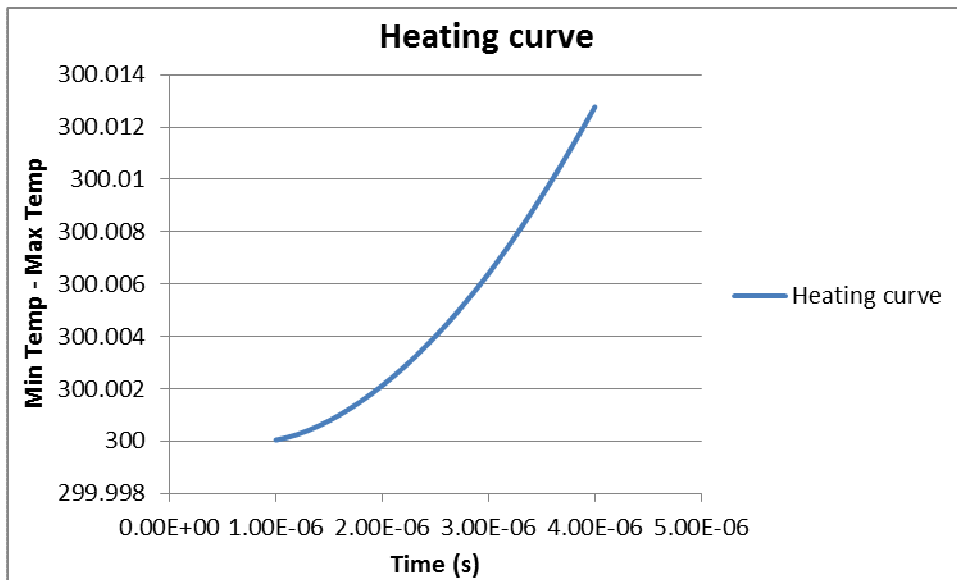


Figure 5-3: Heating Curve for MET 2

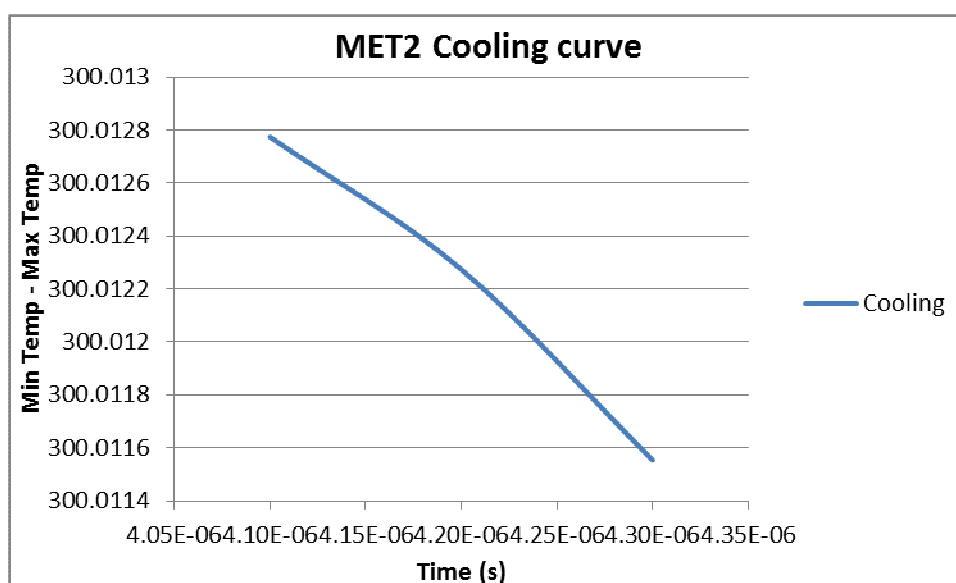


Figure 5-4: Cooling Curve for MET2

These curves can be represented by two exponential equations found using the Excel Trendline. The heating curve is given by $299.99 E14.246x$ while the cooling is represented by $300.04 E-20.34x$.

To determine the thermal time constant, a solution of an exponential equation that satisfy the Newton's law of cooling, expressed by equation 5.9 below have been used.

$$T(t) = T_0 e^{-t/\tau} \quad (5.9)$$

Where τ is the thermal time constant.

Using equation 5.9 with the initial ambient temperature of 300 K, after solving the two parametric equations from excel, the thermal time constant has been determined as shown bellow;

Heating : $T_{\text{HEATING}} = 5.7 E-05$ second and

$$T_{\text{COOLING}} = 8.14 E-05 \text{ second}$$

From this, the thermal time constant is then found

$\tau = 1.38 \text{ E-}04$ second, which is hundred times lower than the analytical value of thermal constant.

In the same way the previous analysis on MET2, MET3 got analysed but the thermal load was applied on the top surface for a time period of $3.0 \mu\text{s}$ (see graph in fig 5.5).

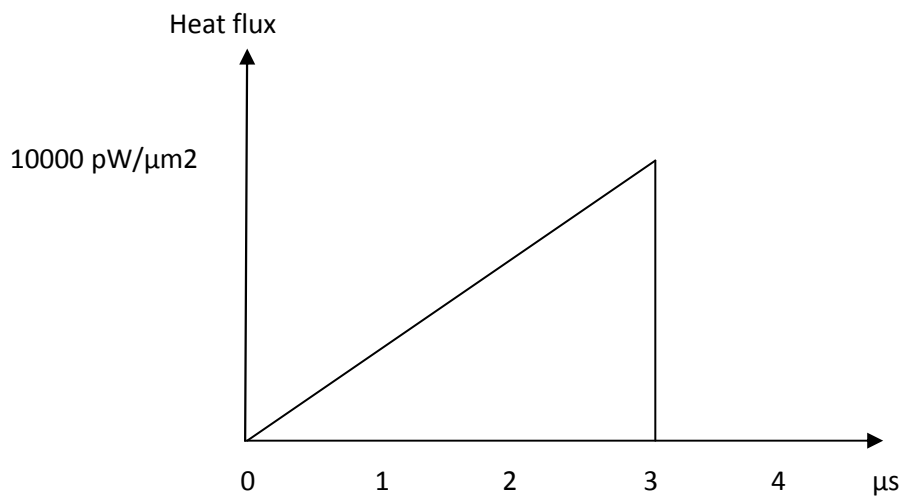


Figure 5-5: Applied heat flux on MET3 @ $4 \mu\text{s}$

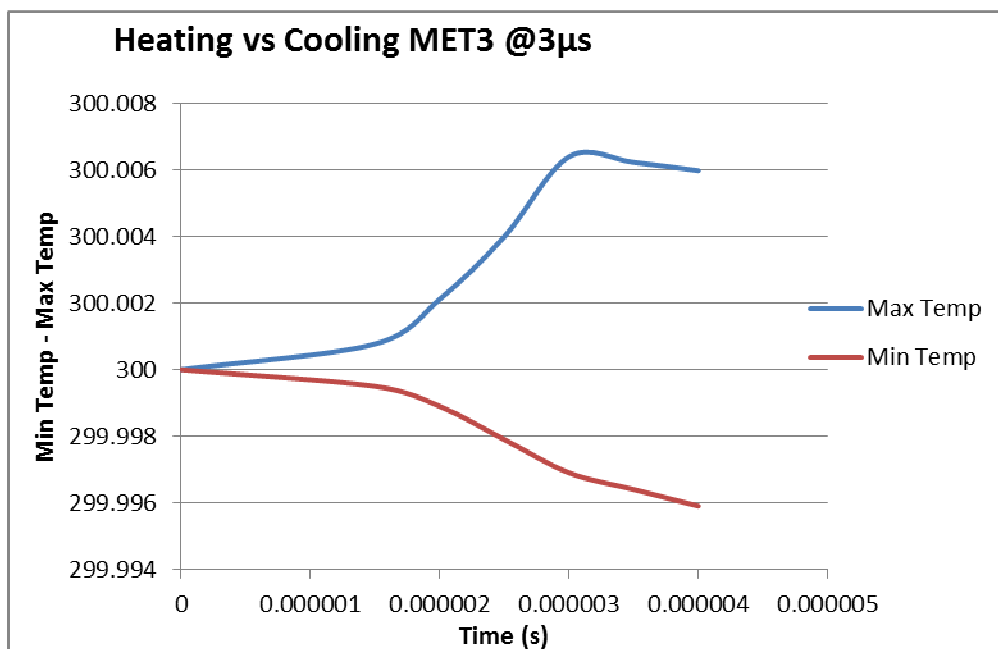


Figure 5-6: Heating and Cooling curve of MET3 over $3 \mu\text{s}$

The heating and cooling curves of MET3 represented separately are expressed by the following two exponential parametric equations

$y = 300e^{6.714 \cdot x}$ for heating and $y = 300.01e^{-1.4}$ for cooling.

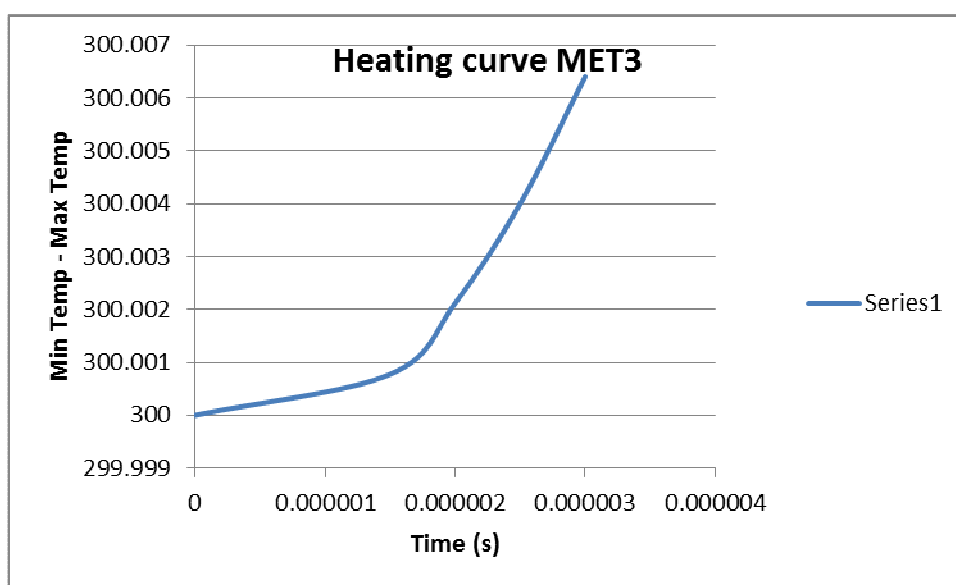


Figure 5-7: Maximum temperature heating curve

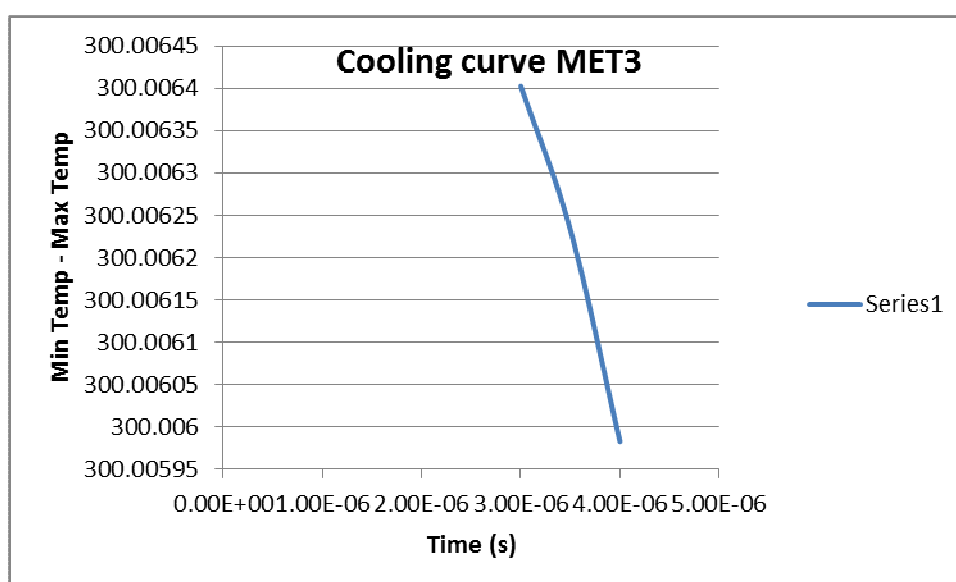


Figure 5-8: Maximum temperature cooling curve

Heating: $T_{\text{Heating}} = 2.6856 \text{ E-05}$ second, and

Cooling: $T_{\text{Cooling}} = 5.6 \text{ E-06}$ second

Therefore thermal time constant of MET3 is 3.25 E-05 second. This has also improved of about hundred times of the analytical results found from literature.

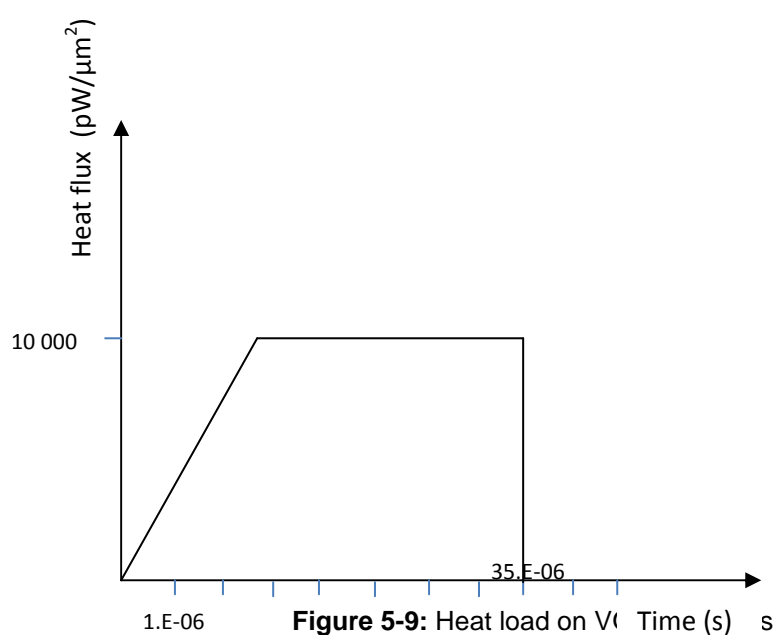


Figure 5-9 shows that a thermal load of 0.0 to $10\,000 \text{ pW}/\mu\text{m}^2$ was applied to the top surface of the membrane of VOX3. The initial ramping of the load, i.e. from 0.0 to $10\,000 \text{ pW}/\mu\text{m}^2$ occurred over a period of $3.0\mu\text{s}$. The load was then held at $10\,000 \text{ pW}/\mu\text{m}^2$ for a further $32.0\mu\text{s}$. The entire analysis time was thus $35\mu\text{s}$. The heating vs cooling curves are shown in Figures 5.10 – 12. And thermal time constants for heating and cooling were found using equation 5.9.

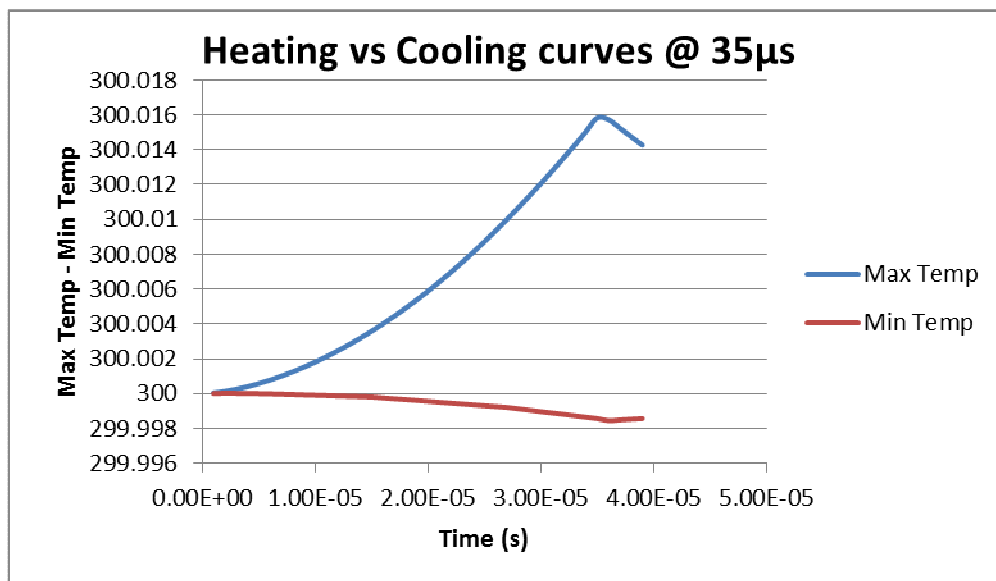


Figure 5-10: Heating vs Cooling curves of VOX3

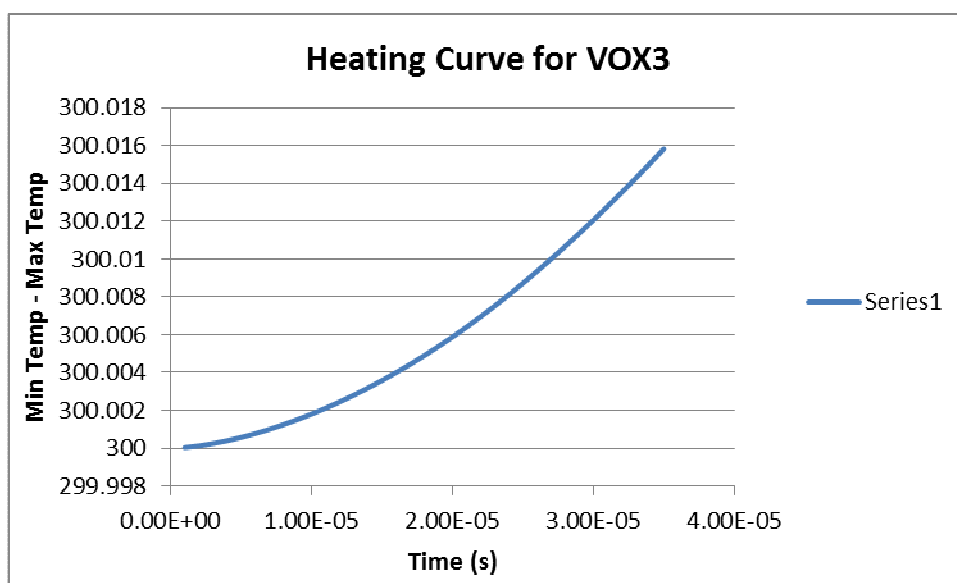


Figure 5-11: Heating curve of VOX3

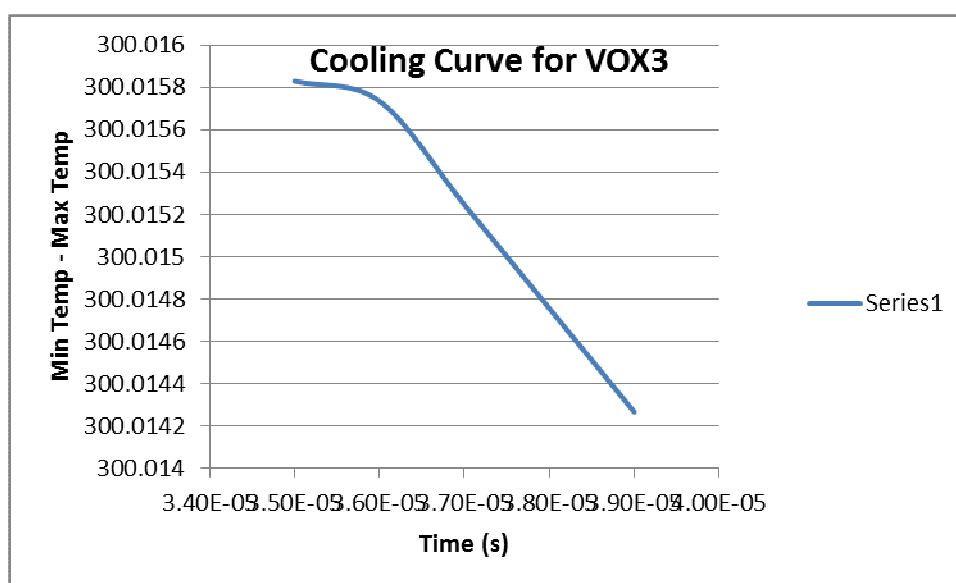


Figure 5-12: Cooling curve of VOX3

From the parametric equations; $y = 300e15.613x$ for heating and $y = 300e3E-30.44.x$ for cooling, the thermal time constant is found.

Heating: $T_{\text{Heating}} = 5.78E-4$ second, and

Cooling: $T_{\text{Cooling}} = 1.126E-3$ second

Therefore the thermal time constant of VOX3 over 35 μs of thermal loading is as below;

$\tau = 1.704 E-03$ second.

For the third set of Vanadium oxide bolometer, dynamic analysis were conducted on two devices VOXA and VOXF. The heat flux was applied the same way as for VOX3 and their curves are shown in figures 5.13 and 5.14 respectively.

Thermal time constants for these devices are found using equation 5.9 and given below.

$\tau = 1.22 E-03$ second for VOXA and $\tau = 1.51 E-03$ second for VOXF

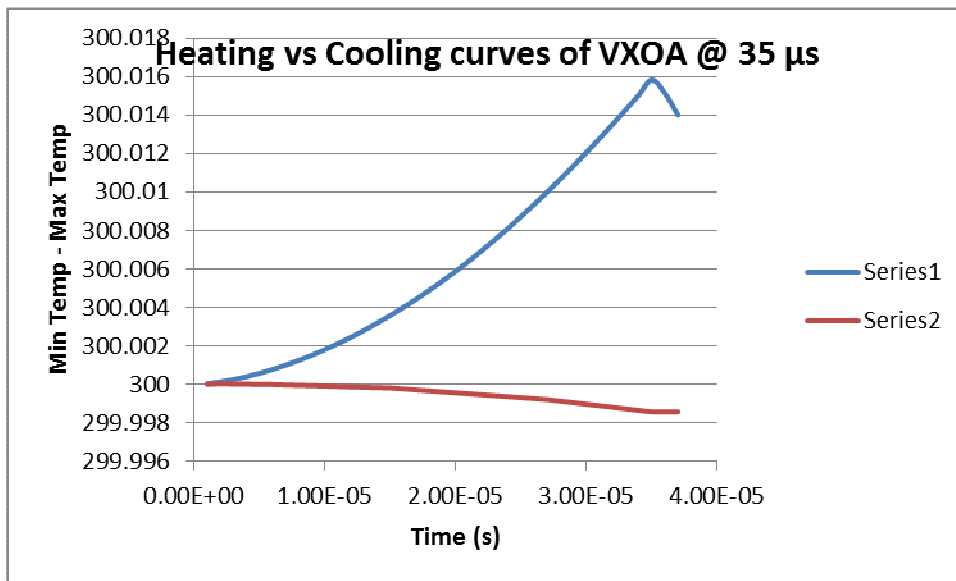


Figure 5-13: Heating vs Cooling curves @ 35 μ s

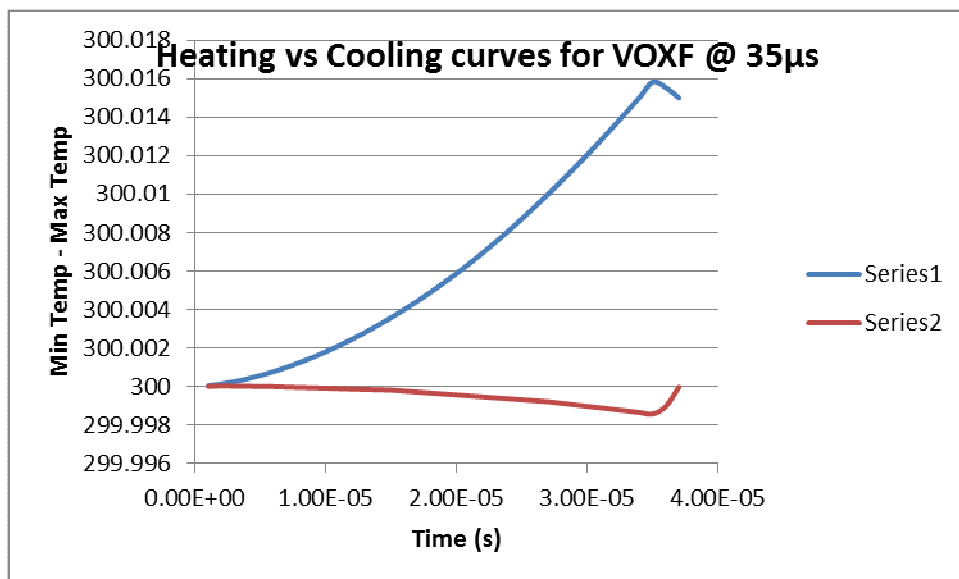


Figure 5-14: Heating vs Cooling for VOXF @ 35 μ s

Figure 5.15 and figure 5.16 present data collected and thermal behavior of VOX3 in CoventorWare from dynamic simulations respectively. Simulations of these analyses took longer than expected up to 590 days as shown in figure 5.17 which limited opportunities for further investigations, reason why only 5 analyses were done. And figures 5.18 shows one Vox pixel membrane at

peak temperature during the transient or dynamic thermo mechanical analyses.

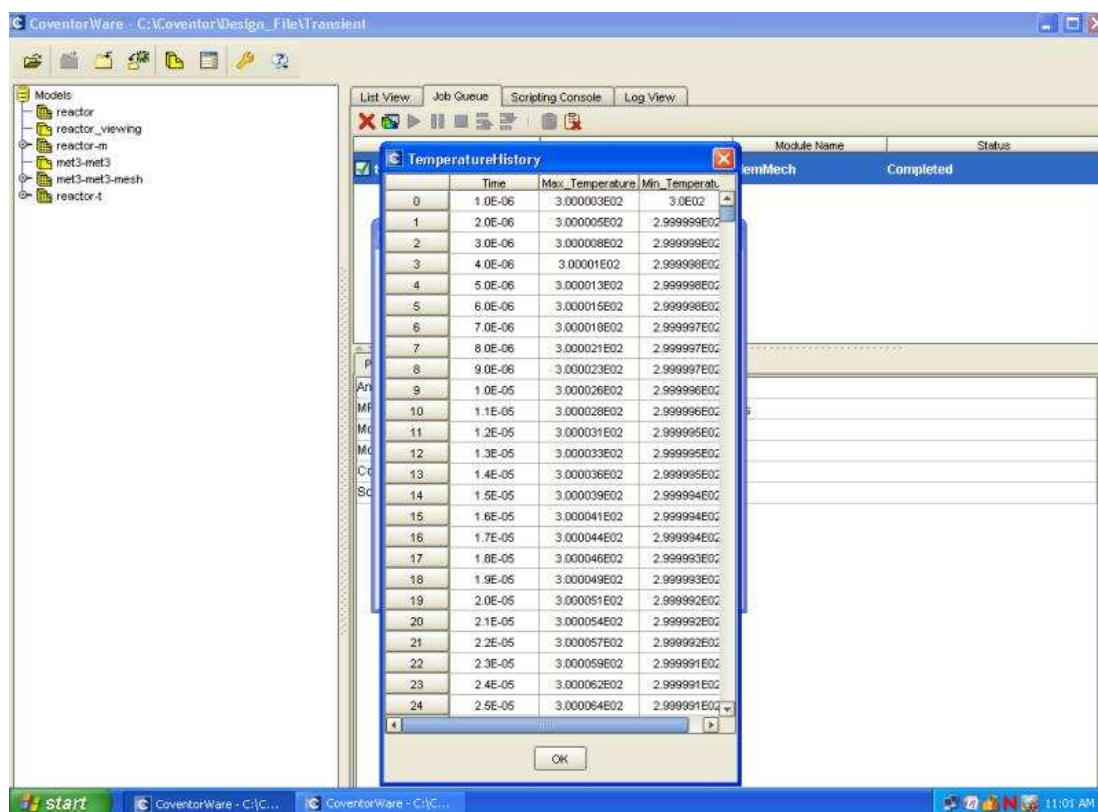


Figure 5-15: MET2 dynamic simulations data collected

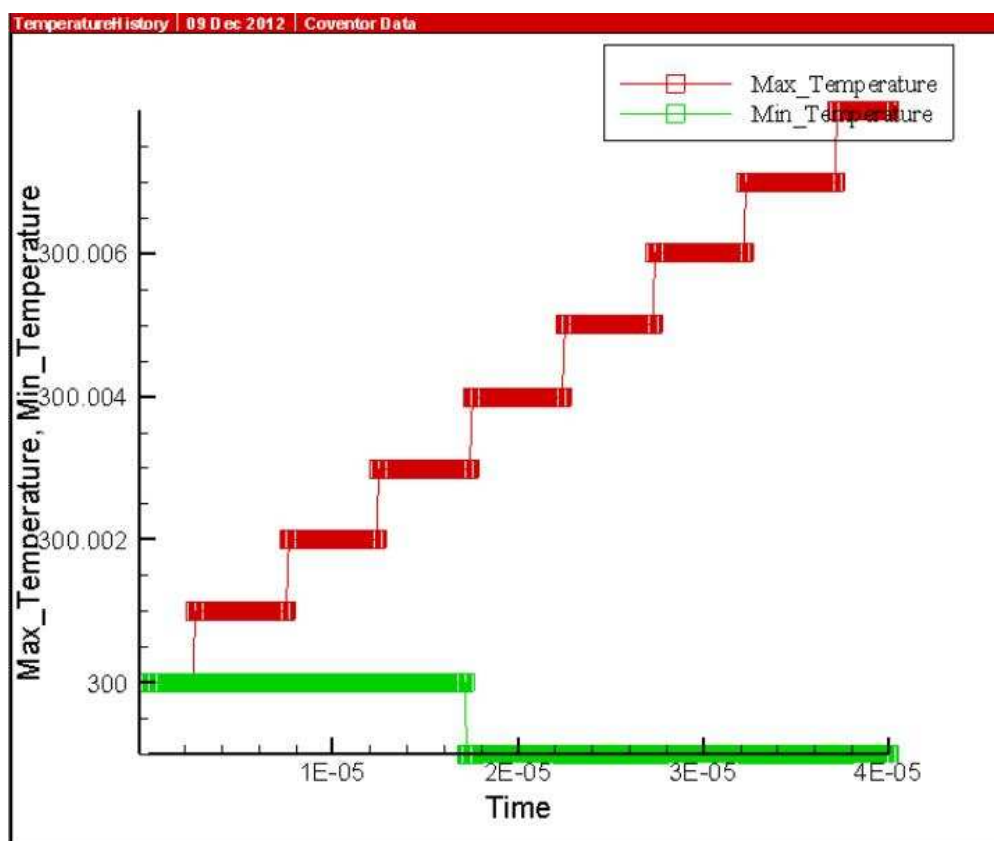


Figure 5-16: Maximum temperature, Minimum temperature vs Time of VOX3

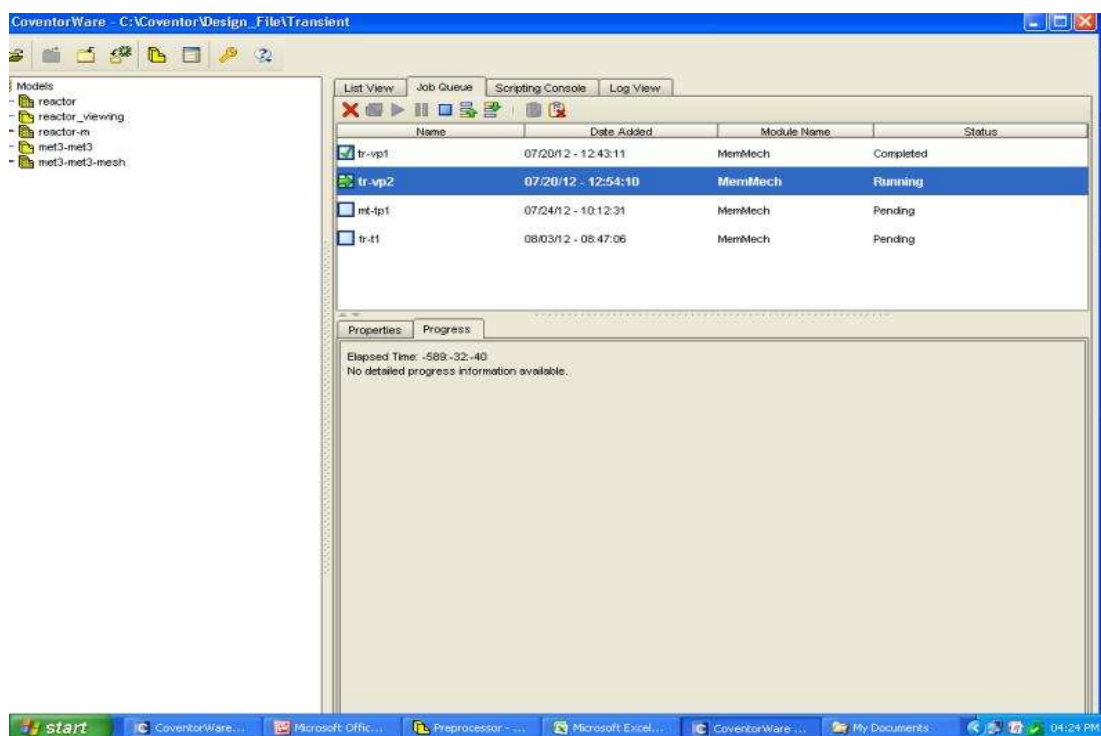


Figure 5-17: Elapsed time for MET2 dynamic simulations

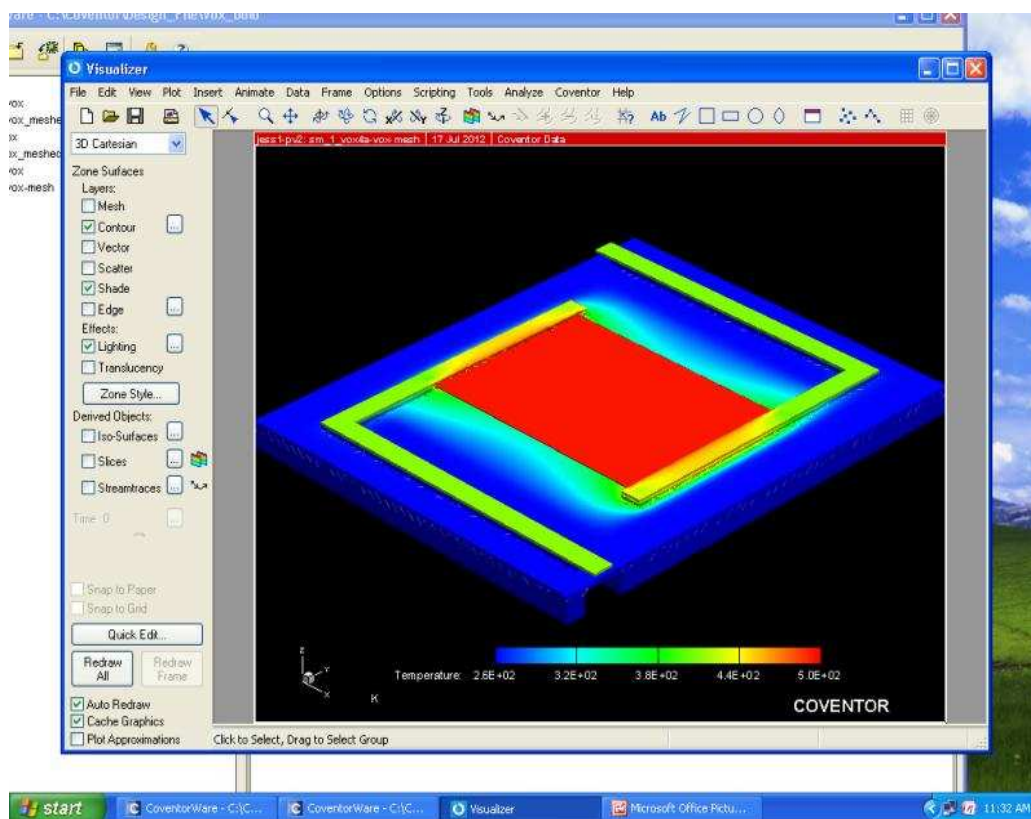


Figure 5-18: Vox membrane pixel bolometer at peak temperature

From dynamic simulations, results were collected and used in Window plot and fit to find the constant γ that is dependent on the thermal expansion of the membrane pixel bolometer as shown in equation 5.10, determined by combining equations 5.3, 5.7 and 5.9.

This constant can help in the understand the time a device subjected to heat flux takes to reach the maximum temperature which is proportional to the deformation of the bolometer as shown in equation 5.7.

$$G(\ln T/T_0) \frac{\gamma}{t} = H \quad (5.10)$$

Where;

G = Thermal conductance,

H = Thermal heat capacitance,

T = Maximum temperature,

To = Initial temperature (fixed),

t = required time the device needs to reach the maximum temperature when subjected to the heat flux.

Figures 5.19 – 21 present some of the results from window plot and fit used to determine the time a device needs to be exposed to heat for it to reach its maximum temperature using.

The equation $Y(X) = P1 * EXP(P2 * X/P3)$ was used in Window Fit and Plot in order to get the constant gamma. In the equation above, three parameters are used;

P1 = Initial temperature

P2 = Analytical thermal time constant, and

P3 = parameter used to find the constant γ , used in its initial state with the value of the deformation.

After iterations from Fit and Plot, new values are found, therefore the constant γ is also found given by the new value of P3. P3 relates both physical and thermal properties; which explains its relationship with the thermal expansion. Using equation 10, the required time for each device to reach the maximum temperature is determined and presented in table 5.5.

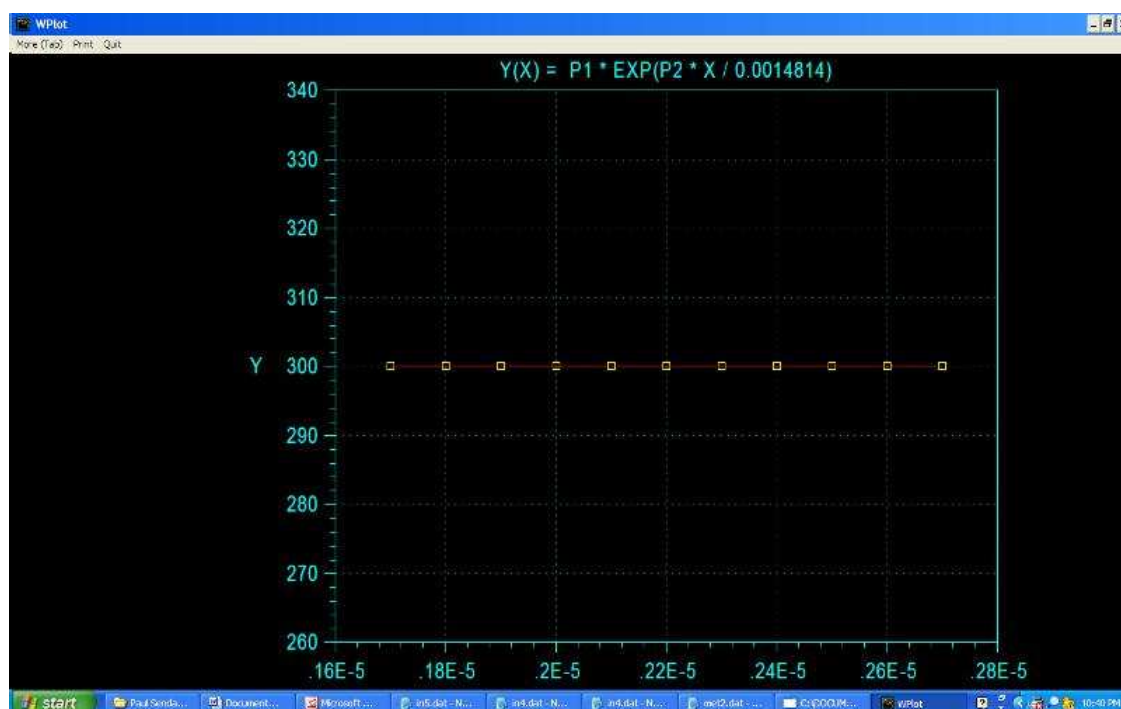


Figure 5-19: window fit and plot applied to MET2

```

C:\DOCUME~1\ADMINI~1\DESKTOP\PAULSE~1\WFIT.EXE
Command? load voxF.dat
read 37
37 data points were read.

numpar 3
y(x) = P1 * exp(P2 * X / P3)
P1 = 300
P2 = 0.0054
P3 = 0.10411
FIT
Please wait ...

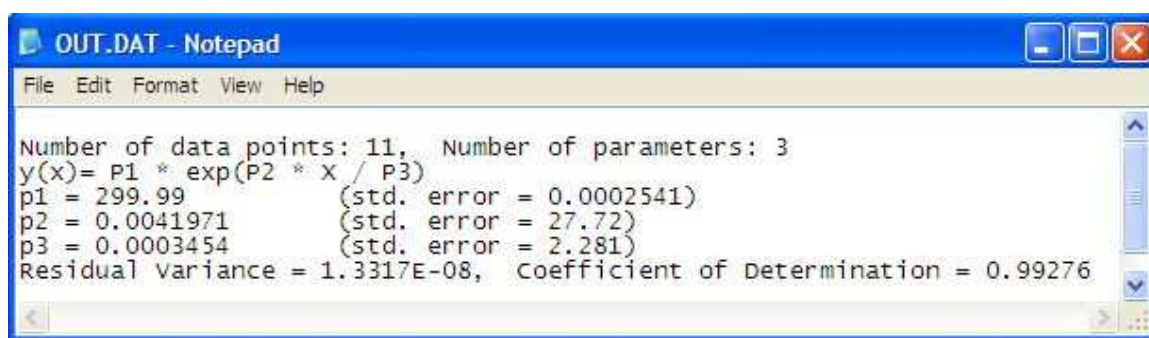
Number of data points: 37, Number of parameters: 3
y(x)= P1 * exp(P2 * X / P3)
p1 = 300 (std. error = 0.0003354)
p2 = 0.012084 (std. error = 397.8)
p3 = 0.0076517 (std. error = 251.9)
Residual Variance = 9.7401E-07, Coefficient of Determination = 0.96621
Iterations = 46, Time = 0.0 sec

OUTFIT OUT.DAT
PLOTFITUsing WPLOT program to make the plot ...

*** PRESS A KEY TO CONTINUE *** _

```

Figure 5-20: Determination of γ in Window Fit and Plot of VOXF



```

OUT.DAT - Notepad
File Edit Format View Help
Number of data points: 11, Number of parameters: 3
y(x)= P1 * exp(P2 * x / P3)
p1 = 299.99 (std. error = 0.0002541)
p2 = 0.0041971 (std. error = 27.72)
p3 = 0.0003454 (std. error = 2.281)
Residual variance = 1.3317E-08, Coefficient of Determination = 0.99276

```

Figure 5-21: Output from Window Fit and Plot for MET3

Table 5-5: required time to reach the maximum temperature

Device	Thermal Conductance G	Thermal Heat capacitance H	Initial Temp To	Max Temp T	Constant γ	t(s)
MET2	4.67E-07	2.33E-09	300	300.0212	0.005694	8.08E-05
MET3	7.16E-07	3.58E-09	300	300.0138	0.006332	5.82E-05
MET4	8.26E-07	4.64E-09	300	300.0121	0.006971	5.01E-05
VOX2	4.81E-07	2.11E-09	300	300.0208	0.005694	8.99E-05
VOX3	7.26E-07	3.12E-09	300	300.0138	0.0031	3.31E-05
VOX4	1.02E-06	4.06E-09	300	300.0098	0.005057	4.15E-05
VOXA	1.08E-06	4.07E-09	300	300.0093	0.001673	1.37E-05
VOXB	1.09E-06	3.28E-09	300	300.0092	0.002132	2.17E-05
VOXC	9.62E-07	2.56E-09	300	300.0104	0.0031	4.04E-05
VOXD	4.78E-07	1.83E-09	300	300.0209	0.000765	1.39E-05
VOXE	9.90E-07	2.97E-09	300	300.0101	0.003465	3.89E-05
VOXF	5.59E-07	2.34E-09	300	300.0179	0.000765	1.09E-05
VOXG	9.80E-07	2.09E-09	300	300.0102	0.003465	5.53E-05

5.3 Summary

This chapter deals with dynamic analyses and determination of thermal time constant and thermal time capacitance in order to find the thermal responsivity of the focal plane arrays microbolometer pixel. Results are shown in table 5.2 to 5.4.

From these results VOXD, VOXE and VOXF seem to be the best devices of all thirteen FPA pixels by their heat capacitance that characterises the amount of heat required to change its properties for both heating and cooling. And they also have the best thermal time constant which are favourable for both military and commercial applications as typical values of thermal time constant are given in the introduction.

In this chapter, it is also noticed that dynamic simulations lasted longer than expected, up to 590 days for only one simulation as shown in figure 5.17; this is due to either the software or the hardware, therefore only Five simulations were conducted; two on MET; MET2 and MET3, and three on VOX; VOX3, VOXD and VOXF.

In these analyses the substrate was kept at 300K and the thermal load applied on the top surface varying from 0 to 10 000 pW/ μm^2 over a time period varying from 3.0 to 35 μs as shown in figures 5.1; 5.5 and 5.9.

different curves representing the heating curve vs the cooling curve were found and interpreted using excel trendline in parametric equations solved in order based on equation 5.9 in order to determine the thermal time constant that were confronted to the analytical thermal time constant and using equation 5.10 to determine the required time for each device to reach its maximum temperature when subjected to thermal load.

In this chapter the sensitivity of each device was analysed by determining the responsivity that explains how sensitive the device is. Some of the devices present better results than the other that put them in a good position for both commercial and military applications as mentioned above.

Chapter Six

6. Conclusion and Recommendations

Development of microbolometer technology in the last ten years has improved dramatically in terms of its performances and resolutions. This research is based on the numerical modelling and analysis of both metal Titanium and Vanadium oxide pixel membrane bolometers that constitute a part of the second prototype of South Africa's bolometer devices. The technique for achieving this has been based on the use of the finite element analysis software package, CoventorWare. This software was utilised for the majority of the work conducted for this study.

6.1 Problems solved in the research

The objectives of this study has been achieved in the following ways:

Thirteen pixel membrane bolometer solid models as chosen by the consortium, i.e. DENEL Dynamics, SST, University of Pretoria and Cape Peninsula University of Technology, were modelled and analysed using the finite element analysis package CoventorWare. (as described in Chapter 3). For further investigations, the solid model of all thirteen membranes were meshed and prepared for thermal and mechanical analyses.

The second objective of the study was to study the deformation behaviours of 13 bolometer pixel membranes subjected to the application of varying thermal loads. Using the calculated results, the Thermal Conductance of 13 bolometer

pixel membranes were determined and is presented in Tables 4.6 – 4.16. The second objective of this research was thus achieved.

The third objective of this study was achieved positively in two phases as it is demonstrated in chapter 5. The thermal time constant and thermal heat capacity for the 13 devices were first calculated analytically using equations 5.1 - 5.4 as given by literature and are presented in Tables 5.2 – 5.4. Then using data collected from the transient thermomechanical analyses in CoventorWare, parametric equations were established and solved in order to determine the thermal time constant as it is also shown in chapter 5.

The fourth and last objective was also achieved positively by studying the sensitivity of the membrane pixels for the devices and results are presented in table 5.4. The required time for each device to reach the maximum temperature that influences the membrane displacement was determined and presented in table 5.5. This was achieved using WFit and WPlot software packages. Three devices out of the thirteen FPA pixel devices, i.e. VOXD, VOXE and VOXF, appeared to present better performance in terms heat capacitance and thermal time constant. The values obtained make them suitable for use in both military and commercial applications.

6.1.1 Solid model

The construction of the solid model was done using the FEA package CoventorWare. Six masks were defined for the device solid models: Cavity, Metal, Gold, Vanadium oxide, Contact and Nitride. These masks were deposited using the lithography technique on a silicon substrate with respect of dimensions specified, such as the width and length of the membrane bolometer.

6.1.2 Thermal conductance

To determine the thermal conductance, steady state thermomechanical analyses using CoventorWare were conducted.

First boundary conditions were defined as discussed. Tetrahedron elements were used to mesh the solid model. These elements conform to problematic shapes especially if they are not orthogonal. Furthermore, the parabolic element order was selected in order to make better approximations of results. The generated mesh for a metal bolometer is shown in Figure 6-1:

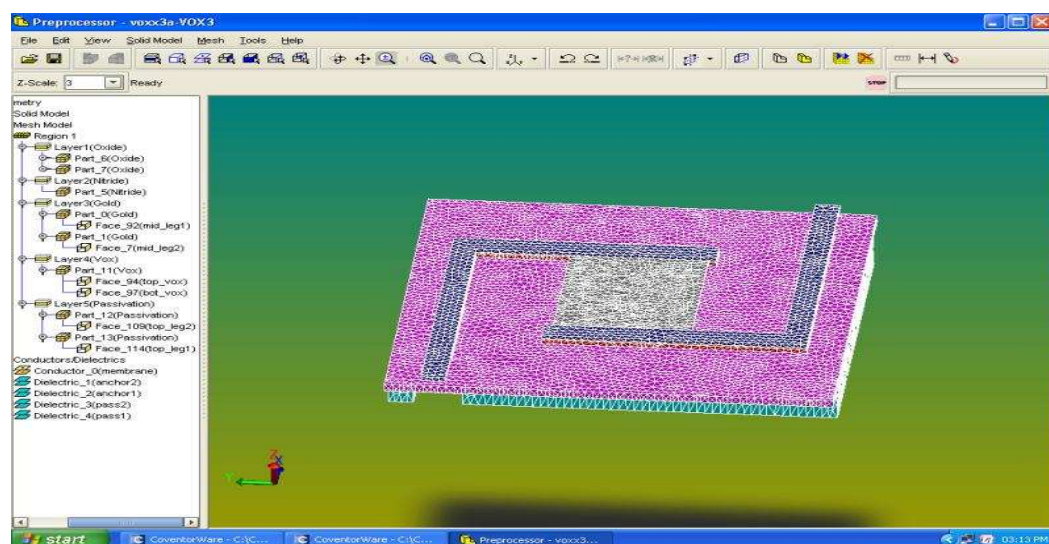


Figure 6-1: Metal bolometer meshed

From these analyses it has been noticed that in a vacuum the bolometer has lower thermal conductance than in atmospheric conditions and thus provides better performance under vacuum, i.e. thermal isolation in the vacuum is higher than that in air. This was demonstrated by M Zimmermann in 2001. MET2, VOX2 and VOXD have the smallest thermal conductance respectively; so that they have the best thermal isolation, however all thirteen pixel bolometers have good thermal conductance.

6.1.3 Thermal time constant

The thermal time constant constitutes the relationship between the thermal heat capacity and thermal conductance. It was determined first analytically using equation 5.2 and Table 4.6.

Then the transient analyses were performed to determine the thermal behaviour of the devices in defined time. This defines the thermal time constant which is dependent on the heating curve and cooling curve. However, as the simulations took many days to finish, a delay was created for further investigations. The relationship between these three parameters defines the responsivity of the device.

After completion of all investigations, four of the thirteen devices qualified for both military and commercial applications by the response time as demonstrated in chapter 5. These devices are; VOXD, VOXE and VOXF as they present time response that is below 45 ms which is the typical value for commercial applications.

The calculated results for each of the devices is given in the Tables below:

Table 6-1: Bolometer properties for VOX2, 3, & 4

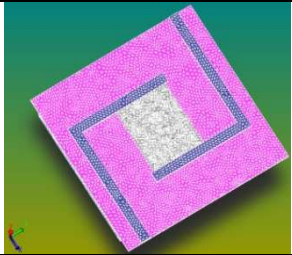
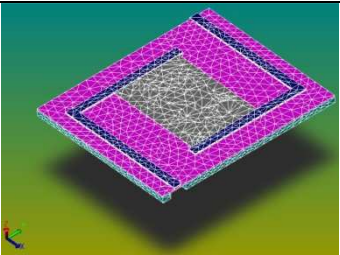
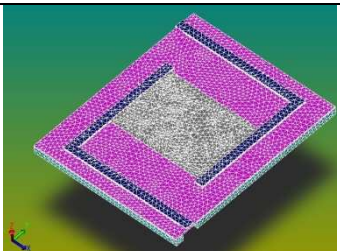
Device	Thermal Conductance G(W/K)	Thermal time constant τ (s)	Thermal Heat Capacitance H(J/K)	Responsivity R_v (s)	Device
VOX2	4.81E-07	4.39E-03	2.11E-09	9.40E-02	
VOX3	7.26E-07	4.30E-03	3.12E-09	6.47E-02	
VOX4	1.02E-05	3.98E-03	4.06E-09	5.23E-02	

Table 6-2: Bolometer properties for MET2, 3 & 4

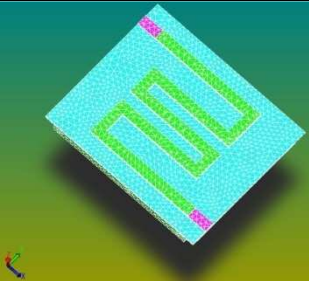
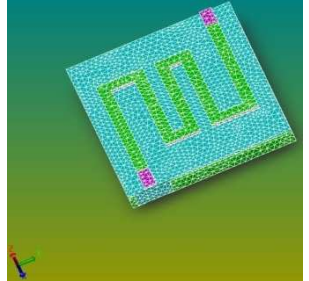
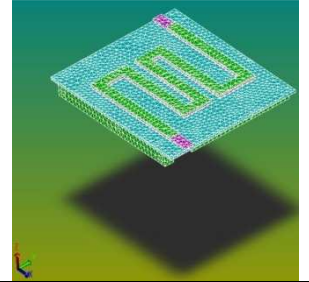
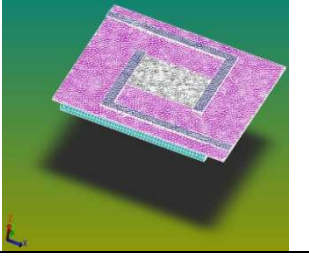
Device	Thermal Conductance G(W/K)	Thermal time constant τ (s)	Thermal Heat Capacitance H(J/K)	Responsivity Rv(s)	Thermal Heat Capacitance H(J/K)
MET2	4.67E-07	4.99E-03	2.33E-09	8.09E-02	
MET3	7.16E-07	5.00E-03	3.58E-09	5.18E-02	
MET4	8.26E-07	5.61E-03	4.64E-09	4.47E-02	

Table 6-3: Bolometer properties for VOXA, -B, -C, -E, -F, & -G

Device	Thermal Conductance G(W/K)	Thermal time constant τ (s)	Thermal Heat Capacitance H(J/K)	Responsivity Rv(s)	Thermal Heat Capacitance H(J/K)
VOXA	1.08E-06	3.78E-03	4.07E-09	6.85E-02	

VOXB	1.09E-06	3.00E-03	3.28E-09	6.95E-02	
VOXC	9.62E-07	2.66E-03	2.56E-09	6.84E-02	
VOXD	4.78E-07	3.82E-03	1.83E-09	3.12E-02	
VOXE	9.90E-07	3.00E-03	2.97E-09	3.67E-02	
VOXF	5.59E-07	4.19E-03	2.34E-09	3.67E-02	
VOXG	9.80E-05	2.13E-03	2.09E-09	4.32E-02	

6.2 Recommendations for future work

This lithography technique has opened up many research avenues. Although the programme shows valuable conclusions in solid designing and thermomechanical analyses in the bolometer field, there is still much more to be investigated in the area of fabrication.

There is much room for improvement that would enhance analyses results and timing to determine the performance of devices. For example, the transient simulations took more than a month; therefore, a verification system and equation solving system built into the program should be implemented for both time saving and valuable results. This will allow both military and civil industries to perform more work, not only in the micro-bolometer field but in all the mems and infrared fields.

The thermal time constant and responsivity for devices with time response above 27 and 45 ms need to be investigated in order to improve their thermal parameters, so that the responsivity can also be improved.

Bibliography

C. Chen, X. Yi, J. Zhang et al., "Micromachined uncooled IR bolometer linear array using VO₂ thin films", International Journal of Infrared and Millimeter Waves , Vol.22, No.1, pp.53-58, 2001.

Wayne S. Holland, William D. Duncan (UK ATC) & Matt Griffin (Cardiff University), pp 20-30, August 2003.

Frank Nicklaus, Christian Vieider, Henrik Jakobsen, "MEMS-Based Uncooled Infrared Bolometer Arrays-A Review" Proc. Of SPIE Vol. 6836 68360D, 4-12, Stockholm 2007.

Jeremie Bouchaud, " High Value MEMS market overview", pp. 4-10, 16-19, DTIP ,Marseilles, May 2011

P.W. Kruse and D.D. Skatrud (Editors), "Uncooled infrared imaging arrays and systems", Semiconductors and Semimetals, Volume 47, Academic Press, London, 1997.

M. Soltani, M. Chaker, E. Haddad, R. V. Kruzelecky, J. Margot, " Effects of Ti-W codoping on the optical and electrical switching of vanadium dioxide thin films grown by a reactive pulsed laser deposition", Applied Physics Letters, Vol.85, No.11, pp.1958-1960, 2004.

Y-H. Han, I.-H. Choi, H-K. Kang, J.-Y. Park, K-T. Kim, H-J. Shin and S. Moon, "Fabrication of vanadium oxide thin film with high-temperature coefficient of resistance using V₂O₅/V/V₂O₅ multi-layers for uncooled microbolometers", Thin Solid Films, Vol.425, No.1-2, pp.260-264, 2003.

J-S. Shie, Y-M.Chen, M Ou-Yang and B.C.S Chou, "Characterization and modelling of metal film microbolometer", *Journal of Microelectromechanical Systems*, Vol.5, No. 4, pp.298-306, December 1996.

C. Chang-hong, Y. Xin-jian, X. Bi-feng, "Infrared responsivity of uncooled VO₂-based thin films bolometer", *Acta physica Sinica.*, Vol.50, Part 3, pp.450-452, 2001.

Y. Lv, M. Hu, M. Wu and Z. Liu, "Preparation of vanadium oxide thin films with high temperature coefficient of resistance by facing targets d.c. reactive sputtering and annealing process", *Surface and Coating Technology*, Vol. 201, pp.4969-4972, 2007.

R. S. Ram et al. "Fourier Transform Emission Spectroscopy of the A₂D–X₂P Transition of SiH and SiD" *J. Mol. Spectr.* 190, 341-352 (1998).

N. Chi-Anh, H-J. Shin, K. Kim et. al., "Characterization of uncooled bolometer with vanadium tungsten oxide infrared active layer", *Sensors and Actuators A: Physical*, Vol.123, pp.87-92, 2005.

Matthew J. Donachie, Jr. (1988). *Titanium: A Technical Guide*. Metals Park, OH: ASM International. Appendix J, Table J.2. ISBN 0871703092.

N. Chi-Anh, S. Moon: "Excess noise in vanadium tungsten oxide bolometric material", *Infrared Physics & Technology*, Vol.50, No.1, pp.38-41, 2007.

A Tanaka et al, "Infrared focal plane array incorporating silicon IC process compatible bolometer", *IEEE Transactions on Electron Devices*, Vol. ED-43, No 11, pp.1844-1850, November 1996.

N. Chi-Anh, S. Moon: "Excess noise in vanadium tungsten oxide bolometric material", *Infrared Physics & Technology*, Vol.50, No.1, pp.38-41, 2007.

J-S. Shie, Y-M. Chen, M. Ou-Yang and B.C.S Chou," Characterization and modelling of metal-film microbolometer", *Journal of Micromechanical Systems*, Vol. 5, No.4, pp 298-306, December 1996

P.Eriksson, J.Y. Andersson and G.Stemme,"Thermal characterization of surface-micromachined silicon nitride membranes for thermal infrared

detectors”, Journal of Microelectromechanical systems, Vol. 6, No. 1, pp 55-61, March 1997.

M. von Arx, O. Paul and H. Baltes, “Process depend –Thin-film thermal conductivities for thermal CMOS MEMS”, Journal of Microelectromechanical systems, Vol.9, No.1 pp. 136-145, March 2000.

G. Eppeldauer, A.L. Migdall and C.L. Cromer “Characterization of a high Sensitivity Composite Silicon Bolometer”, Metrologia 317-320, 1993

Sun B., “MEMS, Mechanics, Sensing and Actuation” lecture Notes, pp 7-17, October 2006.

“Infrared spectroscopy”, online edition for students of organic chemistry lab courses at the University of Colorado, Boulder, Dept. of Chem. and Biochem. 2002.

P. Capper, C.T. Elliot: Infrared Detectors and Emitters: Materials and Devices, Kluwer Academic Publishers, 2001.

“Space Shuttle Main Engine Enhancements” NASA, Retrieved 2009-06-06

<http://www.csa.com/discoveryguides/mems/overview.php>

<http://www.scribd.com/doc/14464450/MEMS-Report>

http://www.chem.ucla.edu/harding/notes_14C_IR.pdf

<http://www.slideshare.net/vinayak.nandi/mems-report>

http://www.eee.metu.edu.tr/~tayfuna/papers/akin_c15_trans99.pdf

<http://www.docstoc.com/docs/40306794/AN-UNCOOLED-MICROBOLOMETER-INFRARED-DETECTOR-IN-ANY-STANDARD-CMOS>

www.memsnet.com

Appendix A

A. Using CoventorWare

CoventorWare is the most comprehensive suite of MEMS design tools in the industry. It acts as a seamless integrated design environment that reduces design risk, speeds time-to-time and lowers development costs.

On starting CoventorWare, the Function Manager window is the first to appear. All CoventorWare functionality is accessed from the Function Manager. The upper portion of the Function Manager window has icons for accessing the Material Properties Database and the Process Editor. The lower portion of the Function Manager has navigation tabs for accessing the ARCHITECT, DESIGNER, and ANALYZER functions. The menu at the top of the window provides options for file management, help, and several ancillary tools.

MATERIAL PROPERTIES DATABASE (MPD)

The first step in creating a design, whether you intend to perform system-level simulations with ARCHITECT or FEM simulations with ANALYZER, is to enter the material properties associated with your fabrication process in the Material Properties Database (MPD). Only the materials that are in the MPD are accessible in the Process Editor and available for simulations.

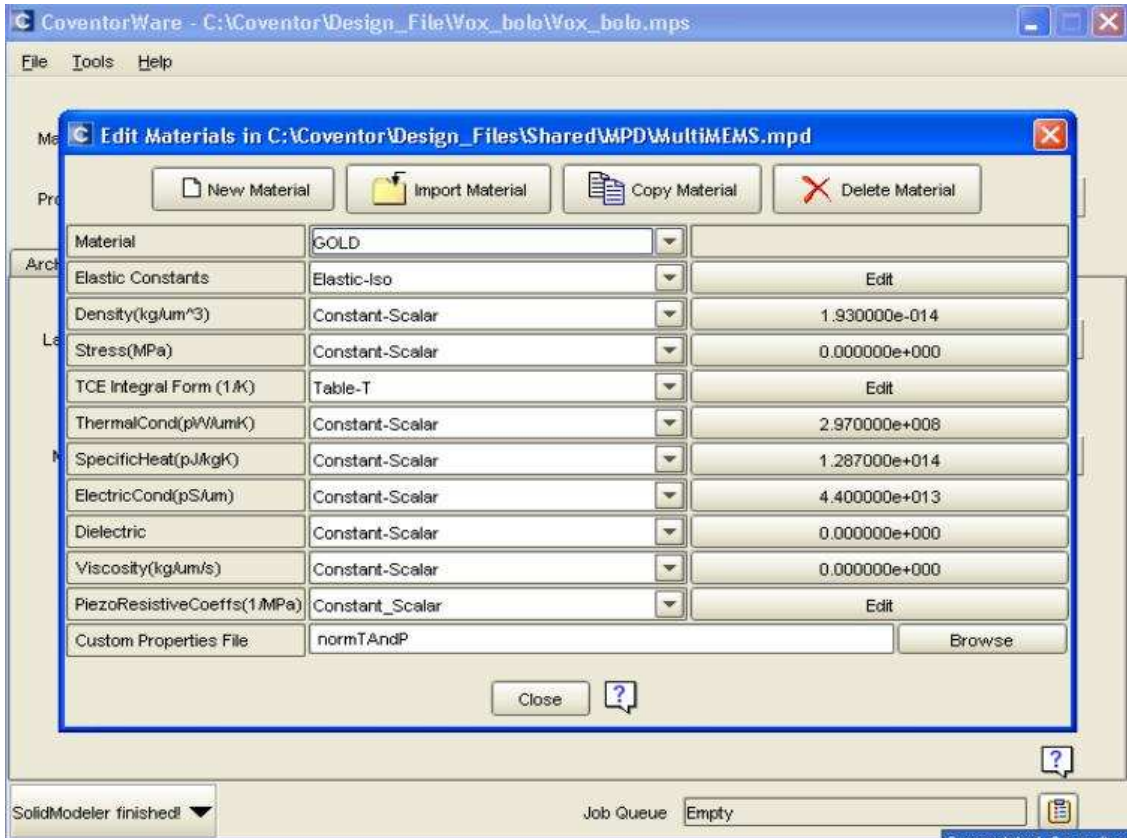


Figure A-1: Gold properties in the MPD

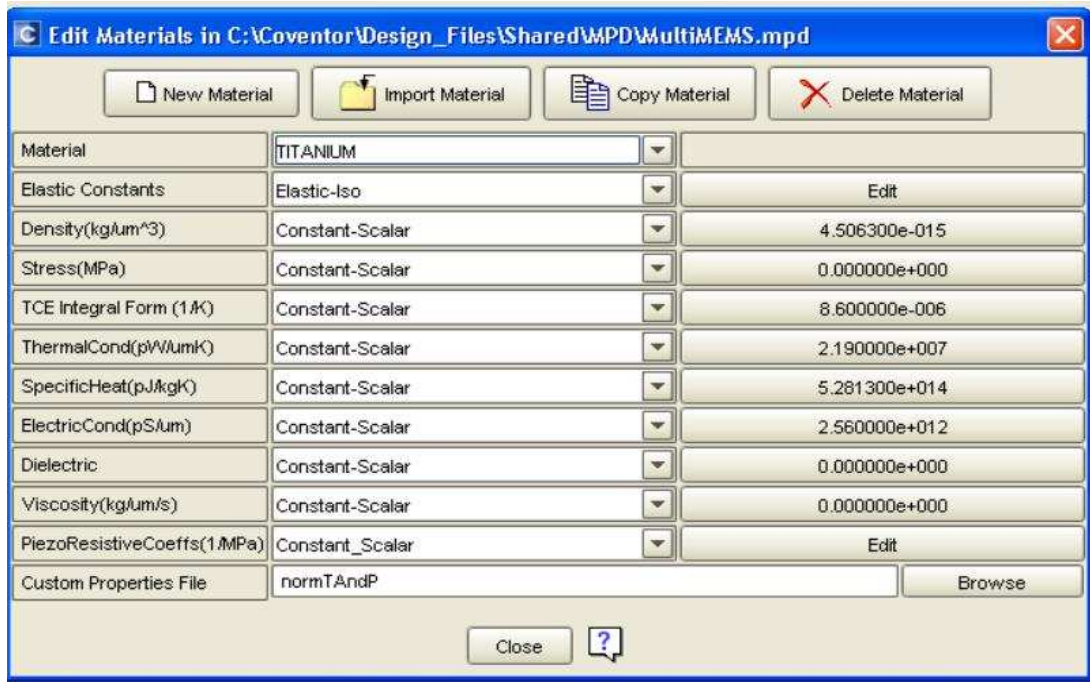


Figure A-2: Titanium properties in the MPD

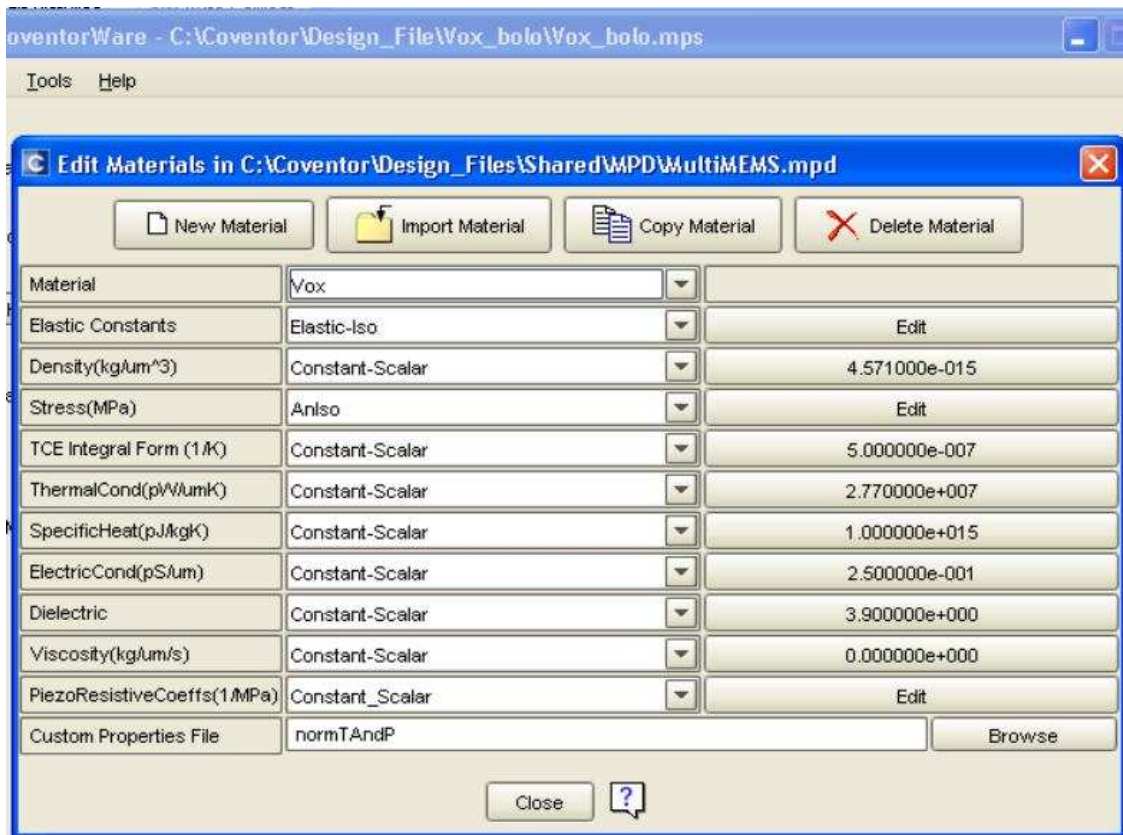


Figure A-3: VOx properties in the MPD

PROCESS EDITOR

The second step in creating a design, whether you intend to perform system-level simulations with ARCHITECT or FEM simulations with ANALYZER, is to enter a description of the sequence of steps involved in the fabrication process in the Process Editor. You create the sequence by selecting prototype steps from a Process Library, displayed by default on the right-hand side of the Process Editor window. Each step has parameters that must be specified. For deposit steps, for example, you specify the material to be deposited and the deposit depth. As an alternative to specifying a custom process, you may select a complete process sequence for an independent foundry from among those listed in the Process Library.

ARCHITECT

ARCHITECT provides a system-level design and simulation environment for MEMS devices. It is comprised of a schematic editor (Saber Sketch), a simulator (Saber Simulator), a plotting tool (Cosmos Scope), a 3-D visualize (Scene3D), and several libraries of parameterized behavioral models (also known as components). Before starting a schematic, you must provide an MPD and process file created with the Process Editor. To create a schematic design in Saber Sketch, you select components from the PEM library and place these components in the schematic view. The design can be viewed in 3-D at any time using the companion Scene3D module. When the schematic is complete, you can run a variety of simulations of the design, including static, transient, and harmonic analyses. Simulation results can be viewed in the form of x-y plots using Cosmos Scope, or the motion of the device can be animated in Scene3D.

DESIGNER

DESIGNER provides a manufacturing-aware method for creating 3-D solid models of MEMS and microfluidics devices. It is comprised of a 2-D layout editor (the Layout Editor), a solid model generator (the Solid Modeler), and a 3-D solid model viewer and editor (the Preprocessor). As a starting point, you must provide a MPD and process file created with the Process Editor. In addition, you must supply a 2-D layout file that has layers that define all of the masks required by the process file. There are several options for providing the layout file. One option is to use the comprehensive editing capabilities in the Layout Editor to draw the shapes that define each mask. Another option is to draw the layout in a third-party layout tool and import the layout in the GDSII, DXF, or CIF file format. ARCHITECT users have the option to generate a layout from an ARCHITECT schematic by selecting the *New from Architect* option on the Designer tab.

MESHING

CoventorWare's automatic mesh generations capabilities are incorporated in the Preprocessor, which serves as a bridge between DESIGNER and ANALYZER. Once a solid model is loaded in the Preprocessor, you select which layers are to be meshed. The Preprocessor automatically groups the layers into regions based on their adjacency. You then select the type of mesh to be generated on each region and can set local refinement options. The types of meshes include surface meshes with triangular or quadrilateral faces and volume meshes with tetrahedrons or hexahedrons (bricks). Several different methods are available for hexahedrons, including extrusion, Manhattan (for near orthogonal geometries) and mapping (for geometries that can be decomposed into 6-sided volumes). You can select any layer, part, face, edge or vertex and specify local refinement options. A Quality Query in the Preprocessor allows you to view a variety of mesh statistics to assess the quality of the mesh, and visualize "bad" elements (elements with characteristics that exceed user-settable thresholds). Generating a valid, high-quality mesh is a pre-requisite for using any of the field solvers in ANALYZER.

Tetrahedron Meshing

The *Tetrahedrons* mesh option should be selected for layers with geometry that would make hexahedral (Extruded, Manhattan, or Mapped) meshing impossible. In principle, tetrahedral meshing can be used to mesh any 3-D geometry.

Tetrahedrons Mesh Settings

If the *Tetrahedrons* option is selected from the Mesh Type drop-down menu, these options appear in the dialog:

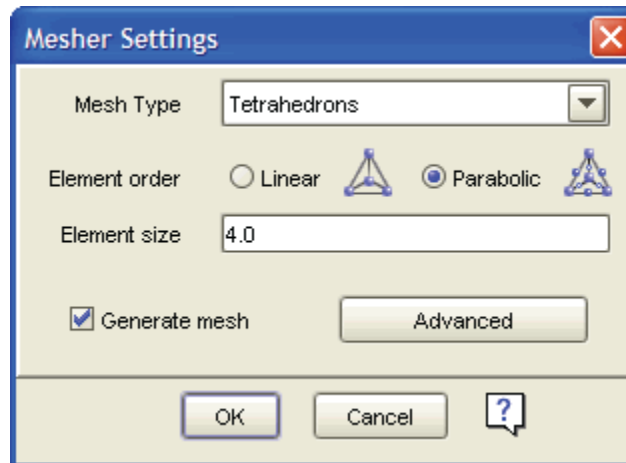


Figure A-4: Tetrahedrons mesher settings

ANALYZER

ANALYZER provides a comprehensive suite of 3-D solvers, including solvers for electrostatics, mechanics, coupled electromechanics, thermomechanics, and microfluidics. With these solvers, you can perform analyses that incorporate or compute the following types of physical behavior and effects:

- capacitance and electrostatic charge;
- deformations from applied pressures or forces;
- coupled electromechanical behavior, including pull-in and lift-off voltage;
- mechanical and coupled electromechanical behavior with full contact boundary conditions;
- piezoelectric effects;
- residual stress (from the fabrication process);
- modal analyses of the natural vibration frequencies of MEMS devices;
- harmonic analyses of MEMS devices;
- steady-state electrothermal (Joule heating), thermomechanical, and electrothermomechanical behavior;
- transient mechanical and thermomechanical behavior;
- thermal boundary conditions, such as film convection, radiation, and heat flux;

- Coupling of package deformation resulting from thermomechanical effects to mechanical behavior of a MS device.
- piezo-resistive sensing of mechanical deformation;
- inductance of electrically conductive components, such as package leads and wire bonds;
- gas damping effects on MEMS device behavior;
- fluidic solutions with static or transient compressible or incompressible flows;
- fluidic solutions with electrokinetic flows and diffusion in microchannels
- fluidic solutions involving species separation using phased voltage channel switching;
- fluidic solutions for multi-phase flows involving droplet ejection or bubble movement; and
- fluidic solutions for chemical reactions

VISUALIZER

The solver output for most MEMS models includes a significant amount of data for analysis and post-processing. The Visualizer tool supplements this capability by enabling users to map these results graphically onto the original model and visually analyze the solution. The Visualizer enables viewing of electrostatic fields, mechanical deformations, stresses, thermal variations, temperature gradients, pressures, current densities, and many other parameters. Selected parameters are color-mapped onto the 3-D model, allowing a complete surface analysis of the model after the solution is complete. An adjustable slice plane and selected probing of interior bricks allow the entire volume to be visualized.

The Visualizer can show a timed sequence of incremental changes to a model from a parametric study and can simulate and animate the modal vibrations from a modal analysis solution. It includes its own animation module for

capturing and replaying a desired sequence. A print module captures the Visualizer screen to an output file in a variety of resolutions.

The user can adjust virtually every aspect of the 3-D view, including lighting effects, perspective, shading, line widths, font sizes, and scale positions, to satisfy individual preferences.

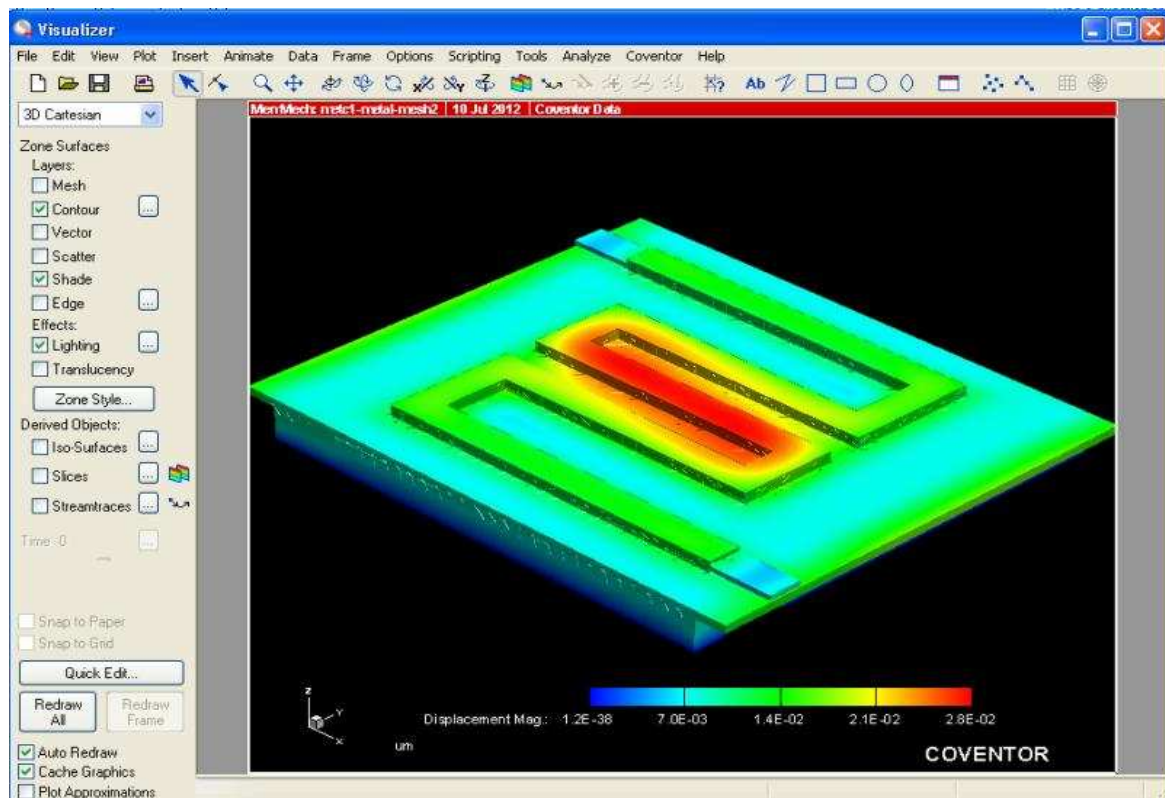
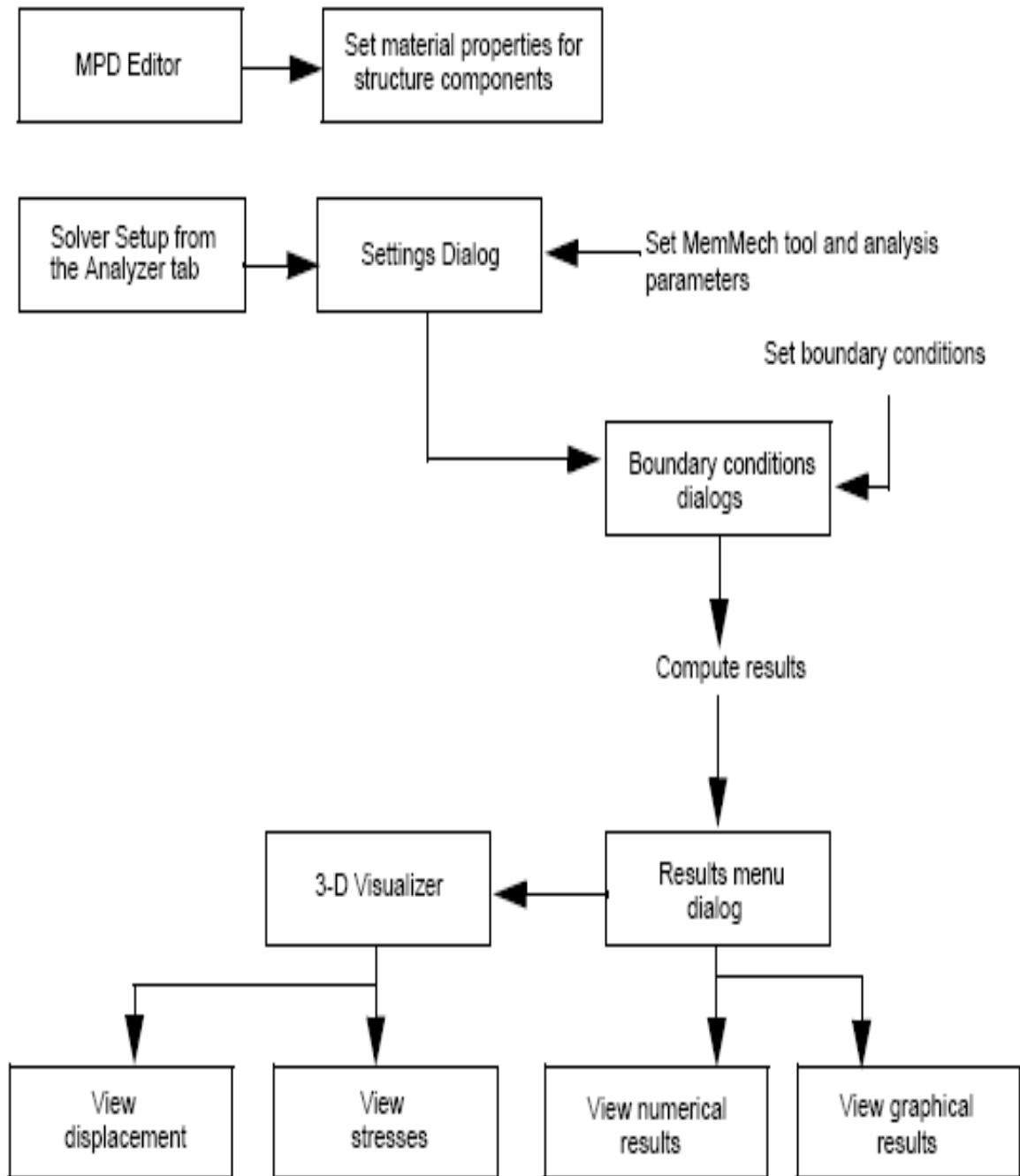


Figure A-5: Titanium bolometer seen in the visualizer

Appendix B

B. MemMech Solver

MemMech is CoventorWare's mechanical solver, which computes displacement and stress results. The user selects boundary conditions from the solver's setup dialogs, and the solver generates output that may be viewed in a tabular form or rendered in three dimensions over the structure's domain in the Visualizer. The flow chart in Figure B-1 provides an overview of the MemMech functions:

**Figure B-1:** MemMech Settings and Results Flow

Appendix C

C. Devices thermal conductance analysis

Table C-1: MET2 Thermal Conductance

Heat Flux Φ (pW/ μm^2)	Max T (K)	Min T (K)	Φ (W/ μm^2)	ΔT	Displacement (μm)	ΔW	Thermal conductance G, (W/K)
500	300.0011	300	5.00E-10	0.00107	0.00833883	4.16942E-12	4.6729E-07
1000	300.0021	300	1.00E-09	0.00214	0.0250165	2.50165E-11	4.6729E-07
2000	300.0043	300	2.00E-09	0.00428	0.0416942	8.33884E-11	4.6729E-07
3000	300.0064	300	3.00E-09	0.00642	0.0583718	1.75115E-10	4.6729E-07
4000	300.0085	300	4.00E-09	0.00856	0.0750495	3.00198E-10	4.6729E-07
5000	300.0106	299.9999	5.00E-09	0.0107	0.0917272	4.58636E-10	4.6729E-07
6000	300.0128	299.9999	6.00E-09	0.01284	0.108405	6.5043E-10	4.6729E-07
7000	300.0149	299.9999	7.00E-09	0.01498	0.1250826	8.75578E-10	4.6729E-07
8000	300.017	299.9999	8.00E-09	0.01712	0.1417602	1.13408E-09	4.6729E-07
9000	300.0191	299.9998	9.00E-09	0.01926	0.1584378	1.42594E-09	4.6729E-07
10000	300.0212	299.9998	1.00E-08	0.0214	0.1751154	1.75115E-09	4.6729E-07

Table C-2: MET3 Thermal Conductance

Heat Flux Φ (pW/ μm^2)	Max T (K)	Min T (K)	Φ (W/ μm^2)	ΔT	Displacement (μm)	ΔW	Thermal conductance G, (W/K)
500	300.0007	300	5.00E-10	0.000698	0.0104562	5.2281E-12	7.16332E-07
1000	300.0014	300	1.00E-09	0.001396	0.0209124	2.09124E-11	7.16332E-07
2000	300.0028	300	2.00E-09	0.002792	0.0418249	8.36498E-11	7.16332E-07
3000	300.0041	300	3.00E-09	0.004188	0.0627374	1.88212E-10	7.16332E-07
4000	300.0055	300	4.00E-09	0.005584	0.0836499	3.346E-10	7.16332E-07
5000	300.0069	299.9999	5.00E-09	0.00698	0.1045624	5.22812E-10	7.16332E-07
6000	300.0083	299.9999	6.00E-09	0.008376	0.1254749	7.52849E-10	7.16332E-07
7000	300.0097	299.9999	7.00E-09	0.009772	0.1463874	1.02471E-09	7.16332E-07
8000	300.011	299.9999	8.00E-09	0.011168	0.1672999	1.3384E-09	7.16332E-07

9000	300.0124	299.9998	9.00E-09	0.012564	0.1882124	1.69391E-09	7.16332E-07
10000	300.0138	299.9998	1.00E-08	0.01396	0.2091249	2.09125E-09	7.16332E-07

Table C-3: MET4 Thermal Conductance

Heat Flux Φ (pW/ μm^2)	Max T (K)	Min T (K)	Φ (W/ μm^2)	ΔT	Displacement (μm)	ΔW	Thermal conductance G, (W/K)
500	300.0006	300	5.00E-10	0.000605	0.010456	5.22815E-12	8.26446E-07
1000	300.0012	300	1.00E-09	0.00121	0.020913	2.09125E-11	8.26446E-07
2000	300.0024	300	2.00E-09	0.00242	0.041825	8.365E-11	8.26446E-07
3000	300.0036	300	3.00E-09	0.00363	0.062738	1.88213E-10	8.26446E-07
4000	300.0048	300	4.00E-09	0.00484	0.08365	3.346E-10	8.26446E-07
5000	300.0061	300	5.00E-09	0.00605	0.104563	5.22813E-10	8.26446E-07
6000	300.0073	300	6.00E-09	0.00726	0.125475	7.5285E-10	8.26446E-07
7000	300.0085	300	7.00E-09	0.00847	0.146388	1.02471E-09	8.26446E-07
8000	300.0097	300	8.00E-09	0.00968	0.1673	1.3384E-09	8.26446E-07
9000	300.0109	300	9.00E-09	0.01089	0.188213	1.69391E-09	8.26446E-07
10000	300.0121	300	1.00E-08	0.0121	0.209125	2.09125E-09	8.26446E-07

Table C-4: VOX2 Thermal Conductance

Heat Flux Φ (pW/ μm)	Max T (K)	Min T (K)	Φ (W/ μm)	ΔT	Displacement	ΔW	Thermal conductance G, (W/K)
500	300.001	300	5.00E-10	0.00104	0.00833883	4.17E-12	4.80769E-07
1000	300.0021	300	1.00E-09	0.00208	0.0250165	2.50165E-11	4.80769E-07
2000	300.0042	300	2.00E-09	0.00416	0.0416942	8.33884E-11	4.80769E-07
3000	300.0062	300	3.00E-09	0.00624	0.0583718	1.75115E-10	4.80769E-07
4000	300.0083	300	4.00E-09	0.00832	0.0750495	3.00198E-10	4.80769E-07
5000	300.0104	300	5.00E-09	0.0104	0.0917272	4.58636E-10	4.80769E-07
6000	300.0125	300	6.00E-09	0.01248	0.108405	6.5043E-10	4.80769E-07
7000	300.0146	300	7.00E-09	0.01456	0.1250826	8.75578E-10	4.80769E-07
8000	300.0166	300	8.00E-09	0.01664	0.1417602	1.13408E-09	4.80769E-07
9000	300.0187	300	9.00E-09	0.01872	0.1584378	1.42594E-09	4.80769E-07
10000	300.0208	300	1.00E-08	0.0208	0.1751154	1.75115E-09	4.80769E-07

Table C-5: VOX3 Thermal Conductance

Heat Flux Φ (pW/ μ m)	Max T (K)	Min T (K)	Φ (W/ μ m)	ΔT	Displacement	ΔW	Thermal conductance G, (W/K)
500	300.0007	300	5.00E-10	0.000689	0.0104562	5.23E-12	7.2569E-07
1000	300.0014	300	1.00E-09	0.001378	0.0209124	2.09124E-11	7.2569E-07
2000	300.0028	300	2.00E-09	0.002756	0.0418249	8.36498E-11	7.2569E-07
3000	300.0041	300	3.00E-09	0.004134	0.0627374	1.88212E-10	7.2569E-07
4000	300.0055	300	4.00E-09	0.005512	0.0836499	3.346E-10	7.2569E-07
5000	300.0069	300	5.00E-09	0.00689	0.1045624	5.22812E-10	7.2569E-07
6000	300.0083	300	6.00E-09	0.008268	0.1254749	7.52849E-10	7.2569E-07
7000	300.0096	300	7.00E-09	0.009646	0.1463874	1.02471E-09	7.2569E-07
8000	300.011	300	8.00E-09	0.011024	0.1672999	1.3384E-09	7.2569E-07
9000	300.0124	300	9.00E-09	0.012402	0.1882124	1.69391E-09	7.2569E-07
10000	300.0138	300	1.00E-08	0.01378	0.2091249	2.09125E-09	7.2569E-07

Table C-6: VOX4 Thermal Conductance

Heat Flux Φ (pW/ μ m)	Max T (K)	Min T (K)	Φ (W/ μ m)	ΔT	Displacement	ΔW	Thermal conductance G, (W/K)
500	300.0005	300	5.00E-10	0.00049	0.104562	5.2281E-11	1.02041E-06
1000	300.001	300	1.00E-09	0.00098	0.24512	2.4512E-10	1.02041E-06
2000	300.002	300	2.00E-09	0.00196	0.385678	7.71356E-10	1.02041E-06
3000	300.0029	300	3.00E-09	0.00294	0.526236	1.57871E-09	1.02041E-06
4000	300.0039	300	4.00E-09	0.00392	0.63455	2.5382E-09	1.02041E-06
5000	300.0049	300	5.00E-09	0.0049	0.634551	3.17276E-09	1.02041E-06
6000	300.0059	300	6.00E-09	0.00588	0.634553	3.80732E-09	1.02041E-06
7000	300.0069	300	7.00E-09	0.00686	0.76431	5.35017E-09	1.02041E-06
8000	300.0078	300	8.00E-09	0.00784	0.894067	7.15254E-09	1.02041E-06
9000	300.0088	300	9.00E-09	0.00882	1.023824	9.21442E-09	1.02041E-06
10000	300.0098	300	1.00E-08	0.0098	1.153581	1.15358E-08	1.02041E-06

Table C-7: VOXA Thermal Conductance

Heat Flux Φ (pW/ μ m)	Max T (K)	Min T (K)	Φ (W/ μ m)	ΔT	Displacement	ΔW	Thermal conductance G, (W/K)
500	300.0005	300	5.00E-10	0.000464	0.304563	1.52282E-10	1.0776E-06
1000	300.0009	300	1.00E-09	0.000928	0.29125	2.9125E-10	1.0776E-06
2000	300.0019	300	2.00E-09	0.001856	0.21825	4.365E-10	1.0776E-06
3000	300.0028	300	3.00E-09	0.002784	0.27375	8.2125E-10	1.0776E-06
4000	300.0037	300	4.00E-09	0.003712	0.308365	1.23346E-09	1.0776E-06
5000	300.0046	300	5.00E-09	0.00464	0.375625	1.87813E-09	1.0776E-06
6000	300.0056	300	6.00E-09	0.005568	0.442885	2.65731E-09	1.0776E-06
7000	300.0065	300	7.00E-09	0.006496	0.510145	3.57102E-09	1.0776E-06
8000	300.0074	300	8.00E-09	0.007424	0.577405	4.61924E-09	1.0776E-06
9000	300.0084	300	9.00E-09	0.008352	0.63407	5.70663E-09	1.0776E-06
10000	300.0093	300	1.00E-08	0.00928	0.690735	6.90735E-09	1.0776E-06

Table C-8: VOXB Thermal Conductance

Heat Flux Φ (pW/ μ m)	Max T (K)	Min T (K)	Φ (W/ μ m)	ΔT	Displacement	ΔW	Thermal conductance G, (W/K)
500	300.0005	300	5.00E-10	0.000458	0.304563	1.52282E-10	1.0917E-06
1000	300.0009	300	1.00E-09	0.000916	0.29125	2.9125E-10	1.0917E-06
2000	300.0018	300	2.00E-09	0.001832	0.291825	5.8365E-10	1.0917E-06
3000	300.0027	300	3.00E-09	0.002748	0.29375	8.8125E-10	1.0917E-06
4000	300.0037	300	4.00E-09	0.003664	0.308365	1.23346E-09	1.0917E-06
5000	300.0046	300	5.00E-09	0.00458	0.375625	1.87813E-09	1.0917E-06
6000	300.0055	300	6.00E-09	0.005496	0.442885	2.65731E-09	1.0917E-06
7000	300.0064	300	7.00E-09	0.006412	0.510145	3.57102E-09	1.0917E-06
8000	300.0073	300	8.00E-09	0.007328	0.577405	4.61924E-09	1.0917E-06
9000	300.0082	300	9.00E-09	0.008244	0.63407	5.70663E-09	1.0917E-06
10000	300.0092	300	1.00E-08	0.00916	0.690735	6.90735E-09	1.0917E-06

Table C-9: VOXC Thermal Conductance

Heat Flux Φ (pW/ μ m)	Max T (K)	Min T (K)	Φ (W/ μ m)	ΔT	Displacement	ΔW	Thermal conductance G, (W/K)
500	300.0005	300	5.00E-10	0.00052	0.304563	1.52282E-10	9.6154E-07
1000	300.001	300	1.00E-09	0.00104	0.29125	2.9125E-10	9.6154E-07
2000	300.0021	300	2.00E-09	0.00208	0.291825	5.8365E-10	9.6154E-07
3000	300.0031	300	3.00E-09	0.00312	0.29375	8.8125E-10	9.6154E-07
4000	300.0042	300	4.00E-09	0.00416	0.308365	1.23346E-09	9.6154E-07
5000	300.0052	300	5.00E-09	0.0052	0.375625	1.87813E-09	9.6154E-07
6000	300.0062	300	6.00E-09	0.00624	0.442885	2.65731E-09	9.6154E-07
7000	300.0073	300	7.00E-09	0.00728	0.510145	3.57102E-09	9.6154E-07
8000	300.0083	300	8.00E-09	0.00832	0.577405	4.61924E-09	9.6154E-07
9000	300.0094	300	9.00E-09	0.00936	0.63407	5.70663E-09	9.6154E-07
10000	300.0104	300	1.00E-08	0.0104	0.690735	6.90735E-09	9.6154E-07

Table C-10: VOXD Thermal Conductance

Heat Flux Φ (pW/ μ m)	Max T (K)	Min T (K)	Φ (W/ μ m)	ΔT	Displacement	ΔW	Thermal conductance G, (W/K)
500	300.001	300	5.00E-10	0.001045	0.00833883	4.17E-12	4.7847E-07
1000	300.0021	300	1.00E-09	0.00209	0.0250165	2.50165E-11	4.7847E-07
2000	300.0042	300	2.00E-09	0.00418	0.0416942	8.33884E-11	4.7847E-07
3000	300.0063	300	3.00E-09	0.00627	0.0583718	1.75115E-10	4.7847E-07
4000	300.0084	300	4.00E-09	0.00836	0.0750495	3.00198E-10	4.7847E-07
5000	300.0105	300	5.00E-09	0.01045	0.0917272	4.58636E-10	4.7847E-07
6000	300.0125	300	6.00E-09	0.01254	0.108405	6.5043E-10	4.7847E-07
7000	300.0146	300	7.00E-09	0.01463	0.1250826	8.75578E-10	4.7847E-07
8000	300.0167	300	8.00E-09	0.01672	0.1417602	1.13408E-09	4.7847E-07
9000	300.0188	300	9.00E-09	0.01881	0.1584378	1.42594E-09	4.7847E-07
10000	300.0209	300	1.00E-08	0.0209	0.1751154	1.75115E-09	4.7847E-07

Table C-11: VOXE Thermal Conductance

Heat Flux Φ (pW/ μ m)	Max T (K)	Min T (K)	Φ (W/ μ m)	ΔT	Displacement	ΔW	Thermal conductance G, (W/K)
500	300.0005	300	5.00E-10	0.000505	0.304563	1.52282E-10	9.901E-07
1000	300.001	300	1.00E-09	0.00101	0.29125	2.9125E-10	9.901E-07
2000	300.002	300	2.00E-09	0.00202	0.291825	5.8365E-10	9.901E-07
3000	300.003	300	3.00E-09	0.00303	0.29375	8.8125E-10	9.901E-07
4000	300.004	300	4.00E-09	0.00404	0.308365	1.23346E-09	9.901E-07
5000	300.0051	300	5.00E-09	0.00505	0.375625	1.87813E-09	9.901E-07
6000	300.0061	300	6.00E-09	0.00606	0.442885	2.65731E-09	9.901E-07
7000	300.0071	300	7.00E-09	0.00707	0.510145	3.57102E-09	9.901E-07
8000	300.0081	300	8.00E-09	0.00808	0.577405	4.61924E-09	9.901E-07
9000	300.0091	300	9.00E-09	0.00909	0.63407	5.70663E-09	9.901E-07
10000	300.0101	300	1.00E-08	0.0101	0.690735	6.90735E-09	9.901E-07

Table C-12: VOXF Thermal Conductance

Heat Flux Φ (pW/ μ m)	Max T (K)	Min T (K)	Φ (W/ μ m)	ΔT	Displacement	ΔW	Thermal conductance G, (W/K)
500	300.0009	300	5.00E-10	0.000895	0.0106523	5.32615E-12	5.58659E-07
1000	300.0018	300	1.00E-09	0.00179	0.0209323	2.09323E-11	5.58659E-07
2000	300.0036	300	2.00E-09	0.00358	0.0414923	8.29846E-11	5.58659E-07
3000	300.0054	300	3.00E-09	0.00537	0.0620523	1.86157E-10	5.58659E-07
4000	300.0072	300	4.00E-09	0.00716	0.0826123	3.30449E-10	5.58659E-07
5000	300.009	300	5.00E-09	0.00895	0.1031723	5.15862E-10	5.58659E-07
6000	300.0107	300	6.00E-09	0.01074	0.1237323	7.42394E-10	5.58659E-07
7000	300.0125	300	7.00E-09	0.01253	0.1442923	1.01005E-09	5.58659E-07
8000	300.0143	300	8.00E-09	0.01432	0.1648523	1.31882E-09	5.58659E-07
9000	300.0161	300	9.00E-09	0.01611	0.1854123	1.66871E-09	5.58659E-07
10000	300.0179	300	1.00E-08	0.0179	0.2059723	2.05972E-09	5.58659E-07

Table C-13: VOXG Thermal Conductance

Heat Flux Φ (pW/ μm)	Max T (K)	Min T (K)	Φ (W/ μm)	ΔT	Displacement	ΔW	Thermal conductance G, (W/K)
500	300.0005	300	5.00E-10	0.00051	0.0104563	5.22815E-12	9.8039E-07
1000	300.001	300	1.00E-09	0.00102	0.0209125	2.09125E-11	9.8039E-07
2000	300.002	300	2.00E-09	0.00204	0.041825	8.365E-11	9.8039E-07
3000	300.0031	300	3.00E-09	0.00306	0.0627375	1.88213E-10	9.8039E-07
4000	300.0041	300	4.00E-09	0.00408	0.08365	3.346E-10	9.8039E-07
5000	300.0051	300	5.00E-09	0.0051	0.1045625	5.22813E-10	9.8039E-07
6000	300.0061	300	6.00E-09	0.00612	0.125475	7.5285E-10	9.8039E-07
7000	300.0071	300	7.00E-09	0.00714	0.1463875	1.02471E-09	9.8039E-07
8000	300.0082	300	8.00E-09	0.00816	0.1673	1.3384E-09	9.8039E-07
9000	300.0092	300	9.00E-09	0.00918	0.1882125	1.69391E-09	9.8039E-07
10000	300.0102	300	1.00E-08	0.0102	0.209125	2.09125E-09	9.8039E-07